Martin, Christopher (2013) Development of a bioelectric nerve conduit using solenoid technology, and nano fabrication. PhD thesis

http://theses.gla.ac.uk/5278/

Microsystem Technology Group

School of Engineering

University of Glasgow

Development of a Bioelectric Nerve Conduit Using Solenoid Technology, and Nano Fabrication

Christopher Martin

Submitted in fulfilment of the requirements for the degree of Doctor of
Philosophy of the University of Glasgow

September, 2013

Abstract

Peripheral nerve repair outcomes have lagged behind comparable surgical techniques for many decades. A number of advanced approaches have been adopted over the last ten years. In particular the application of electrical stimulation during a repair is of great interest. It is clear that electrical stimulation of regenerating nerve tissue has a great many effects and can improve functional outcomes for patients. This work has focused on developing systems capable of applying accurate electric fields on the microscale within a biodegradable conduit, powered wirelessly. Experiments were conducted *in vitro* with a view to making progress towards an *in vivo* implementation.

Electrical stimulation was applied to regenerating sensory neurons *in vitro*, from a rat dorsal root ganglion. Mechanical guidance cues aligned neurons towards different microelectrode configurations in order to record the effect of applied electrical stimulation. This was performed using custom stimulation modules. SU-8 microgrooves and Ti/Au electrodes acted as mechanical and electrical cues respectively. This method was employed to great effect, identifying the effect of a number of electrical stimulation parameters. This led to a stimulation protocol featuring a 1:4 duty cycle, $20\,\text{mV}$ amplitude, $100\,\text{Hz}$ sinusoidal signal. This produced a number of interesting effects, including neuronal turning and a barrier formation. These results, demonstrated at the *cellular* level using a custom device and an autonomous stimulation system illustrates progress towards an optimised electrical stimulation waveform for neuronal growth control.

A novel transfer printing process was developed to produce patterned gold films on the biodegradable polymer, polycaprolactone. Patterned Au, $400\,\text{nm}$ thick, was transferred to a sheet of the polymer, producing a 15 turn, spiral inductor. The inductor was then electroplated to a thickness of $30\,\mu\text{m}$ and wire-bonded. Power and data were transferred wirelessly to the receiver circuit. Receiver circuits, connected to stimulation test modules in planar form, delivered electrical stimulation waveforms to regenerating sensory neurons on polycaprolactone. This stimulation resulted in confinement of the cells between two pairs of electrodes, demonstrating the efficacy of the novel receiver circuits. This was achieved with four electrodes in a twin-barrier configuration. These results illustrate progress towards implantation *in vivo*, using remotely powered electronics to guide regenerating neurons to their targets with microelectrodes.

Sensing cell growth through changes in electrical impedance is a well-documented technique. A receiver inductor has been connected to caco-2 cells in culture. Power was transmitted to the receiver inductor through an inductive link. Changes in the cell-monolayer have been detected at the transmitter output circuit, showing that the impedance changes are of sufficient magnitude to be reflected to the transmitter. Trypsin or EDTA were added to confluent layers of caco-2 cells, detaching them from the surface of the microchannel electrode array. This detachment was seen at the transmitter in the form of transient voltage changes. Data was acquired in using Labview programming and PXI hardware systems. This work illustrates progress towards biodegradable, passive cell sensing inspired by radio frequency identification technology, and electric cell impedance sensing.

Acknowledgement

First, I would like to thank my supervisor, David Cumming. His positive attitude to problem solving and patience ensured this project became a successful one. My second supervisor, Mathis Riehle, helped with the formulation of design ideas and again showed a great positive approach to the problems we faced. Special thanks also go to Andy Hart for helping me understand the requirements of the project and in particular for his contribution in the analysis of the results. I am extremely thankful to the Stephen Forrest Charitable Trust for funding me throughout this project. I would like to thank my opposite number in Cell Engineering, Theo Dejardin for a successful collaboration, ensuring we achieved some good results and overcame many challenges. The work presented here would not have been possible without the assistance of the James Watt Nanofabrication Centre technical staff.

I thank all past and present members of the Microsystem Technology Group for an enjoyable working environment and for any assistance I received. Many of the ideas could not have come to fruition with James Grant's advice and, though it has been said before, the 'top quality chats'. I also thank him for showing me the ropes in the early cleanroom days. I would have completed this work quicker in all likelihood had it not been for the many beers shared with Balazs Nemeth, but I'm sure the quality would have suffered. I thank Marek Piechocinski and Mohammed Al-Rawhani for the long chats about many subjects and for the social activities outside of work.

I thank my friends who have continued to force me to consume alcohol, dance, play FIFA, climb mountains, go on holiday and watch football when I would much rather be working. These guys, Kenny Meikle, Calum Blair, Johnathan Jones; Douglas Macfarlane, Kevin Gallacher, Craig Hunter; have impacted greatly on the quality of this thesis for which I can only apologise. In more recent times, Ross Millar and Scott Watson have joined in on the act, but I thank them for proof reading sections of this work and introducing me to low-level Scottish football. I thank my girlfriend, Kirsty Davidson, for her support throughout this journey and for helping me to unwind. I am thankful to my family for their support throughout. I couldn't have reached this far without them.

Finally, I would like to thank The Knife, Metallica, Bob Marley, Talking Heads and Placebo for providing the soundtrack to this thesis.

Contents

List of Figures

List of Tables

List of Acronyms

AM	Amplitude modulation
BSA	Bovine serum albumin
CMOS	Complementary metal oxide semiconductor
DOD	Drop-on-demand
DRG	Dorsal root Ganglion
ECIS	Electric cell impedance sensing
EDTA	Ethylenediaminetetraacetic acid
EMF	Electromotive force
FBS	Fetal bovine serum
FDA	US food and drug administration
GDNF	Glial cell derived neurotrophic factor
IPA	Isopropyl Alcohol
MEA	Multichannel electrode array
MEMS	Micro-electro-mechanical systems
MIM	Metal-insulator-metal
MRI	Magnetic resonance imaging
NGF	Nerve growth factor
NIL	Nanoimprint lithography
PBS	Phosphate buffered saline
PCB	Printed circuit board
PCL	Polycaprolactone

PDMS	Polydimethylsiloxane
PET	Polytheylene terephthalate
PLGA	Poly(lactic-co-glycolic acid)
PMR	Preferential motor reinnervation
PNS	Peripheral nervous system
PXI	PCI eXtensions for Instrumentation
RFID	Radio frequency identification
SAM	Self-assembled monolayer
UV	Ultraviolet

Publications

Journal Papers

Q. Chen, **C. Martin**, D. R. S. Cumming: *Transfer Printing of Nanoplasmonic Devices onto Flexible Polymer Substrates from a Rigid Stamp*, Plasmonics, Volume 7, Issue 4, p. 755-761, 2012

C. Martin, T. Dejardin, A. Hart, M. O. Riehle, D. R. S. Cumming: *Directed Nerve Regeneration Enabled by Wirelessly Powered Electrodes Printed on a Biodegradable Polymer*, Advanced Healthcare Materials, accepted for publication, December 2013

Conference Paper

C. Martin, Q. Chen, D. R. S. Cumming: *Transfer Printing of Nanoplasmonic Color Filters onto Flexible Polymer Substrates from a Rigid Stamp*, IEEE Photonics Conference, p. 481-482, 2012

Oral Presentations

C. Martin and T. Dejardin *invited talk on behalf of M. O. Riehle*: *Peripheral Nerve Repair Strategies*, Doctoral Training Centre in Cell and Proteomic Technologies, Edinburgh, 2013

C. Martin: *Transfer Printing with AZ4562 Photoresist*, James Watt Nanofabrication Centre Technical Meeting, 2010

Poster Presentation

C.Martin, T. Dejardin, A. Hart, M.O. Riehle, D. R. S. Cumming: *Peripheral Nerve Repair Using Biodegradable Electronics*, Royal Society Meeting, 2013

Declaration

The work in this thesis has been performed by the author in the Electronics Design Centre, the James Watt Nanofabrication Centre and the Centre for Cell Engineering with the following exception.

All instances of cell culture have been performed exclusively by Théophile Dejardin.

Christopher Martin

1 Introduction

1.1 Motivation

Injuries to the peripheral nervous system are complex and extremely difficult to repair using conventional surgical techniques [1, 2]. Functional outcomes for patients are typically poor and have not progressed much in the last three decades. Traditional approaches to repairing these injuries can be divided into suture [3], conduit [4, 5] and advanced techniques [6, 7]. If the two ends of a nerve bundle can be connected together under no mechanical tension, a suture repair may be applied. For those cases where a section of the nerve has been lost, a conduit repair can be used to bridge the gap between the two segments. This can be done with a donor nerve segment, harvested from a trivial nerve function, such as the sensation in a toe [8]. These two techniques do not significantly improve the rate of functionality that is recovered. Loss of function is common and often unavoidable. This is caused by a wide range of factors. The predominant factors are poor-alignment of neurons and support cells to their target, the injury response which prevents immediate regeneration, and the formation of painful scar tissue between the two bundles. This has driven researchers to design a wide range of advanced, functionalised conduits.

Advanced repair strategies have centred on functionalising the conduit, aiming to improve outcomes in a variety of ways. Grooves can be added, aimed at guiding regenerating cells to their targets [9]. Growth factors and Schwann cells can be included or delivered over-time to reduce the rate of cell-death [10, 11]. This project is concerned with one particular function, that of applied electrical stimulation. Applied electric fields have been shown to increase the degree of type-specificity [12]. Other benefits include an increase in the number of sprouting neurons [13] and the improvement of carpal tunnel surgery outcomes [7]. These positive outcomes are almost exclusively demonstrated *in vivo*.

This thesis describes the application of electric fields *in vitro*, documenting their effects on regenerating neurons at the *cellular* level. A number of effects caused by electrical stimulation, assisted by the use of mechanical guidance cues, have been shown here. These experiments aim to identify what electrical stimulation protocol could enhance peripheral nerve repair outcomes, to improve the understanding of how electric fields act upon neurons. A novel transfer printing process has been designed to produce wireless electrical stimulation systems on the biodegradable polymer, polycaprolactone. These systems, powered through a wireless inductive link, have shown how alternating electric fields can confine neurons between electrical barriers. This confinement provides a possible

mechanism for wirelessly powered, electro-activated biodegradable conduits to improve repair outcomes. Confinement of regenerating cells could improve the alignment to their targets, leading to a higher percentage of reinnervation. Finally, efforts to produce a passive wireless sensor, capable of measuring cell-growth through changes in the transmitter output voltage, have been described. This sensor, using caco-2 cells, could eventually be integrated with any stimulation system to provide feedback for a number of healing procedures. It could also be used to indicate the location of unhealthy tissue during a repair procedure.

1.1 Project Scope

The aim of this work is to develop electrical circuits on a biodegradable polymer to demonstrate improvements in the control of regenerating neurons. The circuits should be powered through a wireless scheme and be capable of being wrapped around a nerve conduit. The scope of the project, considering this aim, is to demonstrate and explore the feasibility of five crucial elements that will allow the above aims to be met.

The specific elements that will be studied in this project are summarised as follows:

- The optimisation of the electrical stimulation waveform to allow neurons to regenerate in a healthy manner.
- The demonstration that alternating electrical stimulation can influence the growth of regenerating neurons. In particular, the influence on the growth at the cellular growth should ideally hold promise in guiding neurons in an implant device.
- The development of a technique for patterning metal films on a biodegradable polymer to produce a receiver circuit capable of delivering alternating electrical stimulation to regenerating neurons.
- The delivery of the electrical stimulation signal using a wirelessly powered receiver circuit on a flexible, thin, biodegradable polymer, polycaprolactone, showing its efficacy as a neuronal guidance conduit.
- The design of a wirelessly-powered impedance-sensor capable of charting cell growth over time.

1.1.1 Electrical Stimulation Parameter Space

A number of questions remain unanswered regarding the application of electric fields to regenerating neurons. Whilst the behaviour of neurons in the presence of direct electric fields is well understood, the same cannot be said for alternating fields. This study therefore intends to narrow the electrical parameter space. This will be done by applying

electrical stimulation to regenerating neurons across independent experiments, thus gaining information about the effects that frequency, amplitude, shape, modulation and duration have. Within the scope of this project, it is desirable to identify an operating point that allows repeated experiments to be conducted. For example, it is desirable to find a stimulation waveform that does not inhibit the growth of neurons drastically, which will allow a number of different electric field protocols to be explored. With more scope, the *ideal* stimulation waveform could be found, but this is beyond the scope of this pioneering feasibility study.

1.1.2 Manipulation and Control of Neurons with Applied Electrical Stimulation

By identifying a 'working electrical stimulation', the effect on regenerating neurons can be documented through independent, repeated experiments. By orientating the electric field in different ways, it is hypothesised that a number of outcomes will be displayed, such as turning, barrier formation, guidance and alignment. This will be done with different electrode patterns and ways of applying the electric field, within a narrow operating window as dictated by the previous study point above.

1.1.3 Enabling Technologies for Electronics on Polycaprolactone

The optimum biodegradable polymer for connective tissue repair is polycaprolactone, primarily because of its long degradation time (approximately 2 years). In order to demonstrate that the effective electrical stimulation protocol can be delivered within a biodegradable conduit, a suitable fabrication technique is sought to produce electronic circuits on polycaprolcatone. This will be sufficient to demonstrate the efficacy of the electrical stimulation on biodegradable substrates for guiding regenerating neurons. With more scope, a fully biodegradable system could be implemented.

1.1.4 Design and Set-up of a Wireless Link and Biodegradable Stimulator

To demonstrate that the approach described here could be implanted, a wireless power scheme should be designed to power the electrical stimulator. The constraints on this system are predominantly in the receiver, with a number of biodegradable constraints, such as the size of implanted devices and the number of components. It has been decided that a prototype wireless power system will be implemented and used to stimulate regenerating neurons thus showing the capability of the design to work in its end application. With further scope, an optimised wireless link, either with maximal coupling, efficiency or displacement tolerance could be produced.

1.1.5 Passive Wireless Impedance Sensing

In a nerve repair procedure, it would be of great utility to know how the repair is progressing, providing feedback to patients as they go through the healing process. One way to achieve this could be through the inclusion of a sensing mechanism, capable of operating during the stimulation of the neurons. The design and testing of a sensor system capable of measuring changes in cell growth will be explored here. The system has been designed to be compatible with a biodegradable stimulation system. This will be tested with cell monolayers, measuring changes in electrical impedance between electrodes. With further scope this could be integrated with an electrical stimulation system to demonstrate their combined use as a bi-directional electrical biodegradable nerve repair conduit.

1.2 Thesis Outline

This thesis is sub-divided into six further chapters. A brief description of the purpose of each chapter is provided below.

Chapter 2, the literature review, provides a detailed overview of the published material that has had a significant bearing on the development of this project. The review is split among the four key constituent subjects. The peripheral nerve repair section documents the efforts over the last few years to improve functional outcomes for patients. A wide variety of techniques, from mechanical guidance tubes, electrical stimulation and action potential re-routing have been described, showing where this project's approach fits in and how it aims to improve upon existing studies, particularly in terms of accurately applying electric fields to regenerating neurons. Inductive powering, a technique often employed in bio-medical implants, is explained with the use of contemporary studies. Next, microfabrication techniques for thin-film polymers are examined, with their advantages and disadvantages appraised. Finally, a brief description of some modern cell impedance measurement techniques aims to show what the impedance of cells can tell us about their behaviour, with a view to including a similar system during a nerve repair.

An introduction to the electromagnetic theory used in this study forms the bulk of **chapter 3**. Fundamental laws, such as the Biot-Savart Law, are used to describe the operation of inductors. From this, an understanding of the ideal and non-ideal transformer is provided, providing a means to understand how power may be delivered wirelessly to an implant within a patient. Finally, some of the core sub-systems used within a wireless power scheme are described. These systems form the bedrock of a design approach and are as such vital to understanding what selections must be made.

The next three chapters, beginning with **chapter 4**, describe in detail the three branches of experimentation used. Chapter 4 describes how *in vitro* electrical stimulation of regenerating neurons can have a number of effects. Electrical stimulation applied to free neurons in an MEA and to pre-aligned neurons on a custom device, resulted in different growth profiles. The experiments in this chapter were designed to show how electrical stimulation could influence neurons at the cellular level and how such effects could have a positive influence in terms of *in vivo* peripheral nerve repair outcomes. The electrical stimulation waveform, from an initial estimate, has been honed to produce consistent outcomes. Work is on-going to optimise the parameters but these provisional results show great promise in controlling the growth of regenerating neurons.

Chapter 5 describes the development of electronic systems on the biodegradable polymer, polycaprolactone. This polymer, extremely difficult to work with in terms of microfabrication, was patterned using a novel transfer printing process. Printed receiver inductors allowed the circuits to be powered wirelessly. These systems, used in a planar form, were used to demonstrate confinement of regenerating neurons between two regions of alternating electric field. This development, of confinement at the cellular level on flexible biodegradable substrates, documents progress towards an electro-active biodegradable conduit for use *in vivo* to improve functional outcomes.

Chapter 6 describes the steps taken to design and build a wireless cell impedance sensor. Based on electric cell impedance sensing theory, this approach seeks to use a receiver inductor to reflect changes in impedance with cell-growth and behaviour back to a transmitter inductor. This passive receiver approach is aimed at being implemented on polycaprolactone for a biodegradable implementation. Impedance differences caused by changes in cell-electrode coverage were observed wirelessly using the caco-2 cell line. Work is needed to improve the consistency and to develop the technique further for use with the biodegradable polymer.

Finally, **Chapter 7** concludes the work presented and explores some of the options for future developments.

2 Literature Review

This literature review describes the four key fields of study that have inspired the work towards a functionalised biodegradable conduit, powered inductively, to direct nerve regeneration:

- peripheral nerve repair: surgical strategies and advanced techniques
- inductive power transfer
- microfabrication technology for thin-film polymer systems
- electrical cell impedance sensing: applications

This project is concerned with the development of a suitable electrical stimulation protocol to enhance peripheral nerve outcomes. This protocol should be delivered through a wireless inductive link on a biodegradable, thin-film substrate. A suitable electric cell sensing system should also be developed with a view to implementing it on a biodegradable substrate. It is therefore felt that the four literature review sections are applicable to this task and provide an excellent framework for subsequent design work.

2.1 Peripheral Nerve Repair: Surgical Strategies and Advanced Techniques

Injuries to the peripheral nervous system (PNS) are complex and difficult to address solely through conventional surgical techniques. In a cut-type injury, the nerve is separated into two nerve bundles. After the injury occurs, the bundle closest to the spinal cord (proximal) will attempt to regenerate towards the other bundle (distal). A major consequence of these injuries to patients is the loss of motor and sensor function, caused by poor regeneration accuracy, scar formation and cell atrophy during the regeneration process. This section delineates contemporary approaches to peripheral nerve repair, in particular the use of electrical stimulation, culminating in the identification of the requirements of a state-of-the-art repair conduit.

2.1.1 Suture Repair

If there is no loss of nerve-segment after the injury, a suture repair can connect the proximal and distal nerve stumps together, as shown in figure 2.1. This must be carried out without adding mechanical tension [3, 14]. The repair is often assisted with the addition of Schwann cells (a key support cell) and fibroblasts. However, whilst a large number of neurons will reach the distal stump, a significant proportion will escape the repair site, leading to reduced innervation, loss of function and, in some cases, formation of neuroma

(painful scar tissue). Suture repair is a relatively straightforward surgical technique by today's standards, however the accuracy and outcome is often poor in comparison to other surgical procedures. This type of repair is not suitable for long gaps between the two bundles because of the mechanical tension this would induce in the nerve fibre.
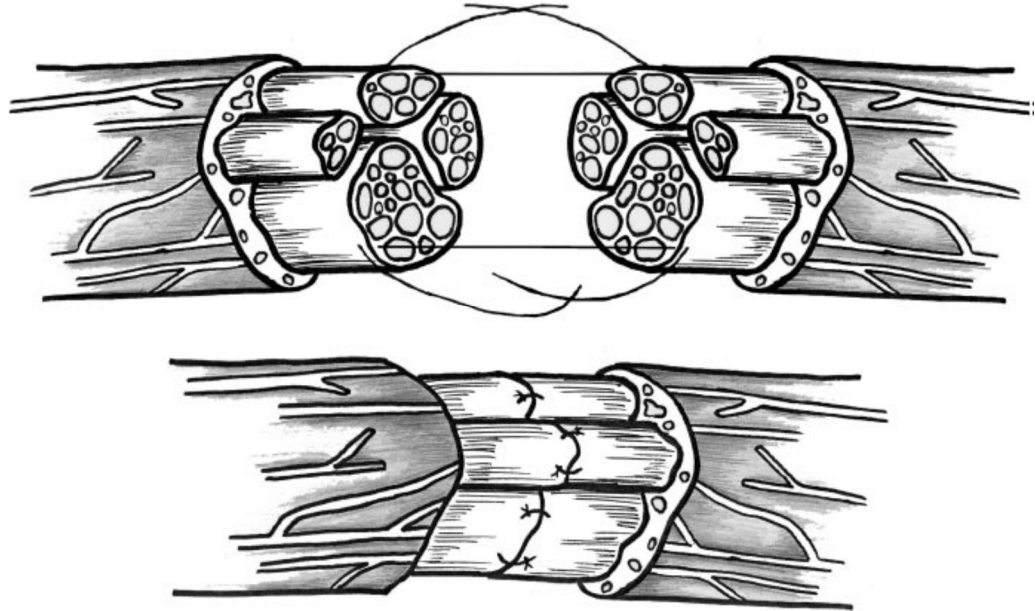
Figure 2.1 a schematic illustrating a suture repair. Often termed an end-to-end repair, individual fascicles within the nerve bundles are connected together. The repair must not induce any mechanical tension in the nerve and is therefore not applicable to long gaps [14].

2.1.2 Tube Repair

Inert tubes or conduits can be used when a loss of nerve segment has occurred in place of a suture repair. Typically the conduit is wrapped around the two nerve bundles, acting as a bridge for regenerating tissue to cross the injury site. These tubes are often made from silicone [4, 5]. The primary advantages of a tube repair procedure is the ability to bridge long gaps, on the order of tens of millimetres, and the ability to confine the regenerating cells within the repair site. However, as is the case with suture repairs, functional outcomes for patients undergoing a conduit repair remain poor. Further complications can arise due to constriction of the regenerating nerve bundle by the silicone tube [15]. Conduit repair is comparable to suture repair in terms of success, however for longer gaps between the nerve bundles, the injury becomes increasingly difficult to repair due to cell atrophy and poor alignment to the target organ caused by the increased distance and time taken to reach the target.

2.1.3 Donor Repair

Autologous donor repair is an advanced form of conduit or tube repair. A donor nerve is added within a repair tube, reducing the effective length of an injury site [8]. The regenerating neurons can reach the donor nerve, finding a supply of support cells, helping them to reach the distal nerve bundle. The donor is often a sensory nerve that fulfils a trivial function, such as the sensation in a toe. However, for some injury gap-lengths and types, a suitable supply of donor tissue may be difficult to harvest. This approach is unique in that, in the case of little or no functional recovery after a repair, the patient has lost the donor function in the process. In general, the outcome from this repair is not significantly superior to that of the suture or tube repair techniques despite the addition of the donor nerve.

2.1.4 Functionalised Tubes with Growth Factors and Support Cells

A promising development is the use of polymers containing materials that encourage the proliferation of neurons, e.g. glial cell-derived neurotrophic factor (GDNF) or nerve growth factor (NGF) [11] and support cells, such as Schwann cells [10]. Schwann cells are known to play a key role in the regeneration process; hence including these support cells in a nerve conduit should enhance repair outcomes by increasing the percentage of axons that cross the repair site. In the same way, the addition of growth factors can provide a boost to regenerating neurons as they attempt to bridge long repair gaps. Advanced nerve repair strategies should seek to deliver these cells, perhaps using drug-delivery techniques in a conduit, in order to further enhance outcomes for patients.

2.1.5 Biodegradable Polymer Conduits

Biodegradable conduits eliminate the requirement for follow-up surgery to remove an implant once a regeneration procedure has ended, but their primary advantage is that they do not compress the nerve fibre in the latter stages of a repair [15]. Instead, the polymer can dissolve over time, allowing the expansion of the nerve bundle. Biodegradable polymers are characterised by their degradation time (in months), mechanical strength, melt and glass transition-temperatures and their level of biocompatibility. Integrating electrical and other functionality within a biodegradable conduit is usually more difficult when compared with other materials.
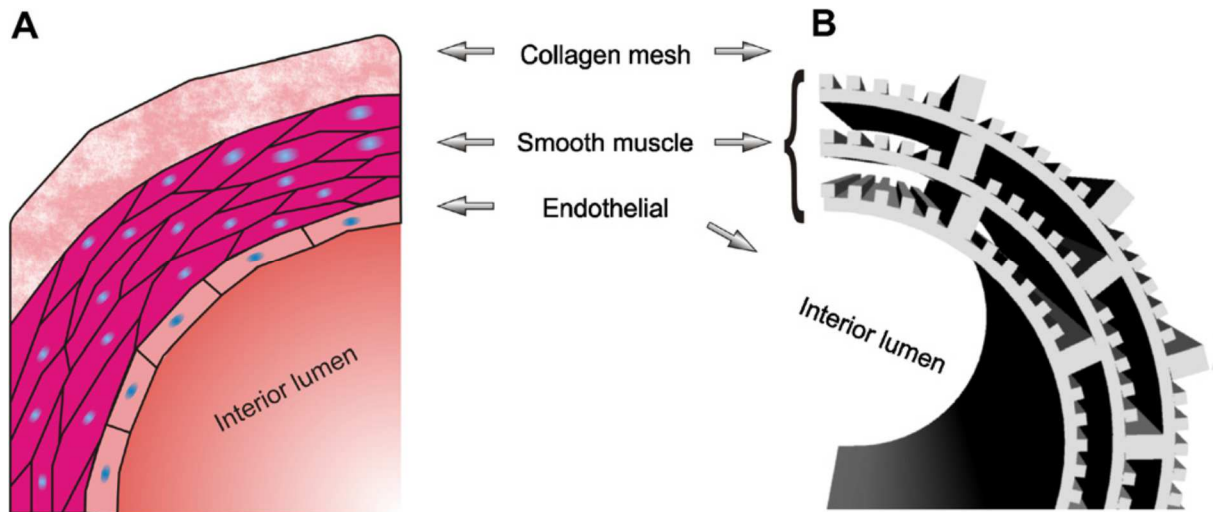
Figure 2.2 (a) a schematic showing the composition of a small blood vessel and (b) a biodegradable tube made from sheets of polycaprolactone designed to determine the tissue type in certain locations within a vascular scaffold [16].

With a range of materials, and the addition of support cells, many authors have sought to alter the surface properties of the conduit to improve the guidance of neurons to their target. This desire for longitudinal alignment is critical to the success of a repair, particularly for longer gaps and is the primary reason that the traditional conduit repairs do not work effectively.

2.1.6   Nano/Microtopography

Patterning sheets of the biodegradable polymer, polycaprolactone (PCL), with nanopatterned surface cues and micro-topography, dictates the location of different cell types within a conduit for vascular tissue engineering applications, as shown in figure 2.2 [16]. This is achieved using patterned surface topography. This approach of copying the conditions within a nerve fibre should prevent negative outcomes, such as the formation of neuroma, whilst ensuring the correct cell type in each location and improving the alignment through the use of topography.

2.1.7   Nanofibres and Microbraids

Nanofibres can be added within a conduit, altering the surface topography. This has been used to great effect, producing longitudinal growth profiles of regenerating neurons [17, 18]. Nanofibres like these have been shown to be effective in aligning neurons and can even induce turning, depending on the orientation of the fibres. These biodegradable fibres have great potential in aligning regenerating neurons towards their targets. Microbraiding of the polymer poly(lactic-co-glycolic acid) (PLGA) [19], has produced large pores in the polymer sheet by altering the braid pattern, increasing the supply of nutrients to the

regenerating cells, particularly in the centre. A combination of nanofibres and microbraiding may yield interesting results in terms of cell growth and directional alignment. These types of conduits require dedicated fabrication tools for the braiding of polymers which has limited the quantity of published studies.

2.1.8 The Action Potential: Indirect Repair Strategies

There are, in general, two types of peripheral nerve repair strategy: direct repair using conduits or sutures and indirect repair using action potential re-routing. Action potentials are electrical signals that propagate through axons, conveying information. Motor neurons send electrical signals in the form of action potentials to muscles, causing them to flex or contract. Sensory neurons work in reverse, taking sensory information back to the spinal cord.

After a nerve injury occurs, action potentials can no longer be transmitted to their target and therefore the muscles cannot respond. This causes a loss of function for the patient. Action potentials can be re-routed through an electronic interface to their destination as an alternative to a repair procedure. This type of interface is used extensively in prosthetic limbs, which use action potentials to control artificial end-effectors, such as robotic hands. Indirect repairs such as this seek to overcome many of the challenges associated with traditional peripheral nerve repair surgery, using microelectronics technology to bypass the injury site.

In vivo recording of action potentials can be difficult as the impedance of the surrounding tissue attenuates a large portion of the signal. Electrical noise caused by crosstalk from other nerve activity can create significant uncertainty in the measured data [20]. Action potential parameters can provide a good indication of the success of a procedure over time [21, 22]; for example the percentage of axons firing their action potentials. Theoretically techniques like these could give real-time feed-back, allowing a surgery to be scheduled if the repair is not progressing as expected. However, transdermal electrodes (often several hundred in an array) increase the risk of infection, are likely to break, and limit the mobility of the patient [23]. A wireless recording interface is much more desirable when interfacing to action potentials.

2.1.9 Advanced tube repair strategies

The standard tube repair has been advanced further by numerous 'Swiss roll' designs, featuring multiple microchannels for regenerating tissue to grow through. Lacour et al [6, 9] have developed systems on polyimide containing both microgrooves and electrodes,

depicted in figure 2.3. The electrodes can measure neuronal activity, indicating how far a repair has progressed along the tube with the microgrooves used as guidance channels to improve the accuracy of the repair. These conduits show good promise in combining guidance cues with action potential recording in a single functionalised conduit. It would be interesting to see such systems adopt a wireless power and data protocol to alleviate the issues associated with transdermal electrodes.
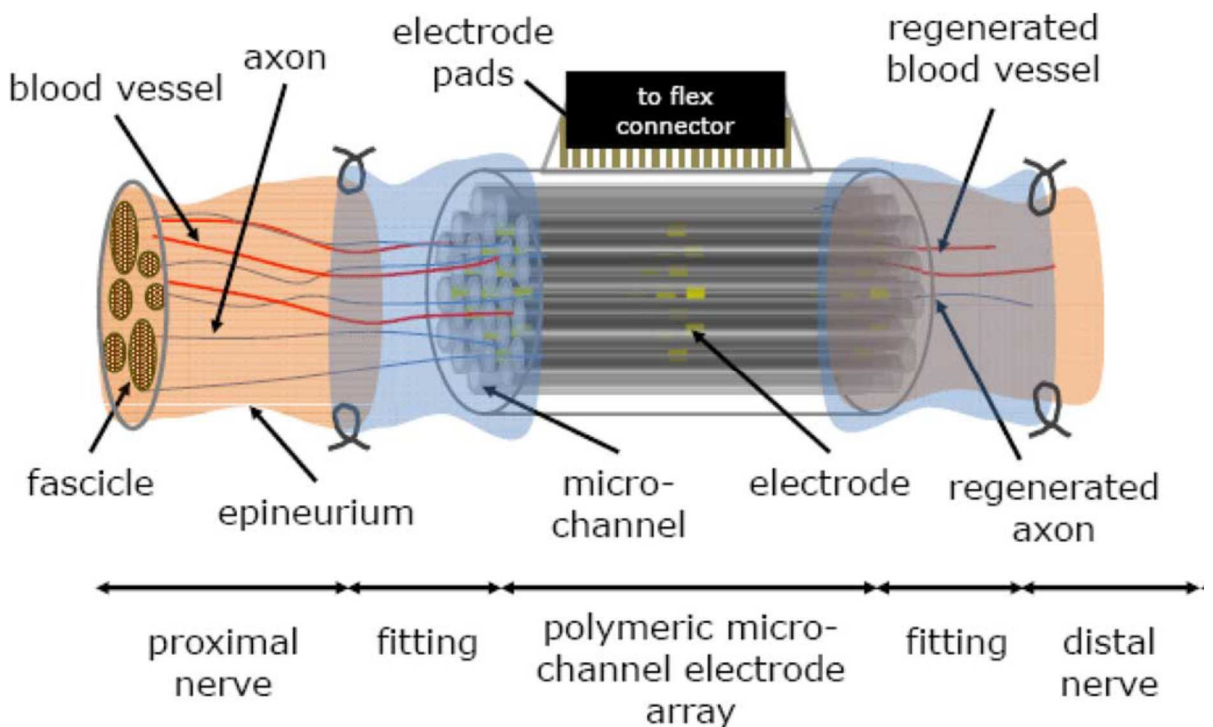
Figure 2.3 the long microchannel electrode array used to bridge a nerve repair site. The implant is sutured to the proximal and distal nerve bundles. This approach uses transdermal electrical connections and contains numerous microchannels used as guidance channels. The length of the implant varies from 0.5 to 5 mm long, with a diameter of 1.5 mm designed to match the rat sciatic nerve [9].

Contemporary conduit repair design is increasingly dependent on the combination of many different repair elements, which can be broadly defined as topographical, biological, chemical and electrical guidance cues. It is useful while designing such conduits to bear in mind some of the fundamental requirements of a conduit [24] as shown in figure 2.4. Progressing from the basic requirement of a conduit acting as a bridge between the two nerve bundles (shown in the centre of the figure), the authors have identified a number of components that could assist the repair process. Conduits that allow nutrients to diffuse into the injury site (Permeability) can increase the percentage of healthy cells within a conduit. Added growth factors and supportive cells such as the key Schwann cells, can have a critical effect on the repair. The three components shown below the basic conduit

illustrate the desire to include directional growth cues for the purpose of alignment and control of regenerating tissue. Conductive polymers may provide electrical guidance cues either as a voltage gradient, or as part of a complex electrical system. Multichannel structures split the repair into sections, mimicking the nerve fascicles and avoiding mass crossover of neurons. In an ideal situation, each axon would have a single microchannel for a perfect repair, but there is a limitation on how thin and complex a polymer conduit can be made. Finally, internal frameworks can offer cell-determination cues to increase the fidelity of the repair, leading to correct tissue type formation and location. The effectiveness of the included features should be examined, particularly for future design iterations [1, 14].
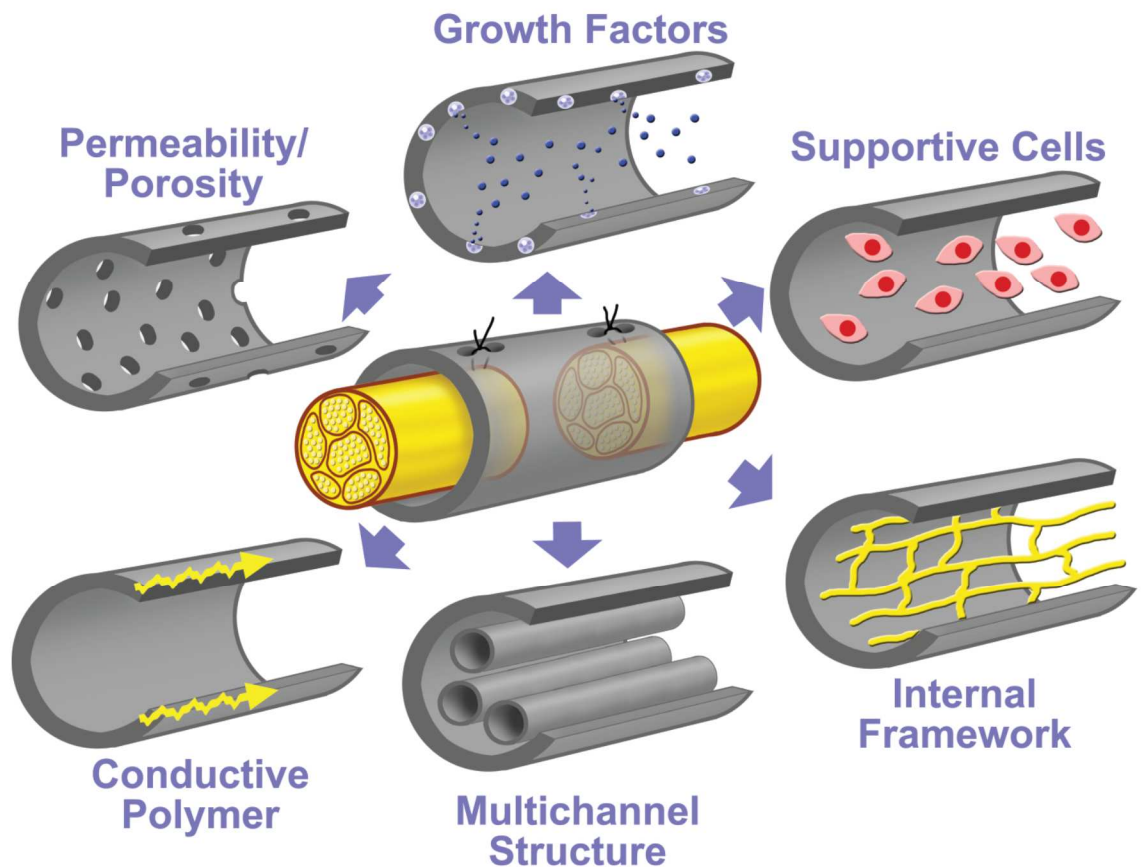
Figure 2.4 depictions of some of the most desirable elements and approaches used for advanced conduit repair strategies. Permeable conduits are required to allow the diffusion of nutrients into the injury site. Growth factors and support cells play an integral role in the repair process. Conductive polymers, multichannel structures and internal frameworks can all provide a measure of control and a degree of guidance to improve the accuracy of a procedure [24].

Both synthetic and natural materials have been utilised for nerve guides. The basic requirements of permeability, biocompatibility, incorporation of growth factors and

Schwann cells, good rate of degradation, good response to swelling [6] and mechanical integrity [3] should be adhered to. Conduit repairs offer the most promise, but linking some of the benefits of action potential recording or re-routing in a wireless manner could also work well if integrated together. It remains a challenge to integrate multiple functions within a single repair conduit. However as the production techniques advance it is thought that these systems may be realised and applied to injuries *in vivo*.

2.1.10 Peripheral Nerve Repair Strategies Summary

Different approaches to peripheral nerve repair, from basic techniques like suture and conduit repairs to more advanced systems containing multiple functionalities, have been delineated. This project is primarily concerned with improving functional outcomes in cases where there has been a loss of nerve segment i.e. any conduit must act as a bridge between the remaining nerve bundles. Conduit repairs with biocompatible tubes are ineffective whilst a follow-up surgery is required to retrieve the non-degradable material. In contrast, biodegradable conduits offer an immediate benefit to patients by eliminating the need for a second surgical procedure, hence this line of research has been selected on the basis that a tangible advantage is achieved immediately. The trade-off here is that biodegradable polymers are, in the main, more difficult to process with traditional microfabrication techniques when contrasted with materials such as silicone and polyimide (which are often used as repair conduits).

Conduit repairs that include a donor repair are not an optimum solution to the nerve repair problem. The concern with these operations is that despite harvesting another nerve from the patient (to the detriment of that function) no significant improvement in functionality is achieved for the patient. Whilst the use of a donor need never be precluded in the design (as there is always space in the conduit for nerve tissue) it is thought that an elegant solution should seek to achieve positive outcomes without harvesting donor tissue.

The work in this project has focused on the inclusion of electrical stimulation within a biodegradable conduit. However, the use of mechanical guidance cues, microtopography to determine tissue type and micro/nanobraids as alignment cues are all excellent elements worthy of inclusion within the conduit. It has been beyond the scope of this project to include these in the conduits documented here, but in the design of the conduit shown in chapter 5, it can be seen that the electronic circuit has been designed to allow sufficient space for other elements to be included in the long-term.

Action potential re-routing strategies are of considerable efficacy, particularly in interfacing between prosthetic parts and healthy nerve tissue. Using electrical stimulation within a biodegradable conduit, the aim here has been to exact a direct repair solution in the long-term by optimising one guidance element. It is hypothesised that the overall aim of improving each prospective guidance element and integrating them together will yield a direct nerve repair approach, without a donor nerve, capable of restoring functional outcomes for patients across a range of injury gap-lengths.

2.2 Electrical Stimulation

The Focus of this review will now turn toward the use of electrical stimulation during a nerve repair procedure as a tool for improving functional outcomes. Electrical stimulation has a variety of effects when applied during a nerve repair surgery. This sub-section aims to outline some of the outcomes reported to date and the contemporary approaches to applying electric fields within a conduit *in vivo*. Electrical stimulation of neurons can be divided into two approaches: that of d.c. and a.c. electric fields.

2.2.1 Direct Applied Electric Fields

Direct electric fields have measurable influence over neurons particularly in terms of alignment. Applying a potential difference, neurons will turn and grow towards the cathode, often resulting in a faster rate of growth than if there were no potential present [25, 26]. It is not well understood why neurons prefer the cathode, and what mechanisms are at play at the cellular level. This effect is comparable with the growth of bone towards a cathode in the presence of a direct field [27]. Direct fields could in theory be included within some of the conduit designs discussed, easily aligning neurons to their target (and at a faster rate). However the long-term health problems associated with prolonged exposure to d.c. fields *in vivo* limit their use [28]. Implanted electrodes will, over time, dissolve toxic ions into the surrounding tissue. Many reported d.c. techniques use relatively large electrical currents, increasing the flow of toxic ions into the surrounding tissue [29]. For these reasons modern research approaches have focused on the application of a.c. fields to regenerating neurons as a safer alternative.

2.2.2 AC Fields
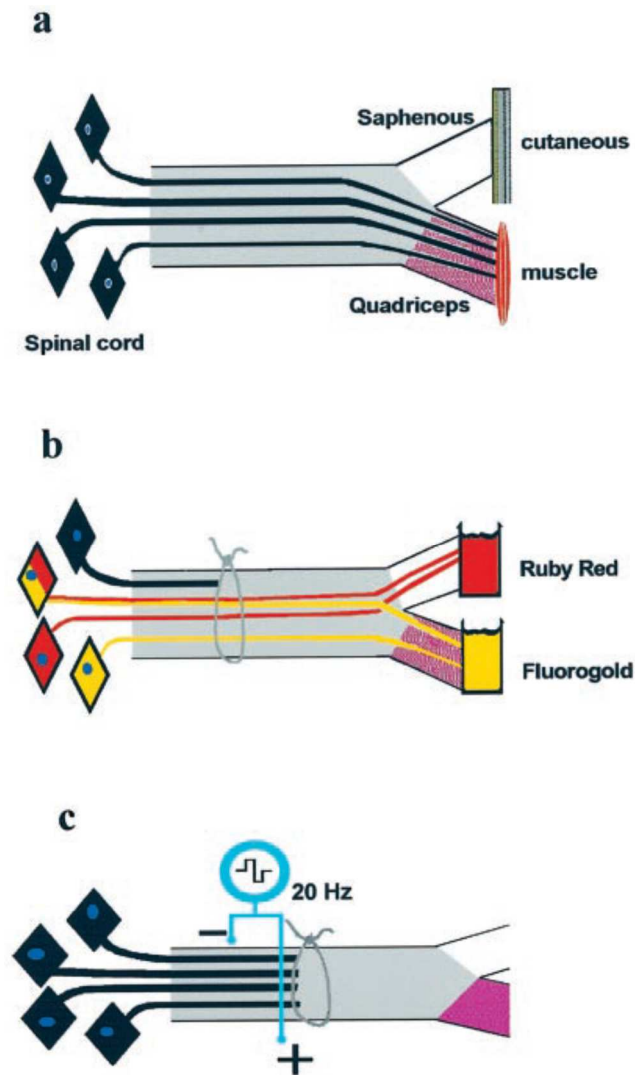
Figure 2.5 the protocol established by Al-Majed et al. (a) a schematic depicting the femoral nerve motoneurons connecting to the quadriceps muscles and the saphenous branch connecting sensory nerves from the skin. (b) the application of retrograde neurotracers to identify the distribution of regenerating motoneurons. If motoneurons successfully reach the quadraceps muscle, this is regarded as good type-specificity. Those motoneurons that grow towards the cutaneous branch have been unsuccessful in terms of regeneration and therefore decrease the rate of type-specificity. (c) the stimulation of the nerve by applying a voltage between the proximal and distal regions of the repair site, resulting in an increase in the number of motoneurons reaching the quadriceps muscles and therefore an improvement in the type specificity [12].

Alternating electric fields, on the other hand, can be applied *in vivo* without inducing harmful tissue effects. The alternating electric field protocol developed by Al Majed and Gordon [12] is the most widely used approach, outlined in figure 2.5. Two electrodes are applied across the conduit during a repair, applying electrical stimulation for a certain amount of time each day. The study found that one hour of stimulation per day produced

the best outcome. The 20 Hz signal applied for one hour per day improved type specificity at the end of the procedure. Type-specificity refers to the percentage of sensory neurons innervating a sensory neuron in the distal stump (the same measurement can be applied to motorneurons). In the work reported in this thesis, electrical stimulation was applied continuously throughout each day. This was chosen in an effort to maximise the chance of observing different growth patterns. It was the aim of varying the duration of the stimulation, in the same way as Al Majed et al, but this proved beyond the scope of this project. Preferential innervation of motor neurons, by regenerating motor neurons (i.e. not by sensory neurons) is termed preferential motor reinnervation (PMR) and many researchers have employed this protocol with varying degrees of success. Since low type-specificity decreases the amount of functional recovery, a positive outcome of this study is that specificity has been increased. N.B. a sensory axon innervating a motor axon will not be able to form a working electrical connection [12, 30].

It has also been shown, using their protocol that the typical injury response can be accelerated by applying alternating fields [7]. If the initial injury response is accelerated by a number of days, the regenerating cells will reach their targets faster, reducing the percentage of cell death in the target organ. This represents a good chance of, in turn, gaining significant improvement in functional recovery. It is thought that the mechanism by which this protocol works is in the reduction of die-back (a process of 'shearing' damaged neurons) and an increase in the number of sprouting axons [13].

2.2.3 Stimulation Frequency

Effects of electrical stimulation at different frequencies have been published, but it is still unknown exactly how the frequency impacts upon the regeneration process [31]. Frequencies in the range of 0-200 Hz are often used in electrical stimulation experiments and the density of fibres after a repair seems to depend on the frequency of stimulation used [32]. Selecting an electrical stimulation parameter and examining how it influences the result of the repair could provide insight into what electrical parameter values form an optimum stimulation waveform for a successful peripheral nerve repair. The frequency of 20 stimulation pulses per second has been used extensively by Gordon et al and is biologically comparable to mammalian firing patterns for motorneurons [33]. In this work, frequencies that are comparable to 20 Hz have been used. Indeed, this frequency allowed much better neuronal outgrowth, perhaps indicating that frequencies in excess of this value do not allow adequate relaxation of the neurons.

2.2.4 Application to Carpal Tunnel Syndrome

A.c. fields may be applied to other types of peripheral nerve injury. Crush injuries and carpal tunnel syndrome are two such examples. Electrical stimulation, again using the same protocol established by Gordon et al, has been shown to be effective in improving the functional outcomes of a carpal tunnel surgery, as shown in figure 2.6.
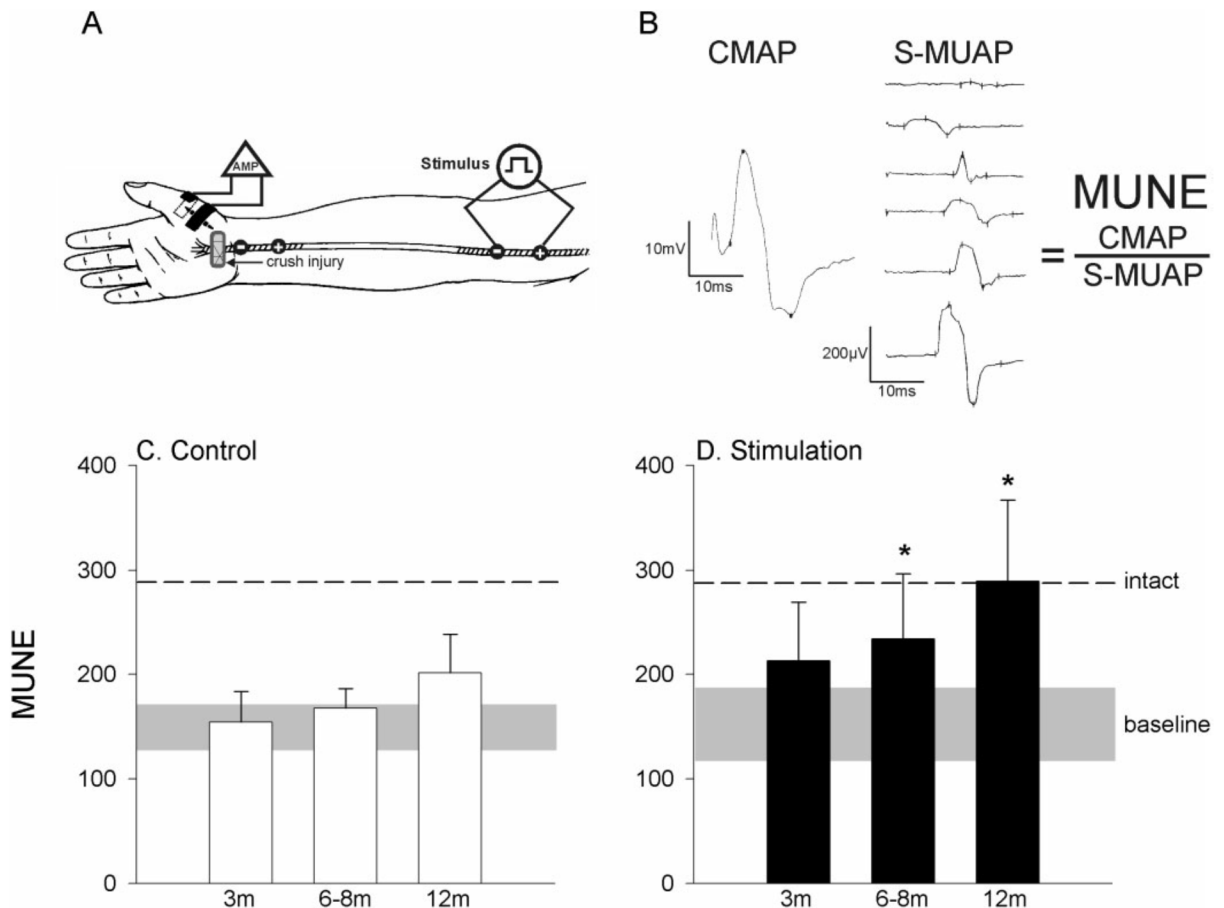
Figure 2.6 (a) electrical stimulation applied to the median nerve in 3 month intervals. The stimulation was designed to recruit discrete all-or-nothing increments in EMG potentials by stimulating progressively more proximal sites. (b) the number of single motor units (MUNE) was achieved through the ratio of the amplitudes of the compound action potential (CMAP) and the single unit action potentials (S-MUAP). (c) the MUNE data for carpal tunnel release surgery without stimulation and (d) with applied electrical stimulation. This is an example of how electrical stimulation can improve functional outcomes for a crush-type nerve injury [7].

2.2.5 Magnetic Fields

The application of magnetic fields in medicine is not unusual, for example they are used in magnetic resonance imaging (MRI) machines. Magnetic fields have been applied during nerve regeneration experiments, though not as commonly as electric fields. An applied static magnetic field did not cause any significant improvements to nerve repair outcomes

[34]. Alternating magnetic fields are, however of more interest [35]. Pulsed electromagnetic fields are used in a number of holistic treatments, but it is not clear what effect, if any, they have on neural repair. A well organised study with accurate control of the alternating magnetic fields at the cellular level has yet to be conducted, with any existing data showing negligible improvement over controls. In all likelihood, any alternating magnetic field of sufficient strength will have an effect based on the *electric fields* it induces in the tissue; therefore it is much better practice to deliver these electric fields with accuracy and control, not as a consequence of applying a magnetic field.

2.2.6 Electrical Stimulation Summary

Applied electrical stimulation after a peripheral nerve injury has a lot of potential for positive outcomes, particularly in the increase of injury response, faster growth rates, and increased type specificity. Direct electrical stimulation, either through the use of constant current or voltage sources, has a definitive effect on regenerating neurons. Neurons indeed prefer to grow towards one electrode over the other. For example, a field magnitude of 0.2-0.3 Vcm^{-1} can cause 55%-73% of neurons to turn towards the cathode [36]. The ability to implement a safe, direct stimulation implant remains elusive primarily because of the harmful effects associated with long-term implantation of direct stimulation. For this reason, alternating electrical stimulation has been the sole focus of the work reported here.

Alternating fields have a complex relationship with regenerating neurons, in that it is difficult to know exactly what their effect is, particularly *in vivo*. The protocol used by Gordon et al [7, 12, 13] has shown some of the positive outcomes described above. They theorise that electrical stimulation applied after an injury may alleviate the effects of Wallerian Degeneration and die-back, which in simplistic terms are the death of supportive and axonal cells in the distal and proximal stumps. Electrical stimulation may override the signals here, initialising the recovery response in a quicker time.

To date, however, an accurate application of these fields at the cell level within a conduit has yet to be displayed. With finer control, outcomes could be better documented and enhanced both by existing authors and new entrants to the field. The difficulty faced by new entrants is in the number of studies operating on different nerves with different electrical stimulation techniques. If the electrical stimulation parameter space could be diminished, a consensus of approach could be reached, leading to greater comparisons between studies and assistance between authors. This has been the central motivation behind this work and in particular the experiments in chapter 4, which attempt to identify what effect the different electrical stimulation parameters have on regenerating sensory

neurons. This approach *in vitro* could help to identify how alternating stimulation could influence And change outcomes *in vivo* by understanding the reaction of neurons when faced with different electrical stimulation protocols.

2.3 Inductive Power Transfer

Many bio-electronic implants use batteries as their source of power. The energy from the battery can be sufficient in some applications or recharged via a wireless link as required [37, 38]. There are many disadvantages associated with the use of batteries *in vivo*. Peripheral nerve repair operations can often last many months, which may be longer than the life-time of the battery. Implantation of a battery inside the body can be dangerous should the battery be exposed to tissue; using a large amount of encapsulation could in turn compromise the space available for the rest of the implant as well as increasing the likelihood of a foreign body response[1]. Wireless charging of an implanted battery is a useful technique. However it is better to power the implant wirelessly, eliminating the battery and in some cases a second surgery to remove it. With these considerations in mind, and in an effort to develop a biodegradable system, a wireless power and data protocol is sought.

2.3.1 Inductive Powering

Inductive powering is a technique used to provide power and data over a wireless link to a receiver circuit. Power is transferred through the magnetic coupling between two inductors operating as a non-ideal transformer. Early wireless schemes demonstrated radio frequency applications, such as transmitting generic clock and data pulses, or power [39]. This early work described how coupling could be optimised, as well as outlining a design of a system. Advanced systems have been designed to operate cochlear implants [40] and retinal devices [41]. These are characterised by long-term implantation and by their data requirements. These devices typically take sound (light) as an input and send it wirelessly to the implant. The implant then converts the data to stimulation pulses; which are applied to the auditory nerve (optic nerve). This is a great example of action potential re-routing as an indirect repair technique. For these systems, a high rate of data transmission and bandwidth is often the most important factor, to ensure the quality of information sent to the appropriate nerve bundle. Inductive powering is used extensively in micro-electro-mechanical systems (MEMS) [42], and in radio frequency identification (RFID) systems [43]. MEMS sensor systems, such as these, are perfect candidates for inductive powering due to their small size and the ease of fabricating an inductor on-chip.

---

[1] Larger objects inside the body are more likely to induce a foreign body response.

2.3.2 Optimisation of Inductive Powering Systems

Approaches to design of inductive powering systems are often grouped according to which parameter is of paramount importance. Seeking optimal efficiency of the link [44] is useful in minimising power consumption, thus allowing the use of a portable transmitter with manageable energy requirements. This translates as a direct increase in the quality of life for the patient, allowing them a certain freedom of movement during a repair. Increased data rates and bandwidth at the expense of the efficiency [45] may be used in a design when the integrity, speed or quantity of data sent via the link is important. Reducing the effect of coupling variations [46-48] is beneficial in medical applications, allowing small movements in the position of the transmitter cuff and the implant, without having an adverse effect on the system performance. A comprehensive power-transfer function for variations in distance, angular displacement and lateral misalignment has been described by Fotopoulou and Flynn [49]. Whereas the majority of studies on this matter have dealt with individual loops of wire, or used simplified models of solenoid coils, their work uses practical inductors which are of most interest to the biomedical field, that of planar spiral inductors, both on PCB and printed. The graphs of power transfer for different cases of misalignment allow the designer to ensure the design is safeguarded against possible coupling variations introduced by the three variables.

The design rules of planar thin-film inductors [50-54] and inductors in general [55, 56] are of assistance when faced with tight geometric constraints, ensuring the designer can make the best use of the space available by selecting the correct inductor parameters. This again can yield improvements in efficiency, penetration depth and cost.

Numerous design procedures for example systems are available and provide useful insight into both the steps involved and the restrictions of the technology [24; 25]. The design of receiver and transmitter and the layout and geometric properties [46, 50, 52, 57] is a useful guide during the design phase of the wireless link.

A power amplifier must be used to drive the large transmitter inductor currents required to induce power in the receiver. There are many amplifiers suitable for this purpose, often divided into their respective classes of operation.

Class E amplifiers are selected in most contemporary inductive powering systems [58]. These amplifiers have very high efficiencies on the order of 90-100% and typically work at one transmission frequency. Class C amplifiers are also used, with an easier design flow

than class E at the cost of lower efficiencies. Class A, AB and B driver topologies may be selected for rapid prototyping.

Class	Description
A	100% conduction angle, simple design flow, low efficiency.
B	50% conduction angle, high cross-over distortion, simple design flow.
AB	A push-pull driver with both transistors conducting for more than a half-cycle. Minimises the cross-over distortion found in class B topologies.
C	Low power dissipation, high output distortion, complex design flow, current output. Often used in inductive powering.
D	Low power dissipation, voltage output, complex design flow.
E	Theoretically no power dissipation, output must be tuned to one or more resonant frequencies, extremely complex design flow, best suited to driving low-coupling inductive powering systems.

Table 2.1 a description of some amplifier classes employed in inductive powering systems.

Data telemetry is features extensively in inductive power technology to fulfil a variety of functions, including monitoring the integrity of transmitted data [59, 60], external regulation of receiver voltage [44], clock recovery at high data rates of 1 Mbps [45], and measurement of electrode potentials in cochlear implants [40]. The transmission frequency is usually in the 100 kHz to 10 MHz range to ensure efficient power transfer and to minimise eddy currents in the surrounding tissue.

2.3.3 Inductive Powering Summary

Inductive powering is ideally suited to the long-term powering of medical implants. The ability to work in a suitable frequency range (100 kHz – 10 MHz) and the ability to use a receiver inductor of suitable geometry for a nerve repair conduit is a significant advantage over far-field radio-frequency solutions. Class E drivers are the optimum transmitter driver for finished products. For rapid prototyping, as is the case in this work, class A, AB or B drivers offer the designer greater flexibility and simplicity in delivering power and data to the implant. A class AB amplifier has been selected for this work to offer a balance between efficiency, design flexibility and a practical implementation for many different electrical stimulation experiments.

Different approaches to optimisation of inductive links have been provided. These are often a trade-off between efficiency, data rates and misalignment tolerance. In addition, for biodegradable systems, it is often desirable to minimise both the number of components in

the implanted receiver, and the complexity of the implant. In the long-term, it is thought that optimising the inductive link for maximal efficiency will improve the quality of life for patients by the largest factor, primarily due to increased battery-life. This will decrease the number of charge-cycles required and thus increasing the mobility of the patient from day to day.

Finally, data transfer methods are numerous and often complex. It is favourable to use amplitude modulation where possible, again to minimise the receiver components and the complexity of the receiver. The transmission and receiving of data has been separated in this work (chapter 5: wireless electrical stimulation, chapter 6: wireless electrical sensing) into amplitude modulation (for transmission) and load modulation (for received data).

2.4 Microfabrication Technology for Electronics on Thin-film Polymers

Advanced conduits, powered through a wireless powering scheme, could greatly improve peripheral nerve repair outcomes. It has been shown that these systems are both complex and difficult to design and build. Biodegradable polymers cannot undergo traditional microfabrication procedures due to temperature, chemical and mechanical limitations. An outline of the processing techniques available for thin-film polymers relevant to this application is therefore necessary to understand what is possible for advanced conduit design.

2.4.1 Inkjet Printing

Drop-on-demand (DOD) inkjet printing may be used to deposit patterned thin metal films onto thin-film polymers [61], operating in a similar way to commercial inkjet printers. The metallic ink often requires a sintering phase, at temperatures far in excess of the melt temperature of some polymers. Sintering at lower temperatures may be achieved using some specialist techniques to avoid damaging the polymer [62, 63]. Inkjet printing onto polymers is commercially advantageous because it is additive, i.e. no metal is wasted, unlike subtractive fabrication techniques such as lift-off and wet-etching. If specialist sintering techniques can be used, inkjet printing is a viable option for the production of electronic circuits on flexible polymer substrates and would be more cost-effective than other microfabrication techniques.

2.4.2 Nano Imprint Lithography

Nanoimprint lithography (NIL) requires a patterned master, or stamp and a target substrate. The master is pressed into a photoresist film on a polymer substrate [64] at a temperature above the glass transition of the polymer, at sufficient pressure to imprint the desired

pattern. Metal can then be evaporated onto the polymer, followed by a lift-off process, leaving patterned metal on the polymer substrate. Alternatively, a wet-etch may be used to yield the same result if a negative photo-mask is used [65]. The polymer substrate must be compatible with the lift-off or wet-etch techniques. In addition, a layer of photoresist must be spun onto the polymer and baked at temperatures on the order of 90 °C which may not be suitable for some polymers.

2.4.3 Cold Welding of Metal Films

If a seed layer of metal can be evaporated or sputtered onto the polymer, cold welding may be used to add patterned metal [66]. This process can be additive [67] or subtractive [68] to produce patterned metal films on the substrate, providing the seed layer can be removed, for example by uniform etching. This technique requires a robust substrate, to cope with the high imprint pressure. The substrate must be compatible with the etching process required to remove the metal seed layer. Cold welding could be best suited to the addition of a small number of via connections, or in the repair of printed features by the addition of replacement metal. This could have great utility in prototyping, and as an auxiliary process to increase the fabrication design options.

2.4.4 Hot Embossing and Nanomoulding

A polymer can be patterned with microgrooves, pores and other topographical features using hot-embossing [16] or micro/nano moulding [69, 70]. These techniques are similar to NIL; with the difference being it is the *substrate* that is patterned here (the photoresist is patterned in NIL). Embossing and moulding can be used with metal transfer techniques to achieve both mechanical and electrical functionality on a polymer substrate.

Polymers may be printed onto other polymeric substrates [71]. The degree of temperature and planarization of the polymer during imprint can alter the nature of the feature produced [72]. A subtractive process may also be used to selectively remove regions of a material [73]. This technique could be used to produce topographical features within a conduit in conjunction with other printing techniques.

2.4.5 Patterning Using a Sacrificial Layer

A sacrificial layer of SU-8 photoresist enables selective metal patterning of polymer substrates [74]. The adhesion properties of SU-8 serve as a good guide when developing this process, as SU-8 is known to delaminate from some materials [75]. Copperfoil can also be used for this process [76] on polydimethylsiloxane (PDMS) substrates. In both cases the resist baking step and the chemicals used for processing must not damage the

polymer. A multitude of sacrificial materials can be selected; based on the design requirements of the fabrication process.

2.4.6 3D Stacking and Printing

Printing may be carried out in subsequent steps, producing three-dimensional stacked polymer structures [77, 78]. This 3D stacking can be used to add polymer features to a substrate, or to print different polymers onto each other. Drug release systems can be designed using two polymers with differing degradation times. Combining sequential stack printing with other fabrication techniques can lead to 3D metal/polymer assemblies. Techniques such as this one could be vital in assembling advanced conduits, allowing each element to be produced on independent stamps.

2.4.7 Transfer Printing

Transferring a patterned metal film from a master, at temperature and pressure, onto a polymer substrate, is often employed when the substrate is not compatible with traditional metal patterning techniques, i.e. lithography, lift-off and/or wet etching. Transfer printing is achieved through the use of a weak-adhesion interface on the stamp. When the stamp is removed from the substrate after a printing step, the weak-adhesion zone is the point of separation, leaving metal on the substrate. Many variations of transfer printing exist and these are often tailored to the choice of polymer and metal. Some metals are easier to print onto substrates and require less pressure e.g. reactive metals like Ti and Al readily adhere to substrates.

A flexible polymer may be spun onto a rigid substrate prior to transfer printing. This ensures the stamp can be brought into good conformal contact with the polymer. Using a release layer between stamp and metal, adhesion energy differences within the stamp/substrate stack cause the metal to transfer to the polymer, providing the pressure and temperature is sufficient [79-81]. Alternatively a bi-layer polymer stamp, with weak-adhesion energy between the two polymer layers, can be used to facilitate pattern transfer to the substrate [82].
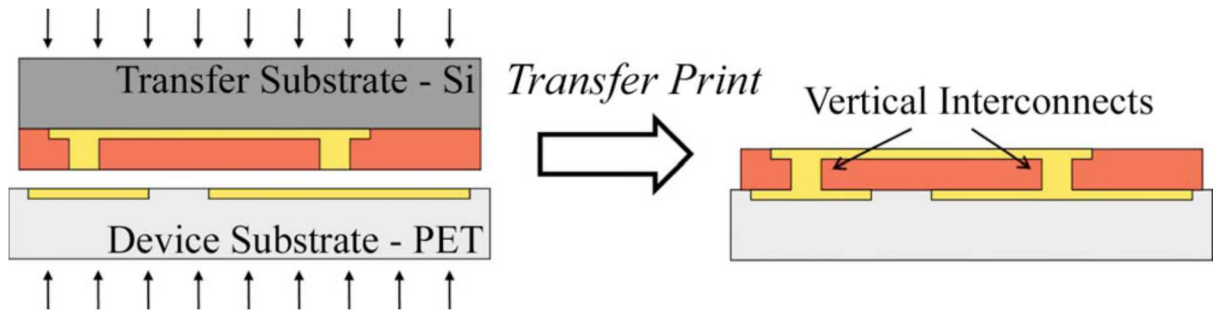
Figure 2.7 a schematic showing the simultaneous printing of a dielectric layer and metal electrodes. (a) the printing stamp, containing electrodes, interconnect and the dielectric is brought into contact with the target substrate. The stamp interconnect makes contact with the electrodes on the device substrate, and after printing and removal of the stamp (b) a two layer structure remains on the device substrate [83].

Metal and dielectrics may be printed simultaneously, as in figure 2.7 [83, 84] or in several sequential printing steps [85] on polyethylene terephthalate (PET) substrates, or on PDMS [86]. Organic transistors and diodes can be fabricated in this way, as well as plasmonic structures. Printing in this fashion could be used to form mechanical guidance cues and electrodes in one or more printing steps. Single printing of multiple materials is advantageous as it avoids multiple heating and pressure steps, which can often deform the previous printing work, particularly under high temperature and pressure conditions.

Careful consideration of the surface chemistry of the stamp and the substrate can increase the quality of the printing process. For example, by coating a stamp in Au/Ti and printing onto PDMS or PET, a TiO_x layer at the interface forms a strong bond, resulting in good pattern transfer [87]. This thin layer of titanium enhances the printing process by acting as a strong adhesion layer (the weakest adhesion interface is within the stamp). Similarly, a self-assembled monolayer (SAM) may be added to a gold covered stamp to act as a 'sticking' layer between metal and substrate. This has been demonstrated on a number of substrates e.g. Si, glass, GaAs and SiO_2/PET shown in figure 2.8 [88].
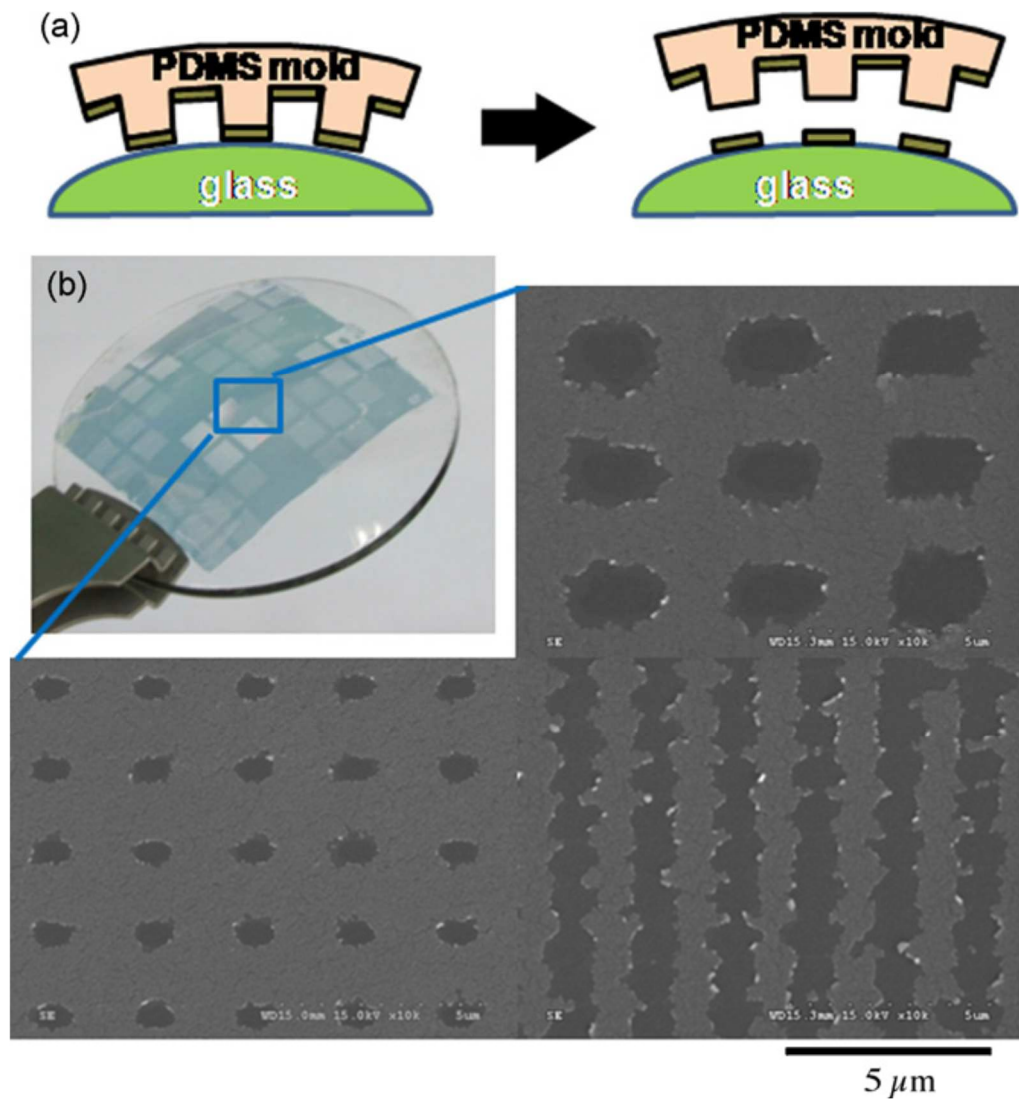
Figure 2.8 a schematic showing the transfer printing process of Au features on a non-planar glass substrate from a PDMS stamp (a) and a photograph and scanning electron micrographs of the nanopatterns produced by the technique [88].

Low-temperature transfer printing, augmented by plasma treatment, may be employed if the target substrate has a low melt-temperature [89]. Using plasma treatment, temperatures as low as 60 °C resulted in pattern transfer. Modification of the surface chemistry has increased the adhesion energy between substrate and stamp. The energy is now strong enough to pull the metal and dielectric stack from the stamp. Printing may also be executed in a subtractive manner, selectively removing metal from a substrate to print a patterned metal film onto a polymer [90].

2.4.8 Electroplating Inductors and 3D Metallisation

The fabrication of complex multi-layer metallic structures incorporated within a polymer may lead to increased levels of complexity and function within the implant. Inspiration and ideas have been drawn from existing technologies, particularly in the electroplating of 3D

inductors [91-94]and transformers [95, 96]. Electroplating of CMOS compatible planar inductors provided good reference material when designing spiral inductors and in particular designs for flexible interconnects and planar inductors [97]. Electroplating of metals on polymers can make them more robust and reduce the resistance of electrodes.

2.4.9 Polymer Microfabrication Summary

There are clearly a number of options available when designing a thin-film polymer microfabrication process. Inkjet printing is a viable option, provided a suitable sintering method can be employed. High-temperature sintering could not be used in this work, as the chosen polymer (polycaprolactone) melts at approximately 60 °C. Laser sintering requires a complex instrumentation set-up and it proved beyond the scope of this project, particularly when compared with the available microfabrication technology in the James Watt Nanofabrication Centre. Electrical sintering of printed features offers a solution for low melt-temperature polymers but this requires large contact areas to every metal node, which impacts upon the possible design in a negative way. Some printers have a resolution of 50 μm at best, which may not be suitable for producing inductors with dense turns-ratios.

Nano-imprant lithography is an excellent technique but is unsuitable for this work due to the incompatibility of PCL with the wet-etching and lift-off techniques that are subsequently employed with NIL. Cold-welding of metals requires an initial seed layer of metal. The weak mechanical properties of thin-film PCL render this technique as impractical.

Hot embossing and nano-moulding are techniques that are perfectly suited to PCL *because* of its weak mechanical and temperature properties. It is envisaged that in future iterations of the PCL construct produced in chapter 5, embossing and moulding could facilitate micro and nanopatterning of the conduit to produce micro-pores for nutrient diffusion into the injury site and microchannels for improved mechanical guidance and control. 3D stacking and printing techniques offer further variations in processing if the PCL substrate should be patterned in any way. This has proved beyond the scope and requirements of this thesis.

Sacrificial layers could not have been employed here as the baking of the sacrificial layer would melt the PCL substrate. Metal sacrificial layers similarly could not be applied due to the wet-etching step which would destroy the polymer substrate.

Transfer printing has proven to be the best processing option for PCL. Producing patterned metal films on a stamp allows standard microfabrication techniques to be employed prior

to printing. A novel variation of this technique has been developed (described in chapter 5) to produce patterned metal films on PCL. Surface chemistry alterations were used successfully, but were not required in the final process.

2.5   Electric Cell Impedance Sensing

Peripheral nerve repair takes place over many months with little or no feedback available to monitor the progress of an operation. Electric cell impedance sensing (ECIS) techniques may provide a route to quantifying how a repair is progressing, allowing medical staff to intervene if progress is slow. This could also help to improve subsequent future peripheral nerve repair operations. Developing a technique like this for use within a wireless conduit could provide the means to chart cell growth over-time. A description of some of the applications and methods of ECIS sensing is now provided.

2.5.1   Electrical Cell Impedance Sensing

ECIS is now a commercial technique used to measure the impedance of the cell-substrate interface *in vitro* [98, 99]. As cells grow, their contact area with the substrate alters. These changes in morphology, if happening on the surface of an electrode, result in changes in electrical impedance. Measuring this impedance can indicate at what stage of cell-growth the cells are in, as well as other indicators, for example ECIS can be used to detect cell death events in response to toxic agents [100-102]. This is of particular interest for nerve repair applications if the nerve conduit is compressing the cells, causing cell death. If this could be monitored wirelessly, surgery could be scheduled to replace the conduit with a larger version, avoiding the compression of the cells. Electrical impedance measurements can be used to determine what type of tissue is surrounding an electrode [103]. In this way, the position of a needle can be adjusted to ensure the correct tissue type is surrounding the tip. This could be of great use during a nerve repair procedure, indicating what types of cells are present at certain locations over time.
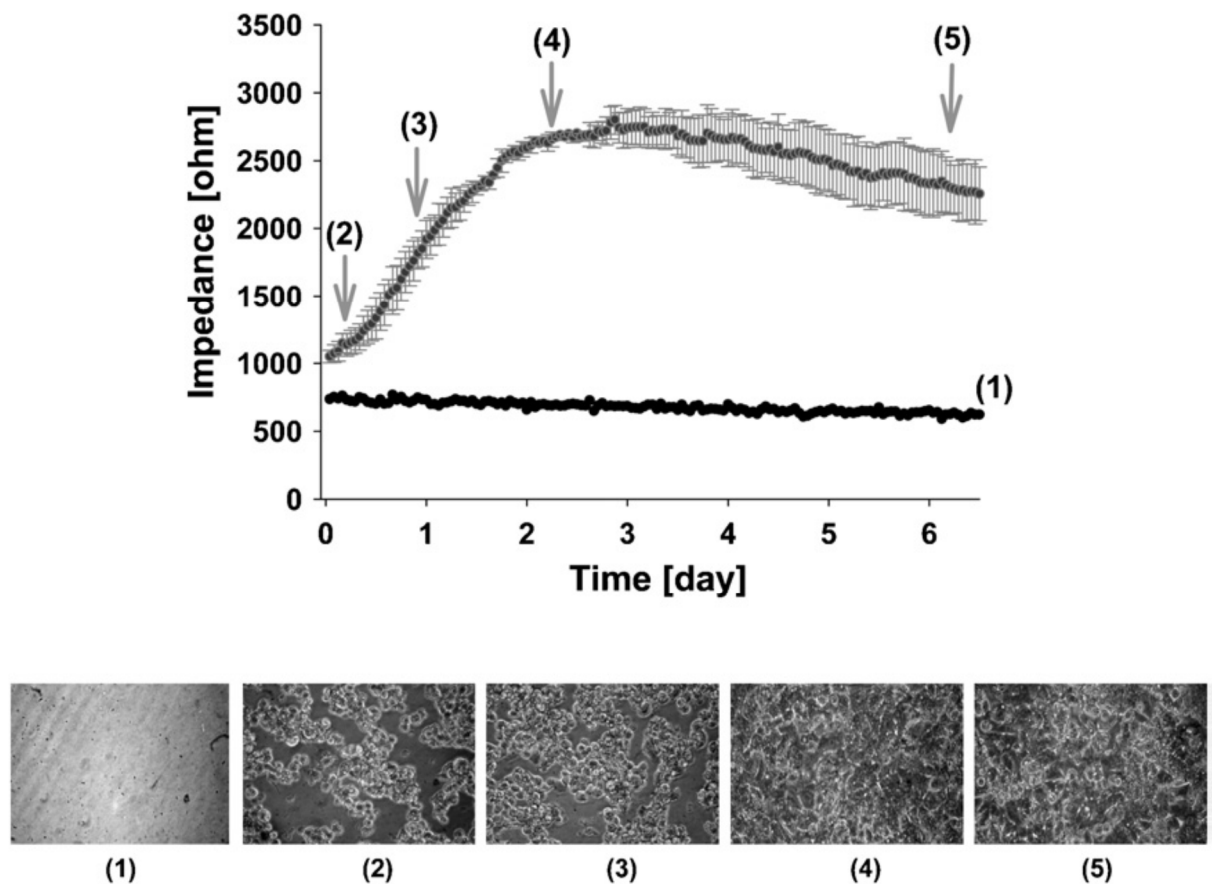
Figure 2.9 changes in electrical impedance in response to different growth phases of HepG2 cells. Data is displayed as the mean impedance and the standard deviation. The phases are described as (1) medium, (2) lag, (3) exponential, (4) stationary, and (5) cell death [100].

2.5.2 Cell Sensing System Design

When designing impedance sensing systems, and in particular when selecting operating frequencies and voltages, good reference material is available showing the electrical response for culture medium and saline across a number of parameters [104]. In addition, the variation of electrical parameters with salt concentration and electrode material has been documented, aiding the design of impedance based measurement systems [105]. Some authors have used current-pulses to calculate one electrical parameter, that of the electrochemical capacitance [106]. Techniques such as these often require dedicated apparatus and specialised instrumentation. Systems capable of inclusion in a conduit would be of great use in many applications. A method of replicating some of the results outlined above, and sent to a cuff circuit worn by a patient would allow real-time monitoring of some injuries as they recover. In addition, the development of a biodegradable impedance measurement system to achieve this would offer the benefit of *in vivo* functionality with all the benefits of biodegradable conduit systems.

2.5.3 Electric Cell Impedance Sensing Summary

Commonly employed with instrumentation, ECIS quantifies cell/substrate impedance information through changes in electrical activity. In order to be implemented as part of a biodegradable implant, a simpler implementation is sought here. To achieve this aim, instrumentation will be used to quantify expected cell behaviour, followed by experimentation with minimalistic electronic circuits designed to be capable of implantation on a biodegradable construct.

2.6 Summary

This chapter has described the four topics that form the foundation of this project: peripheral nerve repair strategies; wireless power and data transmission; microfabrication techniques for flexible polymer electronics; and electrical cell impedance measurements. From studies in the literature it is clear that peripheral nerve repair remains a challenging operation characterised by poor functional recovery. Application of electric fields during a repair, as part of an advanced conduit design, offers much promise in aligning and increasing the rate of repair, towards improving functional outcomes for patients. An outline of inductive powering systems and microfabrication techniques associated with thin-film polymers has sought to explain how such systems could be implemented in a conduit repair. Finally a brief explanation of some contemporary approaches to cell impedance sensing has been provided to show how feedback could be included during a repair to improve outcomes.

3   Electromagnetic Theory

This chapter outlines the electrical and magnetic theory required to design inductively powered biomedical systems. An overview of magnetic field principles is followed by a comprehensive introduction to inductors and their use as electrical transformers. Finally, the inductive powering subsystems and theory are described in detail. It is the aim of this section to provide the reader with an insight into the design of the electrical systems used to apply electric fields to neurons. The work in this project is differentiated from contemporary literature in the use of precise electric field control using microelectrodes. This is in contrast to the common approach involving two large electrodes applied to a conduit repair. The success of this approach relies on an understanding of the concepts outlined below to ensure signal integrity and realistic system performance.

3.1   Principles of Magnetic Fields

3.1.1   Parallel current carrying wires

Ampere's law can be used to analyse the magnetic flux density when a number of conductors are placed in close proximity; important when analysing inductors. Consider the case of two parallel wires, carrying current in opposite directions, as in power delivery cables, shown in figure 3.1.
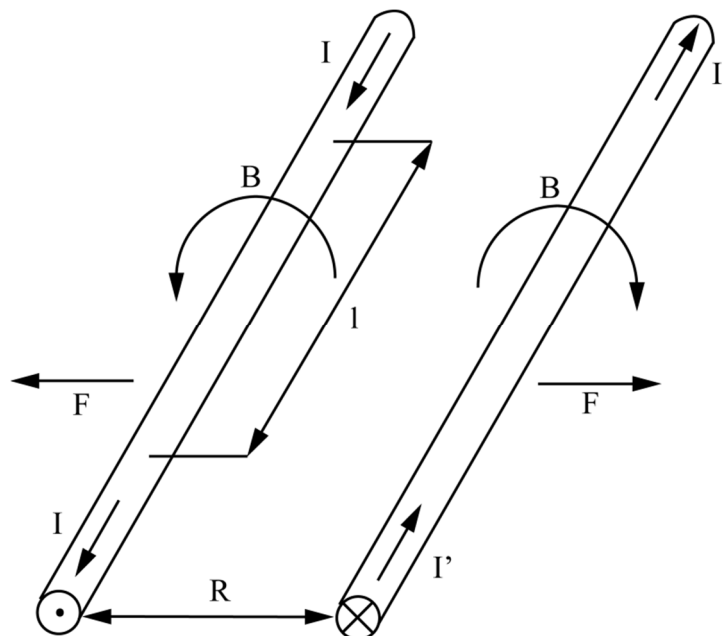
Figure 3.1 magnetic flux density from two parallel current carrying wires in close proximity [107].

Where **B** is the magnetic flux density, F is the force acting on the conductors, I is the current flowing, R is the separation distance and l is a portion of the length of conductor.

Ampere's law is used in figure 3.1 to show how the magnetic flux sums in the gap between the wires, and cancels in the outer regions. Wires carrying power to a circuit are often twisted together, to eliminate the inner magnetic flux density. If the currents flow in the same direction, the opposite effect can be observed. This is the case in inductors; often an inductor will have a strong magnetic field in the centre, caused by the summation of many current carrying wire elements.

3.1.2 The Biot-Savart Law

The Biot-Savart Law describes the magnetic field at a fixed point from a conductor. It can be used, for example, to calculate the magnetic flux density at a point within a solenoid inductor.
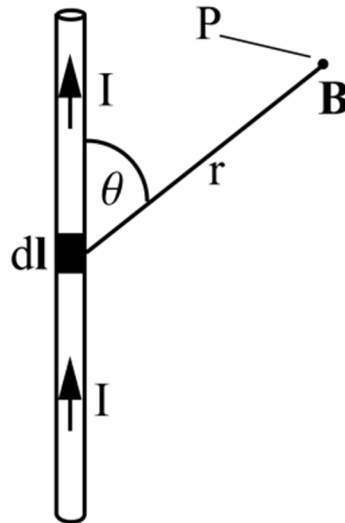
Figure 3.2 the magnetic flux density at a fixed point, P, from a current carrying wire [107].

From the Biot-Savart law, the magnetic field at a fixed point, P from a current flowing in a conductor can be found. Consider a current flowing in an infinitesimal section of length, dl, of a current carrying wire as shown in figure 3.2.

$$d\boldsymbol{B} = \frac{\mu_0 i dl \sin \theta}{4 \pi r^2} \quad (3.1)$$

Where r is the distance to the point, P at an angle θ to the conductor and μ_0 represents the permeability of free space. This relationship is of great use in evaluating a number of complex wire layouts and in calculating inductance values. Inductors typically consist of many loops of wire, hence calculating the magnetic flux density at a distance from a single coil of wire is a fundamental step prior to analysing multiple loops.
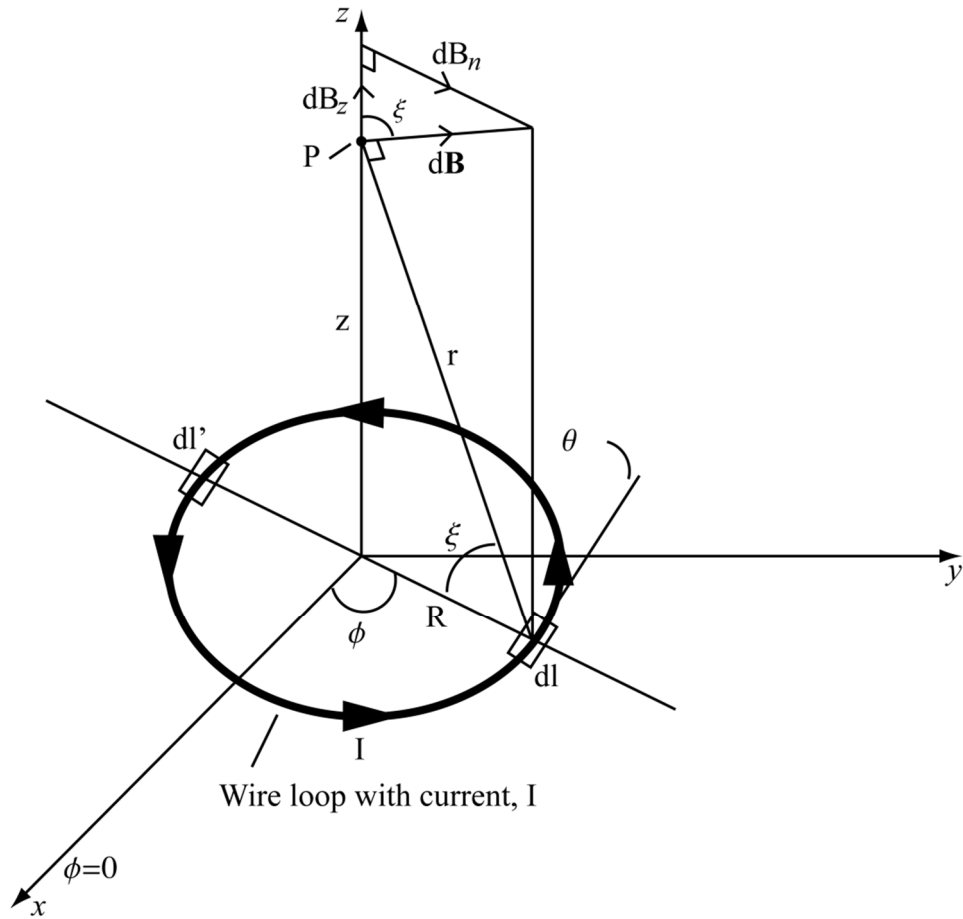
Figure 3.3 the magnetic flux density, B, at a fixed point from a current carrying loop of wire: an

example calculation using the Biot-Savart law [107].

Consider figure 3.3, showing a single loop of wire with a current, I, flowing. At a fixed point, P, from this wire the Biot-Savart law can be integrated to calculate the net magnetic flux density.

$$dB = \frac{\mu_0 I d\mathbf{l} \sin \theta}{4\pi r^2} \tag{3.2}$$

The component of the vector d**B** normal to the z-axis can be written

$$dB_z = d\mathbf{B} \cos \xi = d\mathbf{B} \frac{R}{r} \tag{3.3}$$

Noting from figure 4 that: $\theta = 90°, dl = Rd\phi$ and $r = \sqrt{R^2+z^2}$

$$dB_z = \frac{\mu_0 I R^2}{4\pi (R^2 + z^2)^{3/2}} d\phi \tag{3.4}$$

The net magnetic flux density in the z direction is the integral of this equation around the loop. The normal components cancel leaving the z component as the only remaining flux

$$\boldsymbol{B} = B_z = \frac{\mu_0 I R^2}{4\pi (R^2 + z^2)^{3/2}} \int_0^{2\pi} d\phi = \frac{\mu_0 I R^2}{2(R^2 + z^2)^{3/2}} \tag{3.5}$$

The magnetic field at the centre of the loop, i.e. when z=0, is

$$B = \frac{\mu_0 I}{2R} \tag{3.6}$$

3.1.3 Magnetic Field in the Centre of a Solenoid

The Biot-Savart law can now applied to the solenoid inductor, i.e. a problem with multiple loops of wire. The solenoid is a widely-used inductor type, comprising a long wire wrapped many times around a cylindrical core material. The solenoid is an inductor geometry used in a wide variety of applications due to its ability to generate strong, uniform magnetic flux densities with relatively low currents.
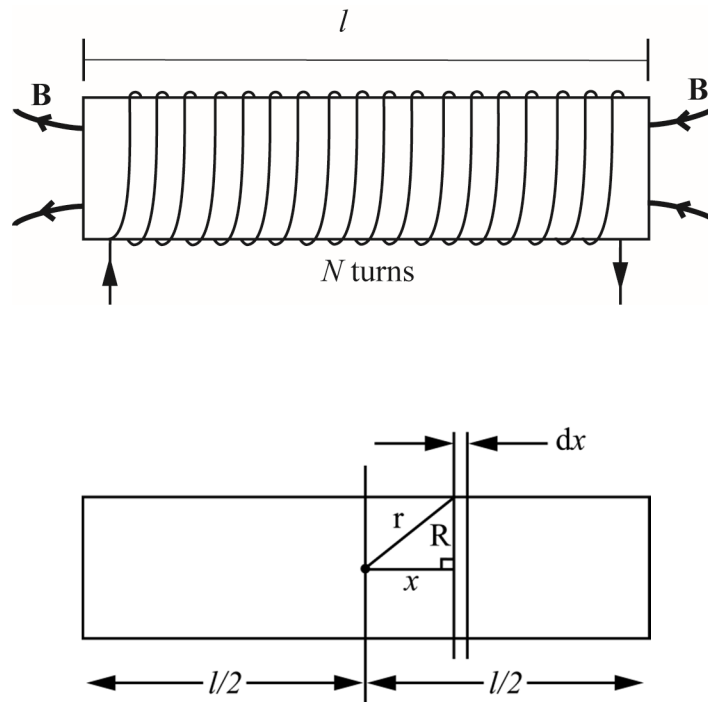
Figure 3.4 a schematic of a long solenoid and its Biot-Savart diagram [107].

For a solenoid with cross-sectional area, A, length, l, inner radius, R and number of turns, N; integration of the Biot-Savart law yields the magnetic field in the z direction as shown in figure 3.4

$$B_z = \frac{\mu_0 I R^2}{(2R + z^2)^{\frac{3}{2}}} \tag{3.7}$$

and integrating along the length

$$B_z = \frac{\mu_0 N I}{\sqrt{l^2 + 4R^2}} \tag{3.8}$$

which, for long solenoids (l>>R) reduces to

$$B = \frac{\mu_0 N I}{l} \tag{3.9}$$

Hence, for solenoid inductors, a large turns-density will yield an increase in the magnetic flux density.

3.1.4 Magnetic Flux

It has been shown how magnetic fields can be calculated at a distance from a wire or loop. It is often convenient to use the magnetic flux, ϕ, passing through an area, A, in electromagnetic design problems

$$\phi = \oiint \boldsymbol{B}.d\boldsymbol{A} \tag{3.10}$$

The magnetic flux ϕ is measured in Webers (Wb). One Weber per square metre is equal to one Tesla. The vector d$\boldsymbol{A}$ represents an infinitesimal part of the total area, perpendicular to the surface.
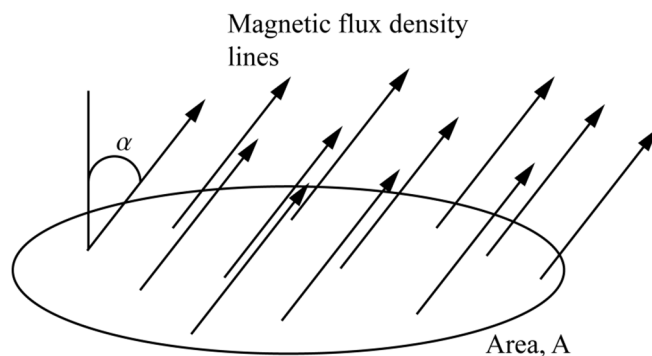
Figure 3.5 uniform magnetic flux density passing through a surface area, A, at an angle, α [107].

For a constant magnetic flux density, as in figure 3.5, the magnetic flux reduces to

$$\phi = BA \cos \alpha \tag{3.11}$$

The above equation reduces to the product, BA, for perpendicular magnetic fields passing through a cross-sectional area.

3.2 Inductance

Some fundamental laws illustrating the direction and value of magnetic flux, flux density and intensity have been described. The following section will apply these laws to inductors, and show how inductors can be used as electrical transformers. In general, an inductor is an electrical component that stores energy in a magnetic field when a current is flowing through them. Inductors are defined by their ratio of magnetic flux to their net current flow

$$L = \frac{N\phi}{I} \tag{3.12}$$

Where L is the inductance in henries (H), N is the number of turns, ϕ is the magnetic flux and I the current flowing through the inductor.

3.2.1 Inductor Core Material

A ferromagnetic material may be used as the core of an inductor, to increase the inductance per unit area. However for biomedical implants it is impossible to implant a ferromagnetic core unless the implant is encapsulated in a biocompatible material, such as silicone. For this reason air-core coils are used those implants that do not use encapsulation, particularly for biodegradable systems. There are no biocompatible materials that improve the value of permeability. For this reason, throughout this chapter any inductors will be analysed as air-core components and thus the permeability will be that of free space.

3.2.2 Inductance of a Solenoid

When analysing inductors, which are often made up of many turns, it is more convenient to calculate the flux linkage. In a solenoid design, it is assumed that all the magnetic flux lines link each turn of wire, therefore the total magnetic flux linkage is the number of turns multiplied by the magnetic flux

$$\Lambda = N\phi \tag{3.13}$$

With the flux linkage expressed in Wb-turns. In order to obtain an expression for the inductance, the magnetic flux density must first be calculated. It is assumed that the magnetic flux density is uniform and the flux outside the solenoid is zero. For a long

solenoid with length, l much larger than the radius, R, and using the expression for the magnetic flux density within a solenoid, the inductance becomes

$$L = \frac{NBA}{I} = \frac{N^2 A \mu_0}{l}$$

(3.14)

The magnetic flux density has been assumed to be entirely in the z direction, perpendicular to the cross-sectional area, A. An important observation is that the inductance varies with the square of the number of turns. Therefore if a large inductance is required for a given design, a higher turns-density should be used, particularly when space is at a premium.

3.2.3 Inductance of a spiral inductor

The spiral inductor is widely used in MEMS and CMOS systems as it can be produced on a single metal-layer (with a second layer used to gain access to the centre connection) with rectangular tracks. Other types of inductor could not be practically implemented on CMOS ICs. Microfabrication of spiral inductors can be accomplished using lithography with precise control over the dimensions; particularly the width of the tracks and the space between them. Spiral inductors have a great advantage over meander and zig-zag geometries in that their tracks have positive mutual inductance (the current in each track flows in the same direction to its neighbouring tack). Meander and zig-zag inductors are useful if one wishes to use only one processing step, as they do not require a via connection, however the inductance per unit area is smaller for these two designs.
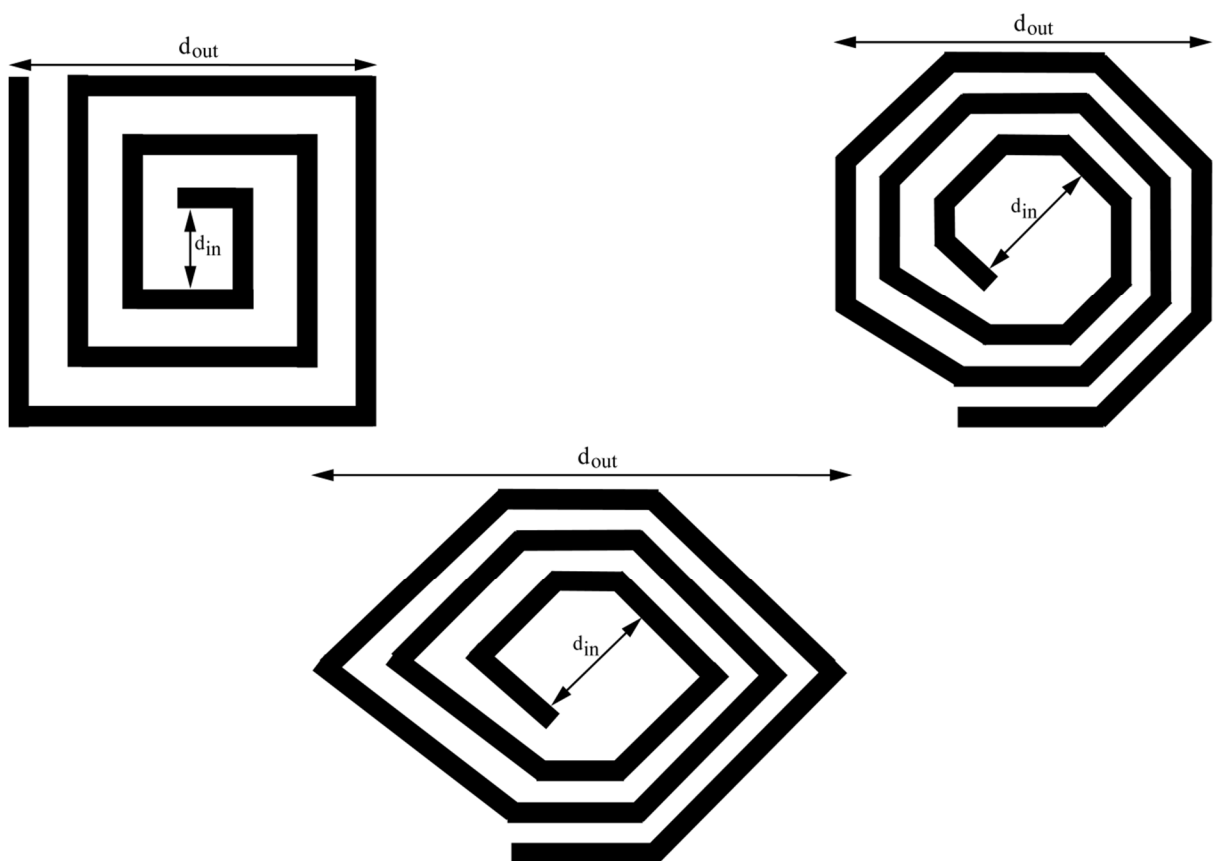
Figure 3.6 (a) square, (b) octagonal and (c) hexagonal spiral inductor designs used when calculating the theoretical value of inductance for planar spiral geometries [53].

Some spiral layout options are shown in figure 3.6 (square, hexagonal and octagonal). A modified Wheeler expression was used to obtain an expression for the inductance [53]

$$L = K_1 \mu_0 \frac{N^2 d_{avg}}{1 + K_2 \rho} \tag{3.15}$$

Where the average diameter has been defined as

$$d_{avg} = \frac{d_{out}+d_{in}}{2}$$

(3.16)

And the fill ratio, ρ

$$\rho = \frac{d_{out}-d_{in}}{d_{out}+d_{in}}$$

(3.17)

The parameters K_1 and K_2 are used to modify the inductance for the different geometrical layout options.

Layout	K_1	K_2
Square	2.34	2.75
Hexagonal	2.33	3.82
Octagonal	2.25	3.55

Table 3.1 K parameter values for different spiral layouts [53].

The expression for the inductance can be used to define an appropriate geometry, given a target value of inductance. Alternatively, an indication of the inductance value for given geometric constraints may be obtained. The value can then be adjusted by varying one parameter e.g. the number of turns. Note that the thickness of the inductor has been ignored as it has a negligible effect on the inductance value obtained.

3.2.4 Energy Stored in an Inductor

Inductors and capacitors are energy storage components, unlike resistors which dissipate energy in the form of heat. The energy in an inductor is stored in the magnetic field when a current is flowing through it. The energy stored is proportional to both the inductance and the current

$$E = \frac{1}{2}LI^2$$

(3.18)

Where E is the energy stored, measured in Joules (J).

The quality factor of an inductor provides a measure of how much energy is lost each cycle due to resistive losses. An inductor with a higher quality factor will consume less energy per cycle. It can be expressed as

$$Quality\ Factor = \frac{Energy\ Stored\ per\ cycle}{Energy\ dissipated\ per\ cycle} = \frac{\omega L}{R} \tag{3.19}$$

where R is the parasitic resistance of the inductor and ω is the angular frequency, expressed in radians. Hence a good inductor should have minimal resistance. The quality factor influences circuit behaviour in a number of ways. In resonant or oscillating circuits, energy must be provided each cycle to replace that which is lost. Therefore larger quality factors cause an increase in circuit efficiency by reducing power loss.

3.2.5 Self-Resonant Frequency

From the lumped equivalent circuit of an inductor, the self-resonant frequency of the inductor can be calculated using the expression for resonance of a parallel LC circuit

$$\omega_0 = \sqrt{\frac{1}{LC} - \left(\frac{R}{L}\right)^2} \cong \sqrt{\frac{1}{LC}} \tag{3.20}$$

Where ω_0 is the self-resonant frequency, R is the resistance of the inductor and C is the inter-winding capacitance, as shown in figure 3.7. This capacitance is the result of windings placed in close proximity, separated by a dielectric, usually air. In order to reduce the winding capacitance, the separation between the inductor wires can be increased. It is important to calculate the self-resonant frequency as it is undesirable to work at frequencies which are too close to this value. At frequencies approaching the resonant frequency, the impedance of the inductor varies drastically. This has an impact upon practical circuits where variations in the inter-winding capacitance can have a large influence over the impedance of the inductor. The frequency of operation should therefore be at least a decade below the self-resonance frequency to avoid large discrepancies between predicted and practical circuit performance.
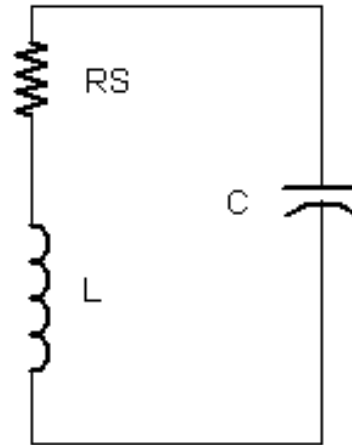
Figure 3.7 the lumped equivalent model for an air-core inductor, showing the resistance of the inductor and the inter-winding capacitance.

3.2.6 Faraday's Law

In order to analyse electrical transformers and inductive powering systems, it is necessary to understand the method of inducing current and voltage in an inductor. Faraday's law of induction states that an alternating magnetic field passing through a loop shaped conductor will induce an electromotive force (EMF) in that conductor.

$$\oint \boldsymbol{E}.d\boldsymbol{l} = -\frac{d\phi}{dt} \tag{3.21}$$

Where **E** is the electric field and d**l** is an infinitesimal line segment of the conductor. The integral of each induced electric field element around the loop will yield a voltage difference between both ends of the loop. Typically an alternating current is used to produce an alternating magnetic field, resulting in an induced emf in the loop. This effect is widely used in electrical transformers. Using Faraday's law of induction, the voltage across an inductor may be found. The magnetic flux through a loop shaped conductor is

$$\phi = Li \tag{3.22}$$

And therefore, the voltage across the inductor is

$$\oint \boldsymbol{E}.d\boldsymbol{l} = \frac{d\phi}{dt} \tag{3.23}$$

$$v = L\frac{di(t)}{dt} \qquad (3.24)$$

Where v is the voltage across the terminals of the inductor. Thus, a change in current through an inductor will cause a voltage difference between the terminals, proportional to the rate of change and the constant, L, the inductance value. In the frequency domain

$$\frac{d}{dt} = j\omega \qquad (3.25)$$

$$v = j\omega LI \qquad (3.26)$$

Lenz's Law states that if the ends of the looped conductor were to be connected, the current would produce a magnetic field that opposes the original changes in magnetic field. This is important when considering the polarity of induced voltages within a transformer system.

3.2.7 Mutual Inductance
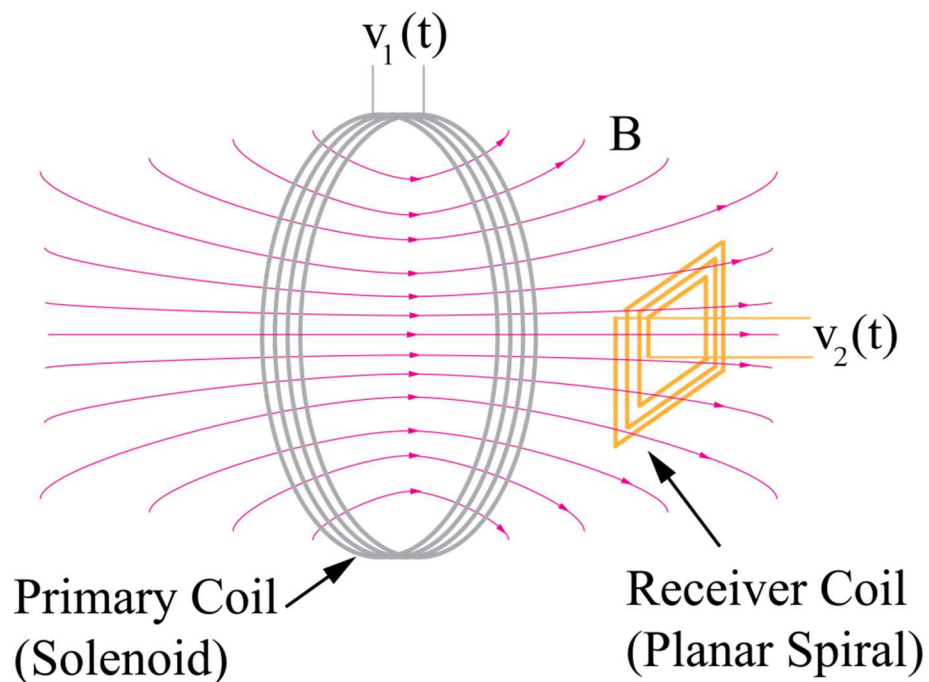
Figure 3.8 use of a large solenoid to power a small, planar spiral receiver inductively.

If two inductors are placed in close proximity to each other, one coil can be used to induce a voltage in the other, as shown in figure 3.8. An alternating current in the 'primary' coil produces an alternating magnetic flux which links to the second inductor, the 'receiver' coil. This alternating flux in turn induces a voltage in the receiver inductor in accordance with Faraday's law.

$$v_2(t) = N_2 \frac{d\phi(t)}{dt} \tag{3.27}$$

Where N_2 is the number of turns in the receiver inductor, and v_2 is the induced voltage between the terminals of the receiver inductor, shown in figure 3.9.
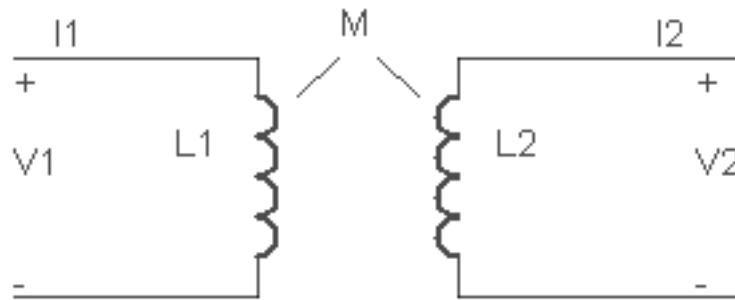
Figure 3.9 circuit schematic depicting two mutually coupled inductors.

Since the magnetic flux is linearly proportional to the current in the primary inductor

$$v_2(t) \propto N_2 \frac{di_1(t)}{dt} \tag{3.28}$$

$$v_2(t) = M_{12} \frac{di_1(t)}{dt} \tag{3.29}$$

M_{12} represents the mutual inductance between the two inductors; the subscript is used to indicate which two inductors in any system are being used for the calculation (note also that $M_{12} = M_{21}$). Many factors influence the value of mutual inductance between two coils, such as the geometry of the coils, the number of turns, the separation distance, angle and displacement, and the properties of any materials in their vicinity. Any materials with high permeability will have a significant effect. For the case of two mutually coupled inductors, the self and mutual inductances both contribute to the voltage. The voltage across an inductor is thus composed of a term dependant on the current flowing through it, and a term caused by alternating currents in any mutually coupled coils. For two mutually coupled coils, the voltage across each inductor is

$$v_1(t) = L_1 \frac{di_1(t)}{dt} + M \frac{di_2(t)}{dt} \tag{3.30}$$

$$v_2(t) = L_2 \frac{di_2(t)}{dt} + M \frac{di_1(t)}{dt} \tag{3.31}$$

3.2.8 The Transformer
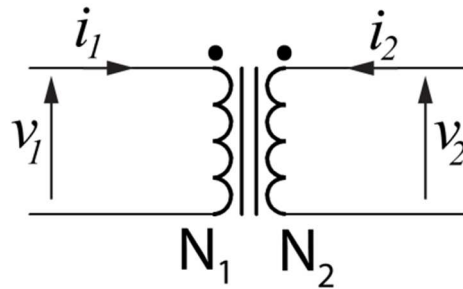
Figure 3.10 the ideal transformer.

If two inductors are wound around a magnetic core material, the magnetic flux from the primary coil can be assumed to link completely with the secondary coil, forming an ideal transformer, shown in schematic form in figure 3.10. Transformers are so named due to their ability to step-up or step-down voltage and currents. The relationship between the primary and secondary power in an ideal transformer is

$$V_1 I_1 = V_2 I_2 \tag{3.32}$$

It can be shown that

$$\frac{V_1}{V_2} = \frac{N_1}{N_2} = \frac{I_2}{I_1} \tag{3.33}$$

i.e. if the voltage is increased at the secondary, the secondary current decreases. Thus the power at the primary is equal to the power at the secondary, for an ideal transformer. Practical transformers typically operate with some losses due to flux leakage, eddy currents in the core, or resistive losses in the windings.

3.3 Wireless Power Transfer Systems

There are a number of different topologies available when considering how best to transfer power and data wirelessly. In biomedical applications the problem faced is how to couple power through the skin, often to an implant buried deep within the patient, at distances on the order of 10-100 mm. In a peripheral nerve repair operation, the distance to the implant

depends on the location and type of injury suffered. Therefore, the chosen power delivery system should be capable of meeting the specifications for this range of separation distances.

3.3.1 Ultrasonic Links

Ultrasonic waves are acoustic signals that have a frequency in excess of 20 kHz. These waves can be used to send signals wirelessly, particularly inside the body where the liquid environment ensures the signal can propagate effectively. They are commonly used to monitor the health of unborn babies in the womb. Overcoming the skin barrier is achieved with a layer of gel. Some researchers have overcome the skin barrier with a pair of inductors (inductive powering); the received power is then sent to an ultrasound transducer to transmit up to 70 mm inside the body [108]. This is an excellent example of combining the merits of inductive powering (short distance, subcuteaneous) with the benefits of ultrasound (excellent and long transmission inside the body). The group were able to couple 29 µW of power at a total distance of 80 mm. Techniques like this can help to reach deep injury or implant sites.

3.3.2 Near-Field Versus Far-Field

At separation distances much smaller than the wavelength of the electrical signal, near-field analysis dominates. In inductive powering, it is the near-field case. The far field case applies at distances much larger than a wavelength from the conductor. This is the case of radiating fields. Inductive powering is advantageous in that the receiver can be much smaller, providing one wishes to operate at a small separation distance (on the order of 10 – 50 mm). At higher frequencies, using a far-field mode of transmission, large eddy-currents would be induced around the receiver antenna inside the body. The practical working range for medical implants, 0.1 – 10 MHz, excludes far-field modes of operation, assuming the receiver space is minimal [109].

3.4 Inductive Powering: Design Theory

Inductive powering is used in a number of applications, from heavy industry as an isolation mechanism, to micropowered implants for biomedical devices. As this project is concerned with bio-implantable electronics, the case of low-power, loosely coupled systems will be outlined. These systems can be thought of as a primary circuit driving a non-ideal transformer connected to a receiver circuit. In the case of biomedical systems, the primary coil is outside the body and the secondary is implanted inside. The characteristics of a biomedical implant powered inductively, in terms of transformer behaviour, are:

- The efficiency of practical power transformers are on the order of 90% and above. Inductive powering systems for biomedical devices can operate with efficiencies below 1%. This is largely dependent on the distance between the transmitter and receiver.

- Practical transformers use a ferrous core material, and are tightly wound concentrically. In biomedical systems both coils are co-planar and separated by a finite distance, on the order of a few millimetres or more. As a biodegradable device is sought here, ferrous materials have been excluded from the receiver design.

- Parasitic effects, particularly in the receiver, must be taken into account. The parasitic resistance and capacitance of the receiver impacts on the efficiency, selectivity and the choice of transmission frequency.

- Biomedical devices should be made relatively insensitive to variations in position of the coils. This often translates into physically large primary coils driving small receiver coils, further reducing the coupling between them.

These factors all serve to reduce the efficiency and the magnetic coupling of wirelessly powered circuits used for biomedical implants. An outline of some of the design considerations required for inductively powered implants is provided in the following sub-sections.

3.4.1 Design Problem

A schematic illustration of the design problem is shown in figure 3.11. A transmitter inductor housed within a cuff worn by the patient, should send power and data to a receiver inductor. The receiver inductor, fabricated on a biodegradable conduit, connects this received power and data to suitable circuitry to extract the data. The electrical stimulation signal is then sent to microelectrodes with the aim of enhancing peripheral nerve repair.
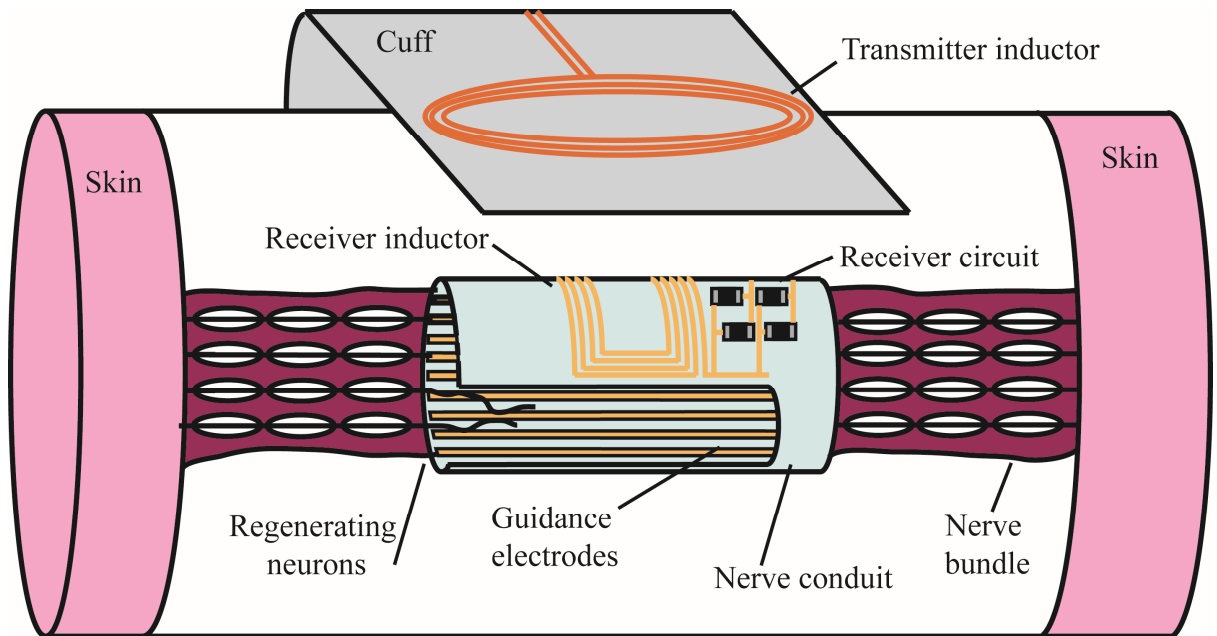
Figure 3.11 schematic illustrating the proposed topology for a functionalised, biodegradable conduit powered through a wireless link. A transmitter circuit worn as an external cuff by the patient is used to couple power and data into the receiver circuit, built on polycaprolactone. The receiver circuit converts the amplitude modulated carrier signal into an electrical stimulation signal, capable of influencing the growth of regenerating neurons. At the end of the repair the conduit will degrade, eliminating the need for a second surgical procedure.

3.4.2   Coupling Factor

The coupling factor is a measure of how much of the flux generated by one coil, links to the second coil; often expressed as a percentage. The flux that does not link to the secondary coil is wasted, i.e. it represents a power loss in the electronic system.

$$k = \frac{M}{\sqrt{L_1 L_2}} * 100\% \qquad (3.34)$$

Where k is the coupling factor; for an ideal transformer, k = 100%. A higher coupling factor represents an increase in efficiency, as less power is required for a given induced voltage in the receiver. A low coupling factor (i.e. biomedical systems) requires a large alternating primary current to generate enough magnetic flux to induce a sufficient voltage at the receiver. Therefore the majority of the energy in the system is consumed in the inductive link as wasted magnetic flux that does not link to the receiver inductor. Figure 3.12 shows how the current flowing in a transmitter inductor can set up a region of relatively constant magnetic flux density around a receiver inductor. The simulation was

performed with Opera (Vector Fields, Cobham Technical Services, UK) using the magnetostatic option. A current of 2 mA was used for the transmitter current. Ideal conductors were used to model an inductor. An air region surrounding both inductors was sufficient to illustrate the spread of the magnetic flux density. Simulations like these can greatly assist in determining the value of coupling factor and in design optimisation.

Map contours: BMOD

- 1.588737E-006
- 1.400000E-006
- 1.200000E-006
- 1.000000E-006
- 8.000000E-007
- 6.000000E-007
- 3.952494E-007

Transmitter inductor: worn as a cuff

Receiver inductor, curved around a nerve conduit
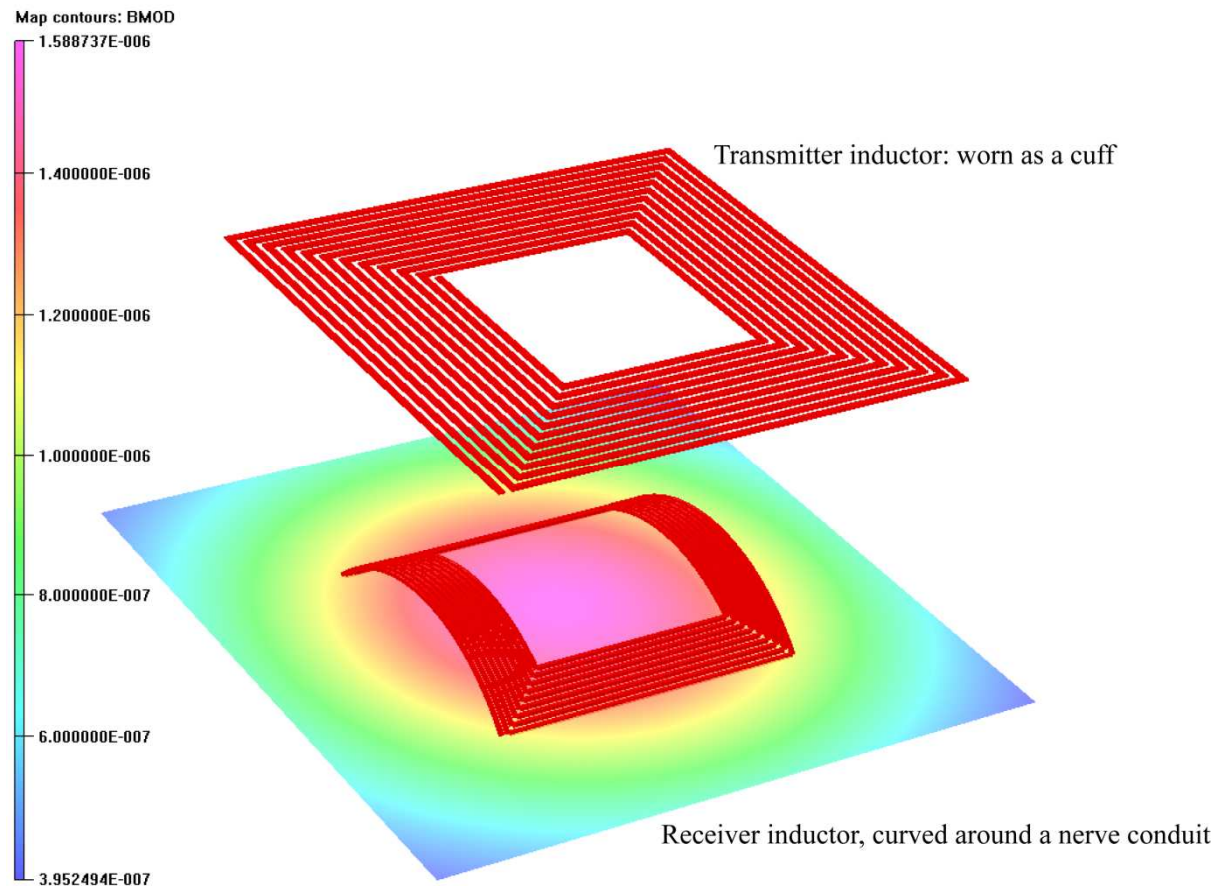
Figure 3.12 current flowing in a transmitter inductor produces a magnetic flux density around the receiver inductor. It is desirable to have a region of near-uniform flux enveloping the receiver.

Since a higher coupling factor is often sought, it is useful to know how to achieve the optimum coupling for a pair of inductors. An expression for the maximum coupling has been derived for a pair of coils, with diameters d_1 and d_2, separated by a distance, D, illustrated by figure 3.13 [39]

$$d_1 = \sqrt{(d_2^2 + 4D^2)}$$

(3.35)
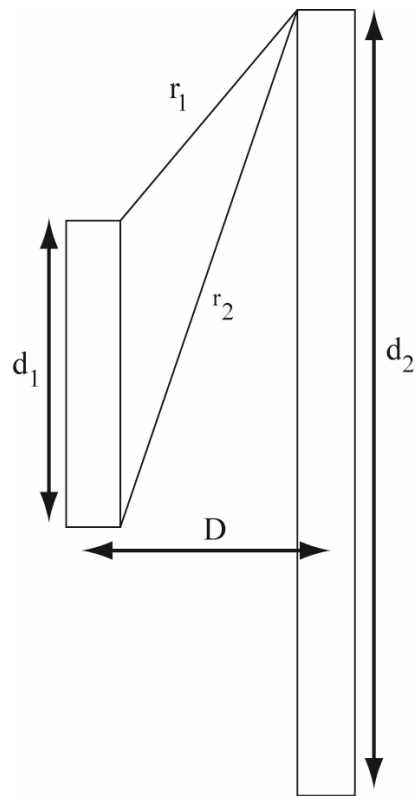
Figure 3.13 coupling factor optimisation between two co-planar inductors [39].

Hence for a given receiver diameter and separation distance, the transmitter diameter can be calculated to ensure maximum coupling is achieved.

3.4.3 Equivalent Inductive Link Circuits

The design of loosely coupled systems can be simplified using equivalent circuits with ideal transformers, or with representative induced voltage or current sources, like those shown in figure 3.14 [110]. These circuits are useful in analysing the primary and secondary circuit together, and in simulating these circuits. This figure represents a non-ideal transformer a a T-model, an ideal transformer with leakage terms, a model with current sources and finally a model comprising voltage sources. The latter model is of most use as it is often easier to work in induced voltages and measured transmitter voltages.
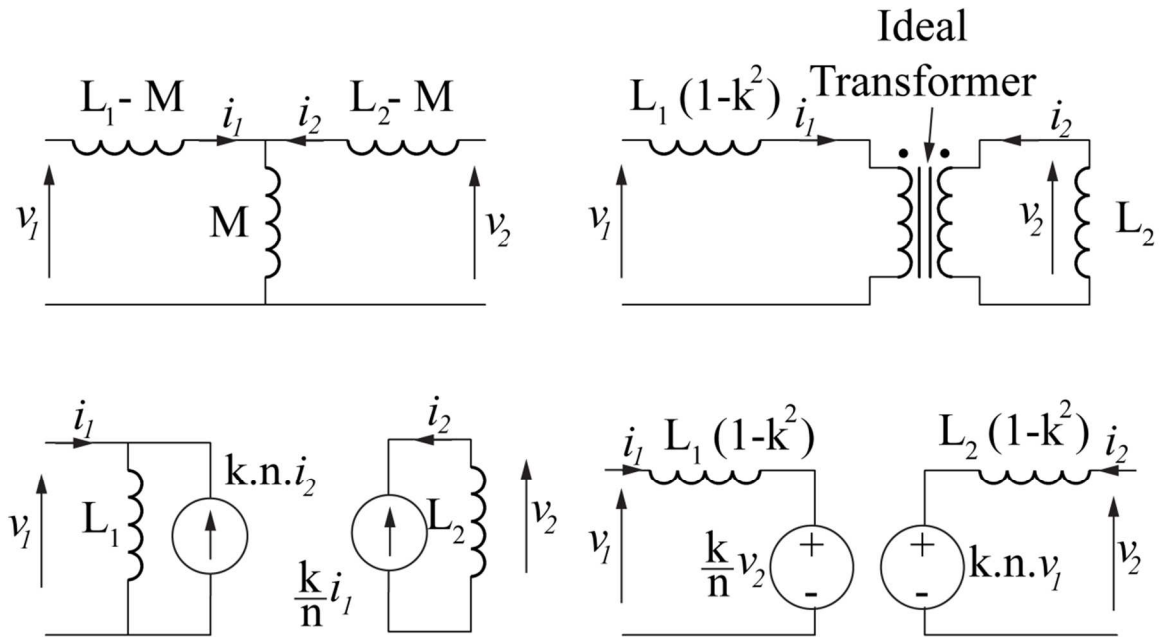
Figure 3.14 equivalent circuit representations of two loosely coupled inductors [110].

The square root of the ratio of the inductors, n, is defined as

$$n = \sqrt{\frac{L_1}{L_2}}$$

(3.36)

3.4.4 Induced voltage in a loosely coupled system

Biomedical implants often require a known value of supply voltage, dependant on what their function is to be, and what components and stimulation signals are required. It is therefore important to know what parameters determine the induced voltage in the receiver. In the case of two coupled inductors driving a nominal load, first assume that the primary current, i_1 is purely sinusoidal and is of the form

$$i_1(t) = \hat{I}_1 \sin(\omega t + \theta)$$

(3.37)

Where i_1 is the transmitter current, $\hat{I}_1$ is the peak transmitter current, ω is the angular frequency in radians^{-1} and θ is the phase angle. Recall that the induced voltage at the secondary is written

$$v_2(t) = M \frac{di_1(t)}{dt}$$

(3.38)

and differentiating i_1

$$v_2(t) = M\hat{I}_1\omega\cos(\omega t + \theta) \tag{3.39}$$

It is useful to express the induced voltage in terms of the peak voltage

$$\hat{V}_2 = M\hat{I}_1\omega = 2\pi f M\hat{I}_1 \tag{3.40}$$

where f is the frequency in Hertz. Finally it can be more convenient to use the coupling factor in place of mutual inductance

$$\hat{V}_2 = 2\pi f \hat{I}_1 k \sqrt{L_1 L_2} \tag{3.41}$$

The induced voltage is directly proportional to the frequency, coupling, inductor values and the primary current. N.B. that increasing L_1 or L_2 may cause the coupling to decrease in some cases. It is therefore better to design the two inductors and maximise their coupling for a fixed distance, before varying the other parameters to achieve the desired induced voltage. These expressions are useful in analysing the effect that a single parameter will have on the induced voltage in the receiver.

3.5 Circuits and Systems of Inductive Powering

The final section of this chapter describes some of the circuit elements used when designing wirelessly powered implants. Receiver circuit elements convert received signals into useful waveforms to be used in the target application, such as stimulation waveforms or cell sensing. Circuits within the transmitter are responsible for supplying large alternating currents to the primary inductor to send power and data to the receiver. They may also be responsible for receiving data from the implant and data logging if required.

3.5.1 LC Tank Resonator
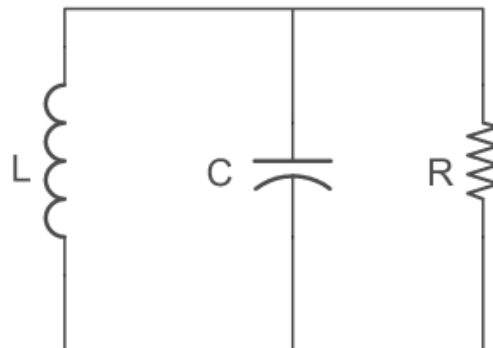
Figure 3.15 a parallel LC tank circuit with a load resistor, R.

A parallel resonant circuit consists of an inductor, a capacitor and a (load) resistor as shown in figure 3.15. Using the admittance of the circuit

$$\frac{1}{Z} = \frac{1}{j\omega L} + j\omega C + R \tag{3.42}$$

The circuit is said to be resonant when the impedance of the inductor is equal to that of the capacitor. It can be shown that the resonant frequency is

$$\omega_0 = \frac{1}{\sqrt{LC}} \tag{3.43}$$

Where ω_0 is the resonant frequency. Figure 3.14 illustrates how, with the use of a parallel capacitor, the voltage drop across the secondary inductor can be eliminated, providing the circuit is tuned to the transmission frequency.
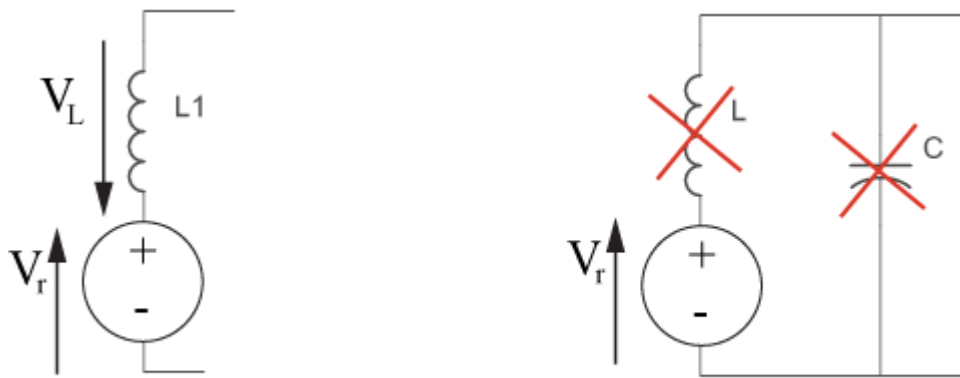
Figure 3.16 cancellation of the secondary leakage inductance using a tank resonator.

Parallel LC tanks are used in the receiver circuit to provide a voltage source output. If a current source output is preferred, a series LC circuit can be used. Voltage outputs are suitable for driving higher resistance loads, whereas current sources are better suited to low resistance loads.

3.5.2 Transmitter design

In order to adequately drive the primary inductor with a large alternating current, an appropriate transmitter circuit must be designed. A wide range of amplifiers are used for this task, with the class C (including saturating class C) and E drivers dominating in the literature due to their high efficiencies. However, these types of driver typically work at a fixed operating frequency, which can make experimental set-up tedious if one wishes to tweak the supply frequency between experiments. Class AB drivers are less efficient, but their ease of design and ability to work at a range of frequencies (with a single component

change) makes them an attractive choice for prototyping. When the experimental set-up has been optimised a high-efficiency driver can be selected to improve the efficiency.

The class AB amplifier uses a push-pull transistor configuration and is shown below in figure 3.17. A low power a.c. signal is applied from a function generator, coupled to the input of both transistors. Each transistor is turned on for half a cycle, that is the npn transistor is on during the positive half-cycle and the pnp is on during the negative cycle. Each transistor acts as an emitter-follower, converting the low-power input signal to a high-power output signal. The output signal drives the primary inductor, inducing a voltage in the receiver. A resonant capacitor is often connected in parallel with the transmitter inductor in order to cancel out the primary leakage inductance.
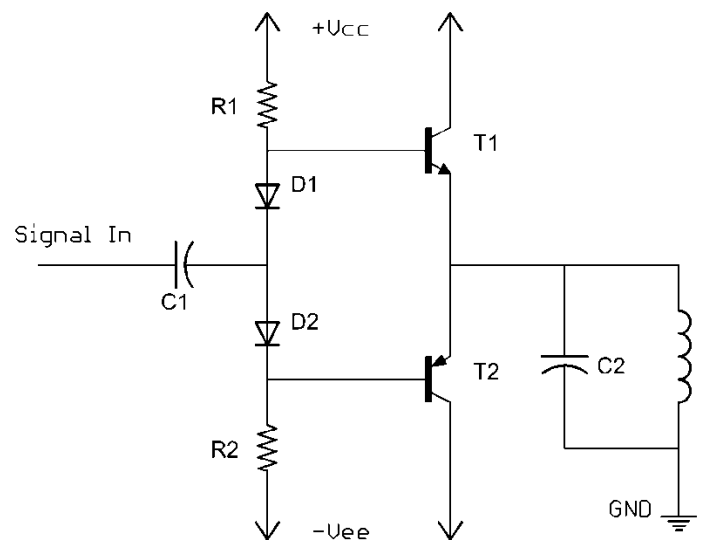
Figure 3.17 a class AB amplifier, driving a parallel LC tank circuit.

Two diodes are used to minimise output distortion, by biasing both transistors on. The downside to this is an increase in quiescent current when there is no input signal applied, but it removes crossover distortion from the driver output.

3.5.3 Amplitude Modulation

Amplitude modulation describes those systems which use discrete variations in the amplitude of the carrier signal to represent information. Two waveforms are generated: the carrier signal and the modulation signal. These signals are modulated to produce the AM output signal for transmission. The data can then be extracted at the receiver by passing the signal through a demodulator. The carrier, signal and output voltages can be expressed as

$$v_c(t) = \widehat{V_c}\sin(\omega_c t) \tag{3.44}$$

$$v_s(t) = \widehat{V_s}\sin(\omega_c t) \tag{3.45}$$

$$v_o(t) = (1 + mv_s(\text{t})).\sin(\omega_c t + \theta) \tag{3.46}$$

Where m is the modulation index, having a value between 0 and 1. The subscripts c and s denote the carrier and data signal parameters. The output, v_o, is the modulated waveform, which appears at the output of the driver.
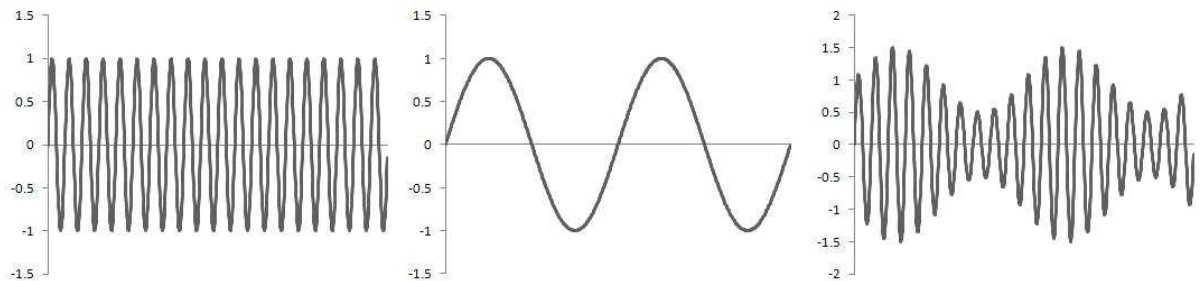
Figure 3.18 a 1 kHz carrier wave (a) a 100 Hz data signal (b) and the amplitude modulated signal

(c). The modulation index is 0.5.

Amplitude modulation may be practically implemented by varying the value of collector (or drain) voltage in the transmitter, thus varying the amplitude of the output voltage, or by varying the collector current by modulating the base, emitter, or driver [111]. Collector modulation may only be used if the transmitter transistor(s) are saturated.

3.5.4 Demodulation

The receiver circuit in an inductively powered implant is used to demodulate the transmitted AM signal in those systems that require data transmission. A typical AM demodulator circuit is shown in figure 3.19.
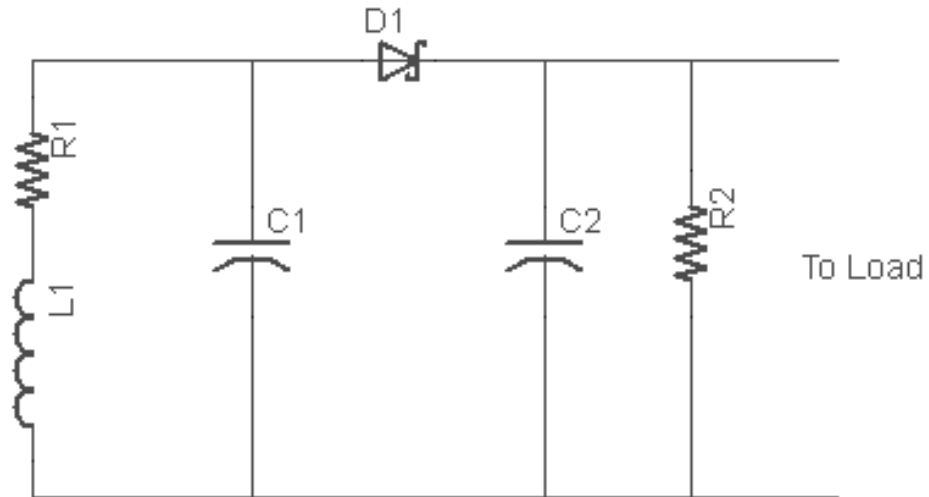
Figure 3.19 a typical envelope detector schematic, consisting of an LC resonant tank circuit and an

envelope detector.

The receiver, shown in figure 3.19, consists of the following parts:

- The receiver inductor converts the alternating magnetic fields from the transmitter inductor into an electrical current
- A resonant tank capacitor tunes the inductor to the carrier frequency, cancelling the leakage inductance
- The AM signal is then half-wave rectified through a semiconductor diode, with a filter capacitor to smooth the ripple voltage. A bleed resistor is used to charge the capacitor during the negative half-cycle. These three components form the envelope detector and the output of this circuit tracks any changes in carrier amplitude.
- The data signal can now be connected to the rest of the circuit and used as desired.

Amplitude modulation has one primary advantage over any other modulation technique, in that it is the easiest system to implement, particularly in biomedical implants due to the simplicity of the demodulation circuit. It can be implemented using a relatively small number of components, which is an important factor in biodegradable systems and in cell-compatibility.

3.5.5 Eddy Currents

If a large conducting material is placed in close proximity to an alternating magnetic field, such as that found in a transformer, electric currents will flow in a closed loop in that material. These currents, termed eddy currents, are induced in opposite polarity to the

alternating field, obeying Lenz's law. In practical transformers, laminated cores are used to reduce eddy current losses. In bio-implantable systems, eddy currents can flow in the tissue surrounding the receiver circuit and this should be avoided for health reasons. Indeed it is the presence of eddy currents that determines the upper limit of transmission frequency for an inductively powered implant. Typically an upper limit of around 10 MHz is imposed to avoid harmful levels of eddy currents, as the induced eddy currents are proportional to the frequency of transmission.

3.5.6 Skin Depth

The skin effect is caused by the internal magnetic fields within a wire, when an a.c. current is flowing in that wire. This internal magnetic field causes the majority of the current to flow in the outer sections of the conductor, where there are less flux lines.

$$\delta = \frac{1}{\sqrt{\pi f \mu \sigma}} \tag{3.47}$$

Where δ is the skin depth in metres, σ is the conductivity of the material and μ is the magnetic permeability. The skin depth is the distance below the surface of a conductor that the current has decreased by $1/e$ of its surface value. This effect is termed the proximity effect when present in tightly wound inductors, such as solenoids, caused by the magnetic fields of adjacent conductors. Both of these effects cause an increase in the effective resistance of the inductor, resulting in a lower quality factor. The resistance of a circular wire conductor can be expressed in terms of its d.c. value, multiplied by a skin depth factor, where r is the radius of the wire and l is the length of the wire.

$$R = R_{d.c.}\left[1 + \frac{1}{3}\left(\frac{r}{2\delta}\right)^4\right] \; for \; \delta > \frac{r}{2} \; (low \; frequency) \tag{3.48}$$

$$R = R_{d.c.}\left[\frac{r}{2\delta} + \frac{1}{4} + \frac{3}{64}\left(\frac{2\delta}{r}\right)\right] \; for \; \delta < \frac{r}{2} \; (high \; frequency) \tag{3.54}$$

$$R_{d.c.} = \frac{l}{\sigma \pi r^2} \tag{3.49}$$

3.6 Summary

This chapter has described the electromagnetic principles that form the basis of electrical induction. Inductors have been described in great detail with a focus on their best known application: the electrical transformer. In biomedical applications, low coupling, wireless power schemes dominate. The sub-systems required to operate these inductive links have been shown with some basic concepts associated with their function. This chapter will be used to design an inductive powering system capable of transmitting power and data to a biodegradable receiver circuit. Inductors are designed using the coupling theory outlined here. The equivalent circuits for inductive powering described here have been used extensively to ensure biodegradable receiver circuits would fulfil the desired functionality at reasonable levels of power consumption.

4 Applied Alternating Electric Fields to Sensory Neurons *In Vitro*: Effects and Outcomes

Electrical stimulation applied during a peripheral nerve repair can have positive outcomes. However, inaccurate attempts at electric field control *in vivo* are invariably seen; with functional outcomes often comparable to control experiments. Throughout this chapter, applied a.c. electric fields are delivered in a precise and controlled manner *in vitro* to examine their influence over regenerating neurons at the *cellular* level. This approach, using many different electrical stimulation waveforms across independent trials, aims to identify the parameters that are most favourable to neuronal alignment, manipulation and growth.

4.1 Electrical Stimulation of Regenerating Dorsal Root Ganglia

The majority of electrical stimulation studies document the use of alternating electric fields *in vivo*. It is clear that the main difficulty lies in selecting the electrical stimulation waveform. This is because, almost without exception, no two authors use the same set of experimental conditions. Reported experiments vary dramatically in the following way:

- The electrical stimulation parameters vary across published studies.
- Some studies do not provide enough information about the applied electrical signal to be able to replicate the experimental technique. For example, some studies quote an amplitude "significant to cause an action potential". This is not a precise value and varies dependant on *in vivo* electrode placement.
- The stimulation frequency can be either continuous, or expressed as a train of pulses occurring a number of times per second. Some studies use bi-phasic pulses 20 times per second, others use a 20 Hz square wave signal. Again it is difficult to compare studies with such a wide set of waveform shapes, frequencies and pulse duration.
- Published literature can be divided by the use of current sources versus voltage sources.
- The value of electric field is often unknown; many authors use two electrodes at either end of a conduit, but do not indicate the separation distance. The electric field will vary at fixed distances along the conduit caused by poor electrode placement. Ideally one should use several electrodes at each end to obtain a uniform field distribution from one end of the conduit to the other.

4.1.1 Experimental Technique

These factors make *in vitro* modelling of the repair extremely difficult. The aim here was to examine the outcome of electrical stimulation using an *in vitro* model. This model began with the use of multichannel electrode arrays (MEAs) to culture dorsal root ganglia (DRG). An autonomous stimulation system was designed using Labview software (National Instruments, USA) and PXI data acquisition hardware (National Instruments, USA). Electrical stimulation waveforms were selected and applied in order to examine their effect at the cellular level using precise control of the electrical parameters. The following section describes the experimental technique and the initial results.

National Instruments Labview software was selected as the best candidate for the design of an automated stimulation generator due to its user-interface, ability to control electrical instruments and compatibility with PXI acquisition hardware. PXI is a platform from National Instruments, used to interface a PC with data acquisition cards. The block diagram of the hardware is shown in figure 4.1. These choices were made with a view to designing a flexible hardware and software set-up to ensure that any design challenges could be met. Flexibility proved to be important in exploring a number of electrical stimulation waveforms and in running experiments in parallel. In the beginning it was not known what the signal parameters would be and this alone called for a flexible approach to waveform generation. A narrowing of the experimental variables could then result in a more fixed approach, leading to the fabrication of custom electrode modules and a more detailed knowledge of hardware requirements with a view to developing a system that closely matches an *in vivo* electrode design.
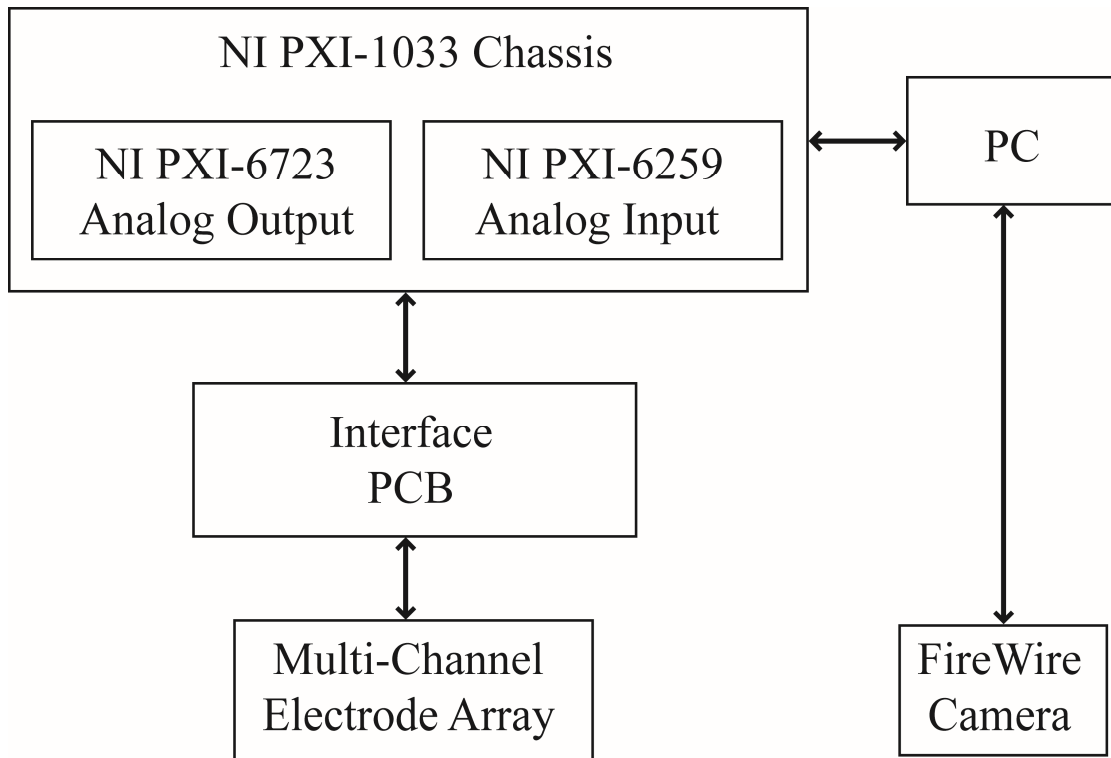
Figure 4.1 the electrical stimulation hardware block diagram. National Instruments Labview software was used to control analog input and output PXI cards within a PXI chassis. A custom interface PCB condensed the signal lines and allowed access to the multi-channel electrode array. A firewire camera provided time-lapse imaging for the duration of each experiment.

The Labview software is used to control two data acquisition cards through a PXI chassis connected via a PXI-express card within a PC. One card is primarily an output card, whilst the other is predominantly an input card. These cards are connected to a printed circuit board (PCB) which forms the interface between the PXI system and the MEAs under test. The PCB efficiently routes signals to the MEA. Several MEAs can be tested in parallel, increasing the rate of experimental data that can be acquired.

The following list summarises the capability of the stimulation system:

1. Control of 32 independent output channels.
2. Control of 2 firewire cameras for time lapse recording.
3. Acquisition of 32 analog input channels.

For each of these experiments, a rat dorsal root ganglion was used as a source of sensory neurons. This DRG was seeded in the centre of the MEA prior to the application of the electrical stimulus signal. It was hoped that by applying different electrical stimulation waveforms across independent experiments, different growth profiles would be visible. In

particular, it was thought that neurons would align along the direction of the applied field. MEAs were chosen as a suitable device for this due to their flexibility and ease of cell-culture (Multichannel Systems, Germany) shown in figure 4.2. These devices contained 60 TiN electrodes on a glass substrate. Connections were made using a gold contact spring connector (Multichannel Systems, Germany).
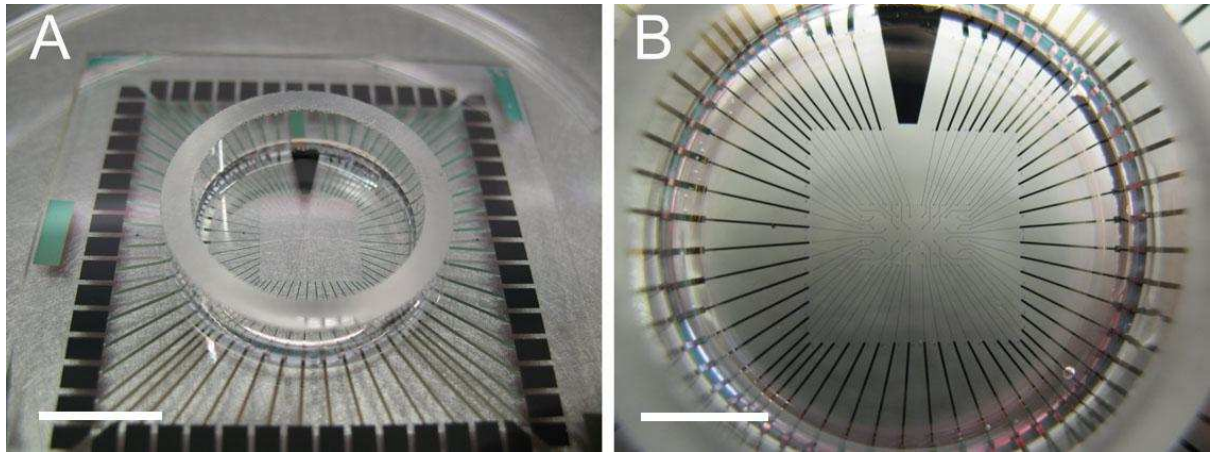
Figure 4.2 the multichannel electrode array used to apply electrical stimulation to regenerating neurons from a dorsal root ganglion. The product used is the 60MEA500/30iR-Ti (Multichannel Systems, Germany). The electrodes were spaced 500 μm apart. Each titanium nitride electrode was 30 μm in diameter. The electrodes are arrayed in a rectangular 6 x 10 pattern. Scale bar (A) 10 mm and (B) 5 mm.

The cell culture technique can be found in appendix C.

4.1.2 Electrical Stimulation Waveform Selection

Two pairs of electrodes were used as a starting point, with an alternating electric field applied between each pair as shown in figure 4.3. The aim was to observe how the neurons regenerating from a DRG were influenced by these regions of electric fields. Control cultures, with no applied electric fields, should see a random growth distribution emanating on all sides of the DRG. Stimulated cultures should see some form of alignment, attraction or repulsion within the electric field regions.

4.1.3 Results

Control cultures evaluated how the DRG and regenerating neurons would behave in the MEA environment. Control cultures showed a good level of random distribution,

indicating a good control environment, as shown in figure 4.3. The control results were used as the reference for any modified growth profile caused by applied electrical stimulation.
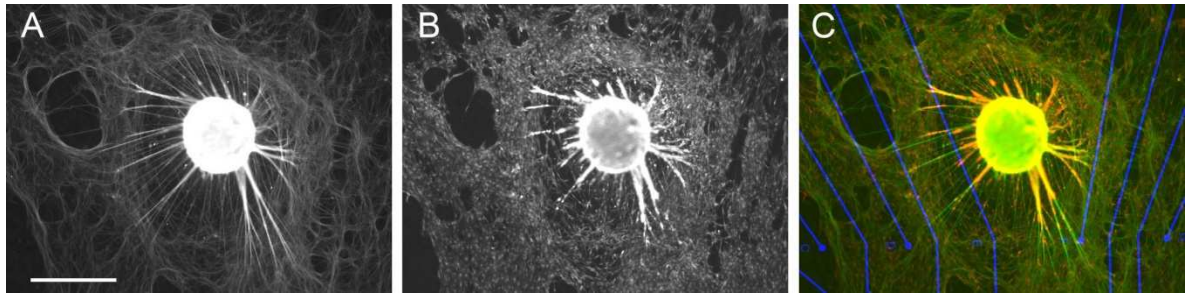
Figure 4.3 control cultures on MEAs (A, B). β3-tubulin has been used in (C) to label the axons (green), with s100 labelling the Schwann cells (red). A non-oriented axonal and cellular network is achieved, indicating a good control outcome. Scale 500 μm. False colouring has been applied for clarity.

Electrical stimulation resulted in aligned regeneration profiles, albeit on a limited percentage of trials. This directed alignment caused by the alternating electric field regions was in some cases highly pronounced, and less so in others. However, the majority of cases were equivalent to a random control distribution. The observed pattern of alignment was inconsistent across the independent trials, which made it difficult to draw any accurate conclusions from the experimental data.
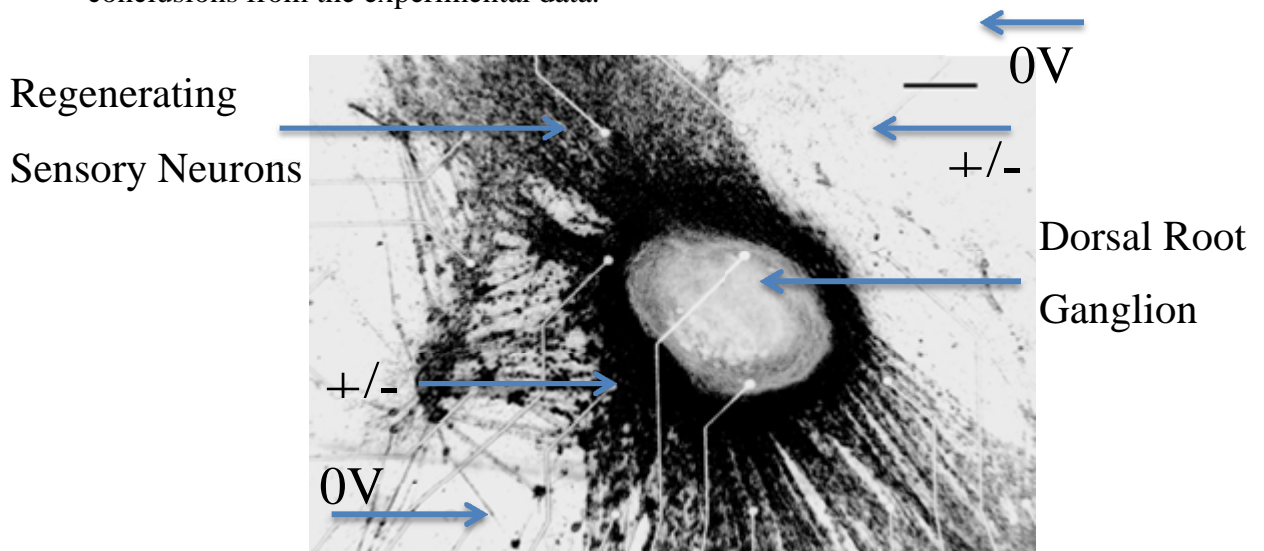
Figure 4.4 directed growth of sensory neurons from a regenerating dorsal root ganglion in response to applied electrical stimulation. Four electrodes were used for the stimulation as indicated on the figure above. These two pairs of electrodes create two regions of alternating

electric field. The voltage applied to the +/- electrodes was 100 mV, with a separation distance of

1 mm. This has had a measurable outcome on the outgrowth of neurons from the DRG. The

original micrograph has been colour –inverted for clarity. Scale: 300 μm.

Figure 4.4 illustrates the directed growth of neurons from a regenerating DRG. The orientation of the neural network is in the opposite direction to that shown in figure 4.5. Note also from figure 4.5 that some neurons have very pronounced, straight, growth profiles in contrast to the majority of the network. These results indicated primarily that electrical stimulation can influence neuronal growth at the cellular level. The directed growth was of particular interest for *in vivo* peripheral nerve repair, where such growth could be used to direct neurons to their targets.
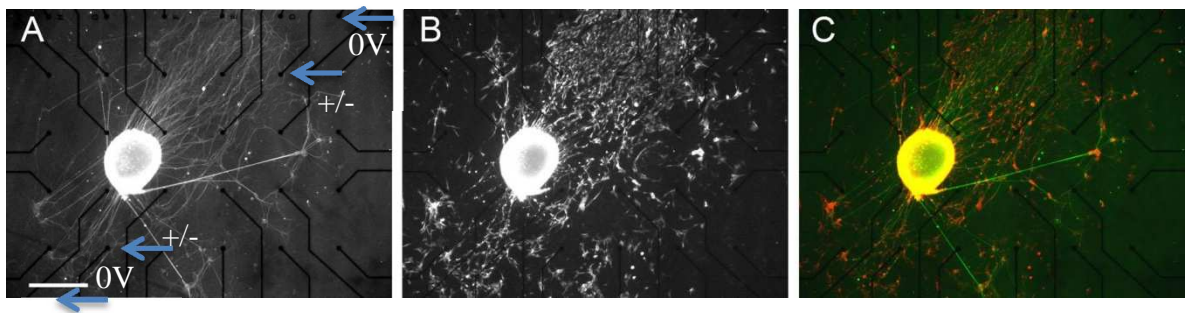
Figure 4.5 directed growth of sensory neurons from a regenerating dorsal root ganglion in

response to applied electrical stimulation, showing a different directionality. A 100 mV, 1Hz

square wave pulse was applied continuously to the electrodes as shown in (A). Axons and Schwann

cells were again stained for β3-tubulin and S-100 respectively (C). Scale 500 μm.

Experiment Number (n)	Stimulation Amplitude (mV)	Stimulation Frequency (Hz)	Stimulation Waveform Shape	Stimulation Time (days)	Culture Time Prior to Stimulation (days)
1	100	20	Square	6	15
2	**100**	**20**	**Square**	**16**	**1**
3a	100	100	Square	8	1
3b	100	100	Square	8	1
4a	500	20	Sinusoidal	4	1
4b	1000	20	Sinusoidal	4	1
5	300	20	Square	6	1
6a	**100**	**1**	**Square**	**25**	**1**
6b	**100**	**5**	**Square**	**25**	**1**
7	100	5	Sinusoidal	38	6
8a	100	5	Square	16	1
8b	100	1	Square	16	1
9a	**100**	**1**	**Square**	**18**	**1**
9b	100	5	Square	18	1
10a	100	1	Square	31	1
10b	100	1	Square	31	1
10c	100	1	Square	31	1
10d	100	1	Square	31	1
11a	100	1	Square	12	1
11b	100	1	Square	12	1
11c	100	1	Square	12	1
11d	100	1	Square	12	1

Table 4.1 electrical stimulation experiments on sensory neurons in multi-channel electrode arrays.

Rows in bold type represent observed directional growth versus controls.

Table 4.1 outlines the experimental parameters used during the stimulation tests. Some of the key observations from this table of results are outlined below:

- Initially, a 20 Hz square wave signal was chosen, influenced by the large number of studies documenting such an approach. As an estimate, it was felt to be a good initial electrical stimulation to induce a measurable effect.

- The amplitude of 100 mV was estimated to be sufficient to produce an effect, whilst being safe enough to allow cells to proliferate.

- A continuous stimulation pulse was selected, conflicting with some published studies that suggest a short period of stimulation per day is optimal. Here the aim was to maximise the chance of observing any effects by stimulating continuously, treating the stimulation duration as a variable to be optimised when fundamental stimulation information was known. If there were any harmful effects from this continuous approach, a shorter duration of stimulation per day could be applied to improve the cell growth.

A series of tests designed to apply high voltages were devised, inspired by the low rate of achieving a measurable outcome, with the results summarised in table 4.2. The amplitude of the electrical stimulation was increased each day, before resting at a final value for the remainder of the experiment. The aim of these experiments was to observe a directional effect and thus identify what the minimum signal amplitude would be to obtain these results on a consistent basis. The frequency was also lowered to 1 Hz, aimed to mimic a d.c. signal. Despite using higher fields, no discernible outcome was observed. However, it was noted with interest that the DRG and neurons could survive for long periods of time in the presence of two high-voltage regions within the MEA. This was a promising development, defining an approximate upper limit of amplitude.

Experiment Number (n)	Stimulation Amplitude (V)	Stimulation Frequency (Hz)	Stimulation Waveform Shape	Stimulation Time (days)	Culture Time Prior to Stimulation (days)
12 a,b,c,d	0.5-0.8-1-1.2	1	Square	23	12
13 a,b,c,d	1.5-3-8-10	1	Square	15	6

Table 4.2 voltage step change, followed by prolonged exposure to high electric stimulus. These experiments showed that the dorsal root ganglion and neurons could survive for long periods of time in the presence of two high electric field regions.

4.1.4 Electrical Stimulation on MEAs: Summary

Some experiments did show a degree of alignment, though the majority of results were in fact comparable to a random control distribution. Repeating any positive outcomes also proved to be difficult and the long experimental times caused a great delay in trying to use new electrical stimulation signals. But, despite this, it proved a valuable exercise in gaining expertise in running such experiments as well as troubleshooting some early problems in experimental technique. These initial experiments on MEAs indicated that alternating electric fields could have a discernible influence on the outgrowth of regenerating neurons. Also, it was shown that regenerating neurons could grow in the presence of these fields if electrical parameters were comparable to those used above. This informed future experiments, providing a range of amplitudes, frequencies and shape of signal that could be applied, safe in the knowledge that an experiment could be conducted. Subsequent experiments would seek to improve the consistency of experiments by achieving different growth patterns in a repeatable fashion. This was made possible through the isolated, significant results achieved here providing a degree of encouragement that positive outcomes, namely alignment, could be achieved in a safe manner (with alternating, not direct fields).

4.2 Electrical Stimulation of Aligned Neurons

The overriding factor determining the lack of success with MEA devices was the large amount of spatial freedom which the neurons had, compared with the electric field area. They therefore had ample room to escape the electric field regions. In addition, the duration of the tests caused large delays in obtaining information on new parameters and gaining feedback. These two factors have been addressed by introducing a new hybrid testing module. These devices consist of two distinct parts: A central groove region where the DRG is seeded, providing mechanical guidance cues to the regenerating neurons, followed by patterned metal electrodes, providing electrical cues when the neurons exit the groove region. After approximately 5-10 days the axonal outgrowths from the DRGs reach the electrode area on both sides of the microgrooves. This design allows for good comparisons to be made, as each DRG will regenerate along the mechanical guidance cues i.e. their growth in the first week has been standardised by the microtopography of the SU8 grooves. These devices 'force' the neurons to interact with the electric field region by aligning them towards it. For each device, two tests can be executed at each end of the groove region, increasing rate of data collection.

4.2.1 Hybrid Device Design

Four electrode layouts within the hybrid devices have been designed in an attempt to show how the growth of regenerating neurons depends on the electric field orientation, shown in figure 4.6 as an illustration of predicted outcomes and in figure 4.7 as a detailed schematic. The four different electrode designs used are as follows:

1. Four electrodes perpendicular to the grooves: the "perpendicular" design. The perpendicular design is aimed at demonstrating how regenerating neurons react to an electric field normal to them.

2. Four electrodes parallel to the grooves: the "straight" design. The straight design allows for a number of field patterns to be investigated, particularly when using all four electrodes. The primary aim of this type of device is to guide the regenerating axons between the two central electrodes. N.B. the electric field in this design is perpendicular to the aligned neurons coming from the groove region.

3. Four electrodes with right angled bends: the "hairpin" design. The hairpin design is a modified straight design with added bends aimed at inducing turning in the regenerating neurons. Four electrodes are used to allow experimentation with different electric field patterns as required.

4. Two electrodes with wider squared areas: The "square" design. The square design was used to investigate the effect of having two distinct regions of electric field. In the narrower sections the field would be three times less intense than that of the wider regions.

By aligning neurons before the application of electrical stimulation, a consistent set of outcomes was achieved. It was still unknown what influence the electrical stimulation would have, particularly across each device, but it was known that these devices would allow for rapid identification of electrical waveform parameter values, in comparison to the slow MEA experiments.
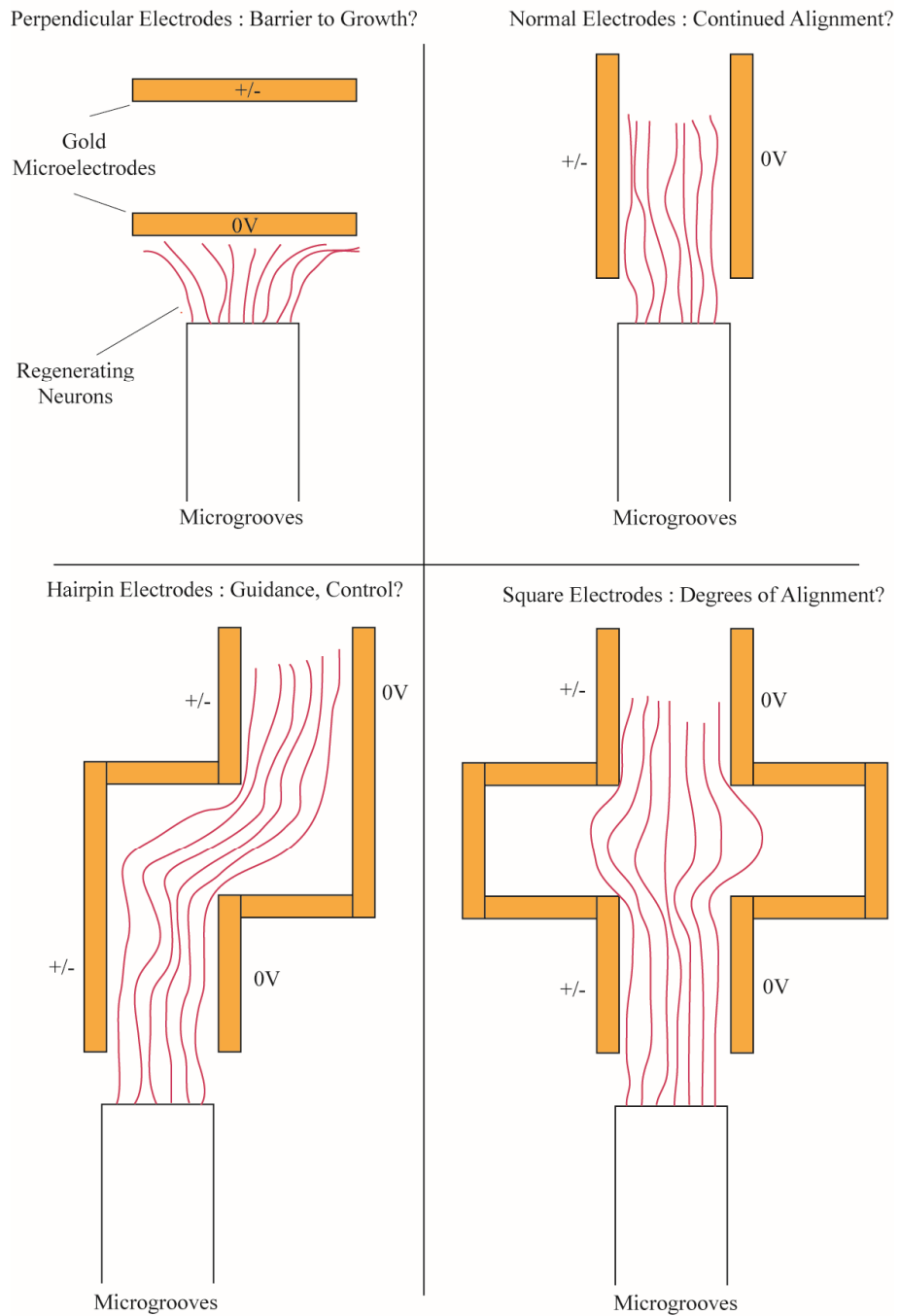
Figure 4.6 schematic illustrating the predicted distribution of neuronal growth in the presence of different electrode layouts. The neurons will be first aligned using SU-8 microgrooves. These aligned neurons then encounter an alternating electric field. These four patterns have been designed to investigate the effects of a number of field patterns, to further the understanding of how neurons are influenced by alternating electric fields.
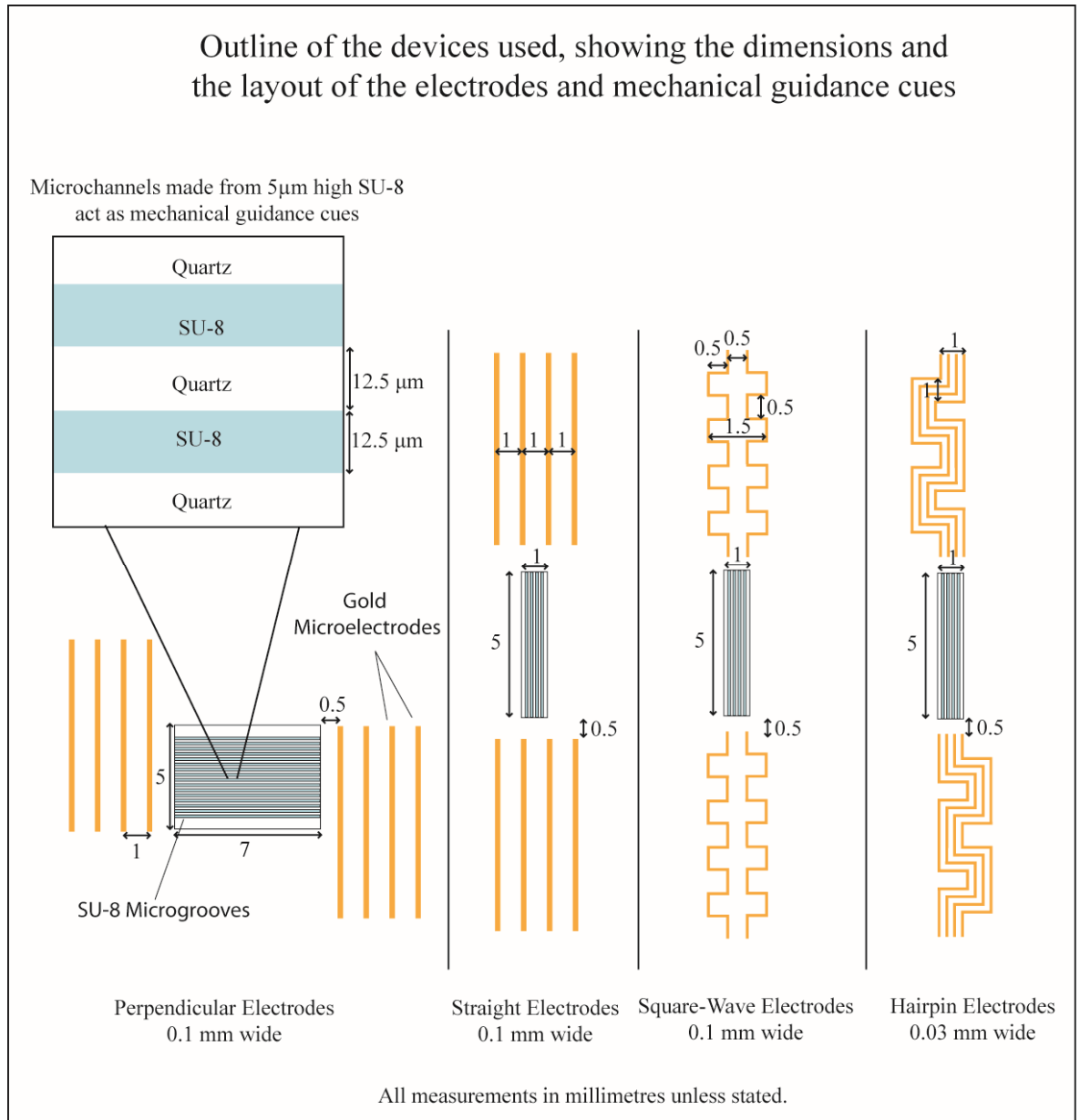
Figure 4.7 hybrid device schematic illustrating the electrode designs used. The SU-8 microgrooves are 12.5 um wide, spaced 12.5 μm apart. The microgroove area was reduced in subsequent designs to reduce the time taken for neurons to reach the electrodes. The electrodes are made from 20 nm Ti, and 200 nm Au. For each experiment, a dorsal root ganglion was seeded in the centre of the microgrooves.

4.2.2 Fabrication of Hybrid Devices

SU-8 microgrooves have been shown to be effective in aligning neurons, which when coupled with the fact that SU-8 is transparent, makes it a suitable choice as the material for the microgrooves. The fabrication process consists of two stages, the metal electrode

patterning and the topographical groove section, depicted in figure 4.8, a detailed description of which is provided in appendix A.
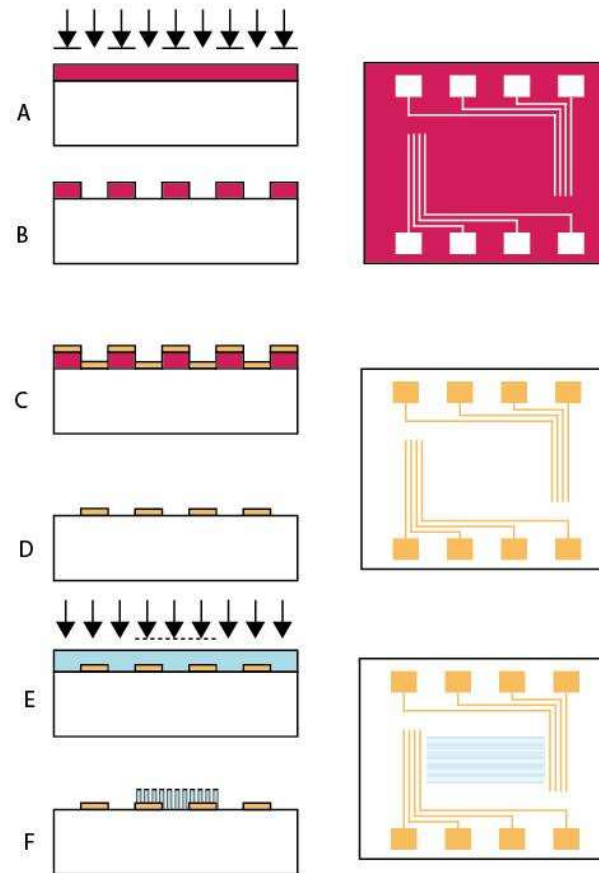
Figure 4.8 exposure of S1818 photoresist (A) followed by pattern development (B). Evaporation of Au electrodes (C) and metal lift-off (D). SU-8 groove definition using UV exposure (E) followed by pattern development in EC solvent (F).

4.2.3 Electrical Stimulation Test Modules

After completion of the above fabrication process, each hybrid device is attached to a PCB interface, shown in figure 4.9. The microelectrodes are connected to the PCB terminal blocks using low temperature soldering at 250 °C. This assembly is termed a 'stimulation test module'. The interface PCB used in the previous experiments can now be connected to each of the stimulation test modules, connecting them to the PXI hardware used. This modular device approach allows many hybrid device experiments to run in parallel. It also allows the devices to be unplugged from the interface board in order to exchange the culture media each day. The same Labview software sent stimulation signals to the hybrid devices via the hardware set-up.
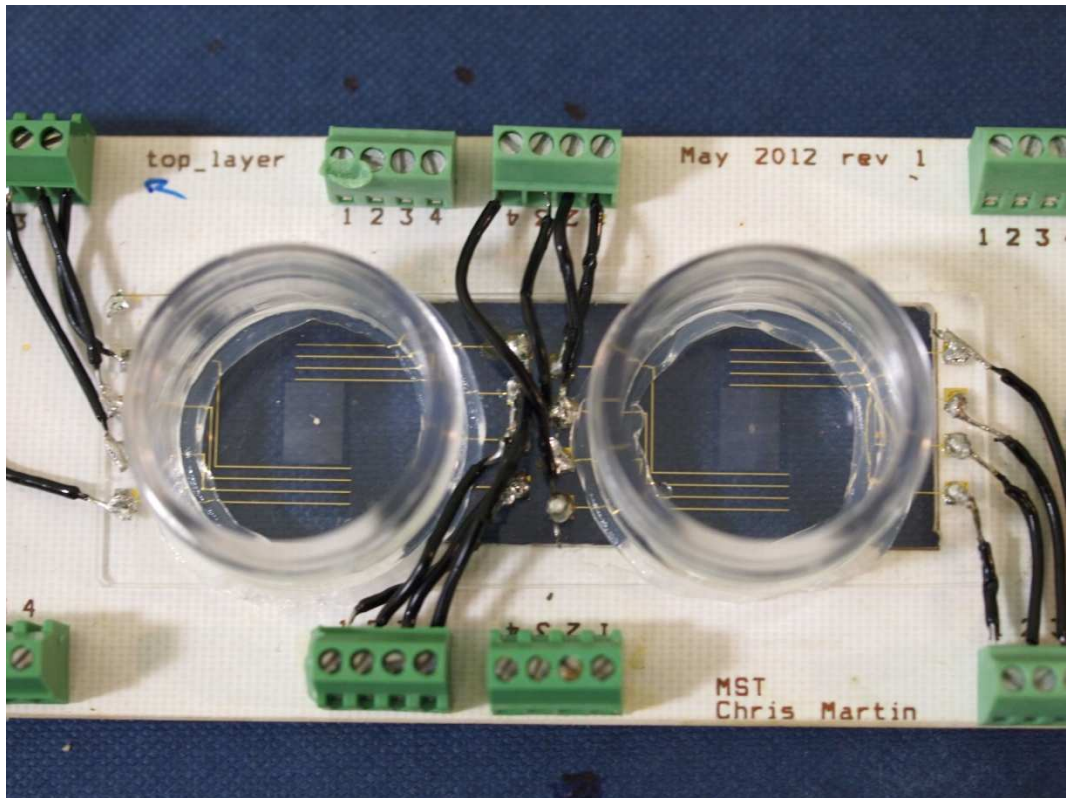
Figure 4.9 a stimulation test module, containing two perpendicular electrode configurations. 20 nm Ti and 200 nm Au electrodes are soldered at 250 °C. A section of the PCB has been removed, facilitating the use of time-lapse recording.

Perpendicular devices contained two culture wells, shown in figure 4.9, made by attaching plastic tubes to the substrate, whilst the other three designs contained a single culture well. Wires were soldered at temperature of 250 °C to prevent damage to the thin-film metal electrodes. A rectangular cross-section was removed from the PCB to allow time-lapse recording during the stimulation experiment, showing the effects of electrical stimulation on the neurons.

4.3 Hybrid Device Results

The results achieved using the hybrid devices are described in detail in the subsequent sections. These devices saw consistent results and outcomes varied across device design. The outcomes are divided into the control cultures and the four electrode designs. The control cultures will be described first, to provide a baseline for the behaviour on the new devices without applied electrical stimulation.

4.3.1 Control Culture on Hybrid Devices

For each control experiment a DRG was seeded in the centre of the SU-8 microgooves. The culture was allowed to grow past the grooves, with the growth in the electrode region of interest. It was expected that the neurons would align along the direction of the microgrooves, followed by spreading upon exiting the grooves. However, each control experiment caused a peculiar result. Independent of the electrode design (i.e. for all devices) the neurons were indeed aligned by the grooves, but both sides of the network *turned right*, moving back towards the DRG, shown in figure 4.10. In some cases, neurons re-entered the microgrooves, performing a 180° turn. Attempts have been made to identify the cause of this behaviour, but as yet no solution has been found for this uneven outgrowth. This behaviour was observed for electrodes connected together (equipotential) and for unconnected electrodes. Discrepancies caused by the fabrication process are often to blame for these types of outcomes. However, one would not expect both sides of the culture to turn in the same direction every time. The microgrooves were effective in aligning the regenerating neurons, which was an expected outcome.
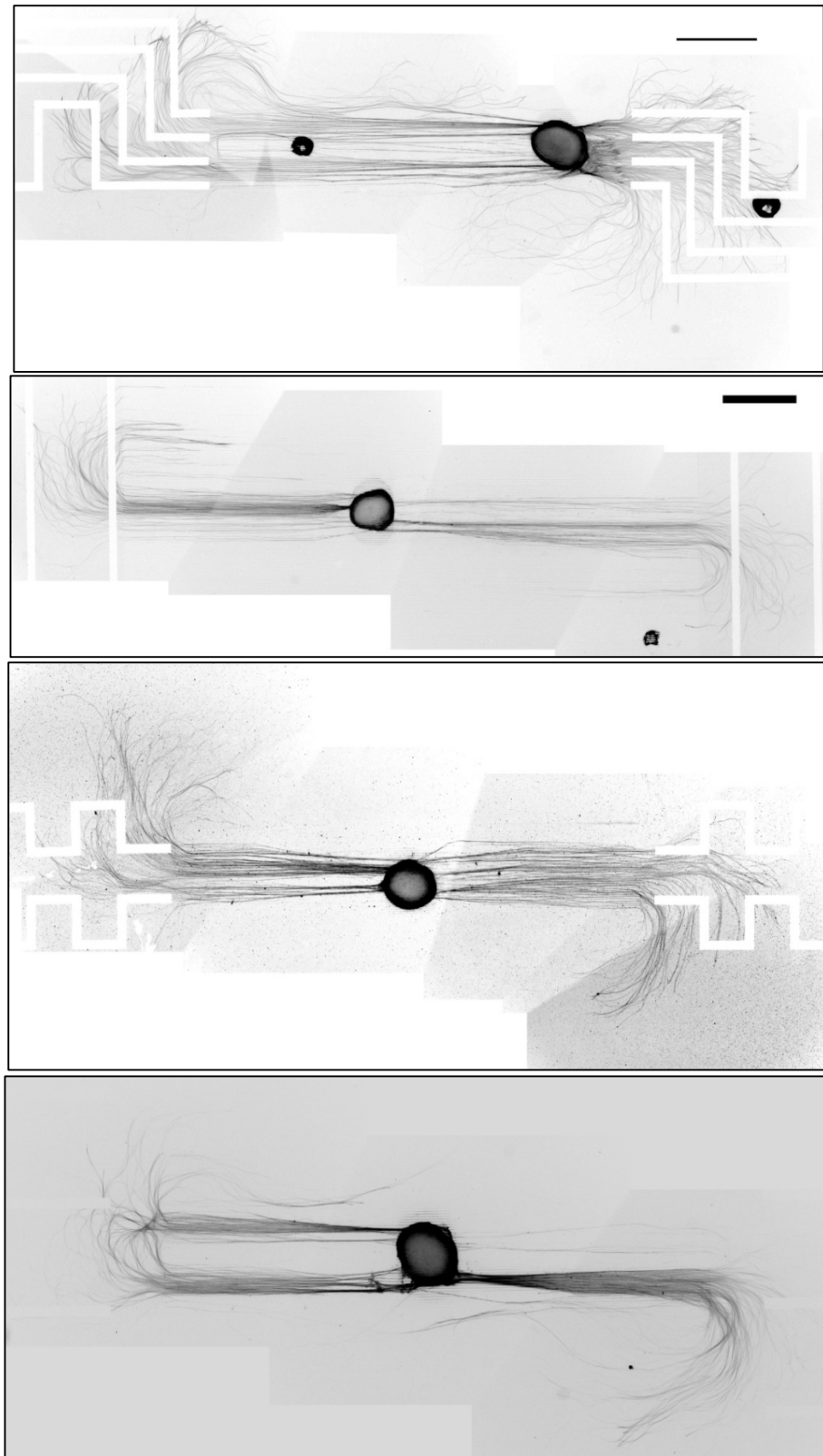
Figure 4.10 distribution of regenerating neurons from a dorsal root ganglion using hybrid devices with perpendicular (A), hairpin (B), square-wave (C), and straight (D) electrodes. The neurons turn right upon exiting the microgrooves for all devices that do not apply electrical stimulation i.e. the control cultures. Scale bar: 1 mm. Colour inversion has been applied for clarity.

These control results made comparison between stimulated and control experiments rather difficult. Stimulated results are usually compared to a random control distribution. A total of 24 control experiments were carried out, all featuring the same outcome. In the following sections, stimulated results will be compared to the control outcomes above. This is less than ideal, but it is hoped that when the control cultures are improved, a proper comparison can be done. The stimulated experiments are divided into four sub-sections, one for each electrode configuration:

1. Perpendicular
2. Straight
3. Square-wave
4. Hairpin

4.3.2 Perpendicular Electrode Results

The results from the MEA experiments were used as a starting point for the perpendicular electrode experiments. Considering the large electric field results, that seemed to indicate that neurons could survive in the presence of high voltages, it was decided that continuing this type of experiment would be a good starting point. The initial experiment involved applying a 1 V, 1 Hz square-wave stimulation signal to the aligned neurons exiting the microgrooves. It was hoped that the neurons would reach the electrodes and grow differently by exposure to this high intensity field. The hypothesis was that the electric field, directed parallel to the neurons, would continue to direct their growth.
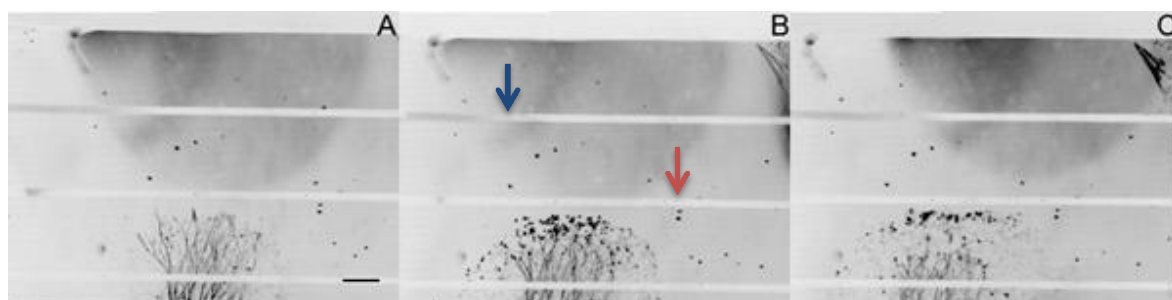
Figure 4.11 regenerating neurons, aligned from microgrooves, approach the electrodes (A). The red arrow denotes the stimulating electrode, with the blue arrow indicating the 0V electrode. A 1V square wave signal, oscillating at a frequency of 1Hz is applied between the pair of electrodes (B). The neurons are held at the stimulating electrode for a time, with some retraction of the network present (C). This indicates that alternating electric fields, placed normal to the direction of growth, can act as a barrier to the regenerating neurons. Scale 5 mm.

As expected, and in stark contrast to the MEA experiments, differences in the direction of the regenerating neurons in response to applied electrical stimulation were consistently observed. Initially, the dominant effect was a retraction of the neural network upon reaching the region of electric field, shown in figure 4.11. The axonal network was unable to grow back towards the electrode at any time, suggesting a mechanism inhibiting the regrowth after the regenerating axons contact the electrical field. This would seem to indicate that the field must be decreased to prevent the retraction and allow the neurons to continue to grow. This effect has potential for therapeutic applications in terms of inhibition of growth of cancerous cells, scar formation and axonal deviation.
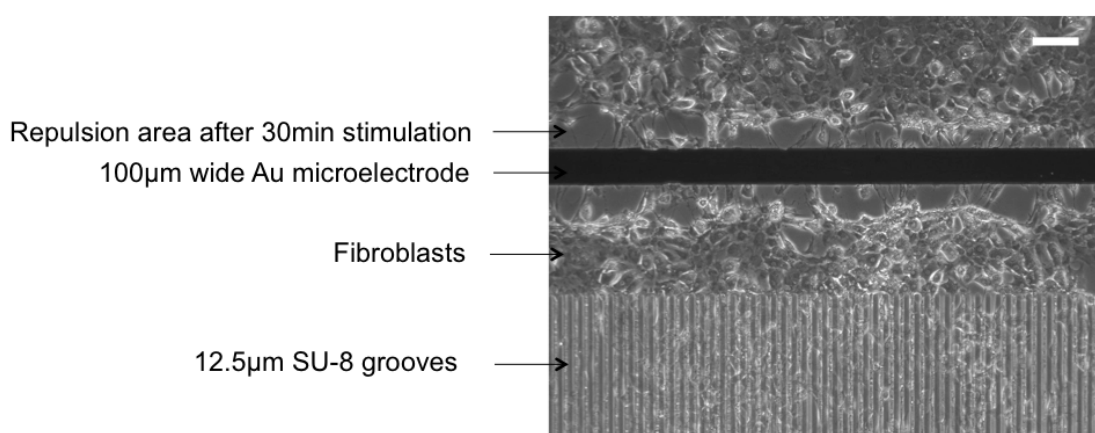
Figure 4.12 fibroblast monolayer from a neonatal rat dorsal root ganglion (DRG) culture repelled by an electrical field. The fibroblast layer was ripped and repelled by a 1V 1Hz square wave electrical stimulation signal. Scale 150 μm.

In the second experiment, shown in figure 4.12, aligned neurons from the microgrooves were allowed to grow over the electrodes prior to the application of the stimulation signal. Using the same electrical stimulation signal, a tear was induced in the neuronal network (including in the support cells). Again, this demonstrated the effectiveness and repeatability of the new hybrid devices in obtaining measurable outcomes quickly and reliably. It was now known at this point that an amplitude of 1 V mm^{-1} would induce an effect, that of extreme repulsion or tearing. It was therefore desirable to identify what a safe level of amplitude would be.

A series of experiments, using step-changes in the electrical stimulation parameters was devised. These experiments sought to identify what parameters had an influence on the level of retractions and thus eliminate them by proper selection of the electrical stimulation signal.

The first step-change experiment began with a square wave signal with 10 mV amplitude, increasing by 10 mV after every hour (i.e. 10, 20, 30 mV in discrete intervals). A retraction of the neuronal network was observed despite using such a low initial value of electric field. Since such a small amplitude still induced retractions, this indicated that a different waveform parameter must be the root cause of this behaviour.

The experiment was executed again using the same electrical parameters, but with a sinusoidal signal. This test aimed to directly compare sinusoidal and square wave signals by observing any difference in retractions. A slower rate of retraction was observed for sinusoidal signals when compared with the previous square-wave experiment. This suggested that the decreased rate of change of voltage seen with a sine wave had a favourable effect on the level of retraction. All subsequent experiments used a sine wave shape of stimulation signal based on the results from this experiment.

Experiment Number (n)	Initial Voltage (mV)	Voltage Increment (mV)	Frequency (Hz)	Start of Retraction (Minutes)	Stimulation Waveform Shape	Experiment Observation
1	100	0.05	1	30	square	retraction
2	10	0.01	1	30	square	retraction
3	0	0.05	1	120	sinusoidal	Retraction with growth
4	10	0.01	1	60	sinusoidal	slow retraction

Table 4.3 step-change experimental results on the perpendicular electrode design.

Table 4.3 shows the summary of four experiments used to execute the amplitude step-change, comparing sinusoidal and square-wave signals. The difference in the speed of retraction indicated that other parameters could now be changed in an effort to reduce the retractions further.

Step-changes in the frequency of stimulation, with the aim of attributing differences in the rate of retraction with frequency, were performed. An initial value of 2 kHz decreasing by half every hour (2 kHz…1 kHz…500 Hz) was selected as an estimate, using an amplitude of 20 mV. It was expected that a frequency of this value would not have any influence over the neurons. As the frequency decreased, the retraction would start at a certain value of frequency. With knowledge of this value, a good estimate of the optimum frequency could be made. A retraction was observed consistent with the amplitude ramps, at the beginning of the experiment. No meaningful conclusions about the stimulation frequency could be drawn as a result.

4.3.3 Modulated Stimulation Results

With a frequency ramp showing no meaningful data, there were a number of options on how to proceed further. A higher frequency could be chosen, on the order of a few MHz, and the ramp test repeated. At this stage it was felt that the near 100 % rate of retractions pointed to a different solution. In published literature, a relaxation phase is often included within the electrical stimulation waveform. This allows the neurons to come to rest prior to the next pulse. A suitable electrical stimulation signal was designed with a relaxation phase, with the aim of further reducing the retractions.

Following some published studies, 20 Hz was selected as a good candidate for the relaxation frequency. That is to say, 20 electrical stimulation pulses would be applied every second. A duty cycle was selected, that of 1 stimulation pulse to 4 periods of rest (1:4). This translated to a stimulation frequency of 100 Hz. The amplitude was chosen to be as low as the stimulation system could provide whilst maintaining a good level of signal integrity. The value chosen was 20 mV. A sinusoidal signal was chosen as outlined in the ramp section. This new, *modulated* waveform is shown in figure 4.13.
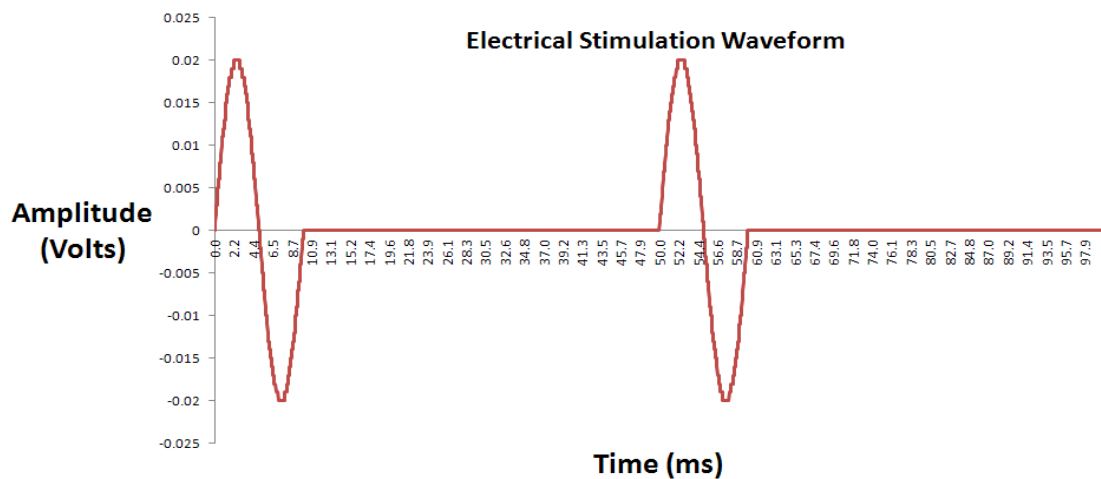
Figure 4.13 a stimulation waveform featuring a 1:4 on/off ratio. This waveform enhanced the observed outcomes by minimising neural retractions.

A stimulation frequency of 20Hz, that is 20 stimulation pulses per second, has been used due to its relevance to the neuronal firing patterns. For example, the cat hindlimb motoneurons are characterised by different relaxation times, ranging from 20 to 40 milliseconds [33]. Therefore, a period of 50ms ensures that every motoneuron has sufficient time to reach equilibrium, prior to receiving the next burst of electrical

stimulation. This has been the foundation of the hypothesis here that 20 stimulation pulses (each with a 100Hz frequency) allows equilibrium to be reached on each cycle.

The retraction of the network happened at a slower rate using this new modulated electrical stimulation signal. It also allowed some growth of the regenerating axons in close proximity to the electric field area. This was an improvement in terms of the rate of retraction. With this protocol, a barrier could be formed to neuronal growth resulting in *confinement* rather than *repulsion*.

Stimulating Electrode
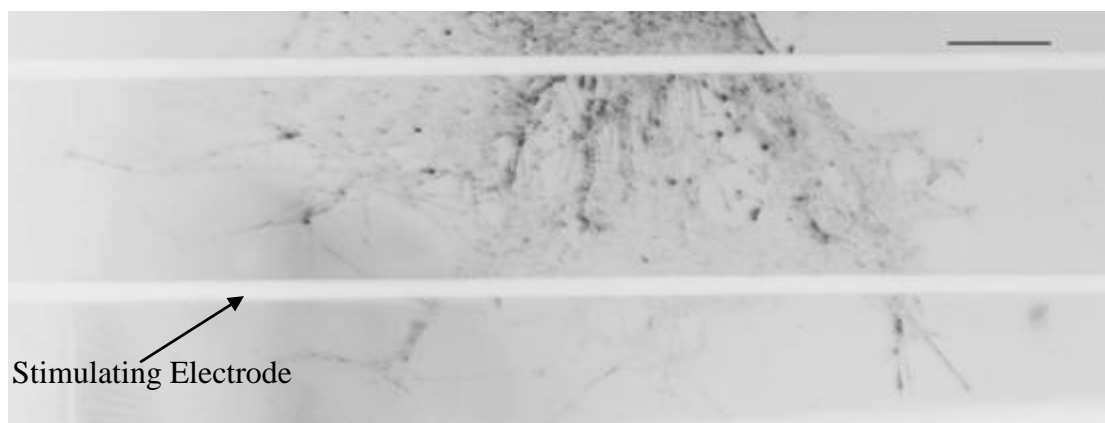
Figure 4.14 demonstration of the electrical barrier effect without a retraction of the network. Cells were held at the stimulating electrode in response to the applied stimulation waveform. Scale: 500μm. The 0V electrode is below the stimulating electrode.

Figure 4.14 shows a neuronal network after 23 days growth in the presence of the a.c. barrier region while applying the new, modulated stimulation waveform. This result heralded a dramatic leap forward in comparison to the retractions observed for previous signals. It is clear that the barrier is confining the cells to a region close to the electrode, with a small number of cells able to cross the barrier. The majority of cells are held behind the electric field region, comparable to published studies showing the formation of a barrier using a.c. fields [112].

4.3.4 Neuronal Turning on Perpendicular Electrodes: A new Effect Induced with a New Stimulus Protocol
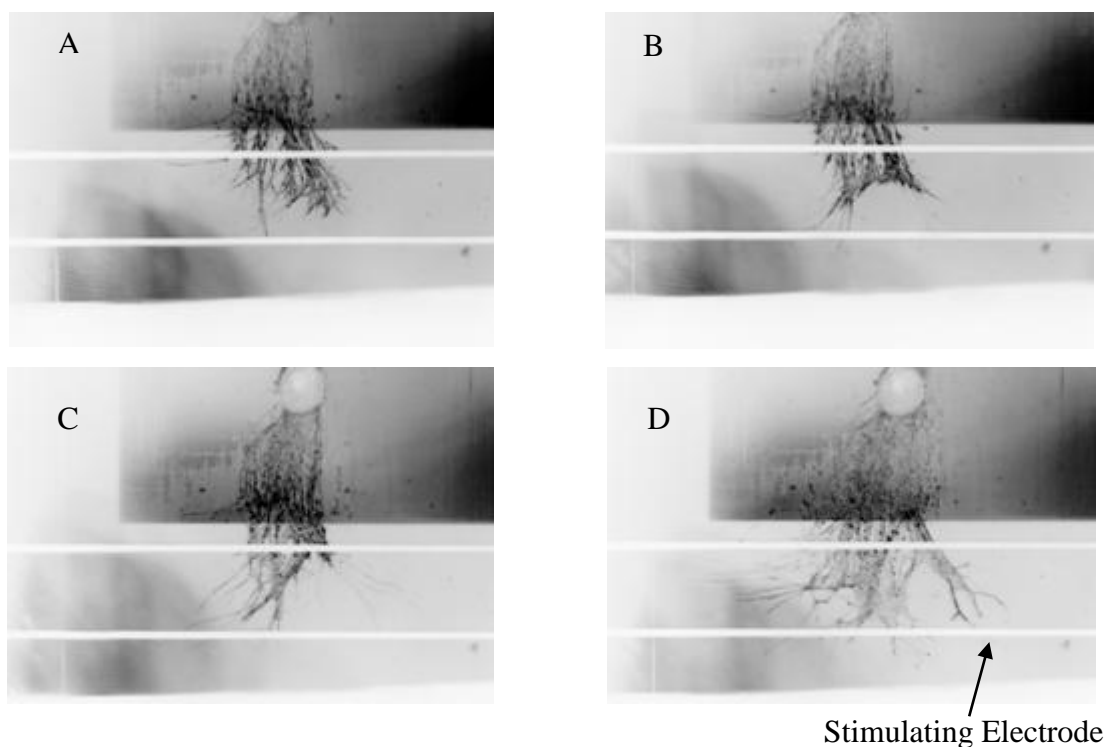
Figure 4.15 Neurons held at the second electrode (top left), followed by reshaping of the network (top right). Spreading of the network (bottom left) and finally perpendicular turning of the network (bottom right). The 0V electrode is below the stimulating electrode.

Another interesting outcome was observed using this new electrical stimulation waveform. Upon reaching the perpendicular electrode, the neurons were held at the electrode for approximately 7 days (figure 4-15 A, B). After this time neurons on both sides of the network turned at right angles and continued to grow (figure 4-15 C, D). This represents the first such directed turning caused by alternating electric fields. This is analogous to turning induced by d.c. fields [26]. Manipulation and control of neurons in this way illustrates real progress towards electronic confinement and control systems for improved peripheral nerve repair outcomes.

4.3.5 Perpendicular Barrier and Turning: Numerical Analysis

Further experiments were executed using the same modulated stimulation signal, aimed at repeating the electrical barrier behaviour. The three results shown below illustrate the same effect, that of containment at the stimulating electrode, followed by some moderate turning. This behaviour contrasts with the control cultures, in that the right-turning has

been replaced with straight growth towards the stimulating electrode. Subsequent containment and turning further demonstrates that an alternating electric field normal to the regenerating axons has a pronounced effect when compared with controls.
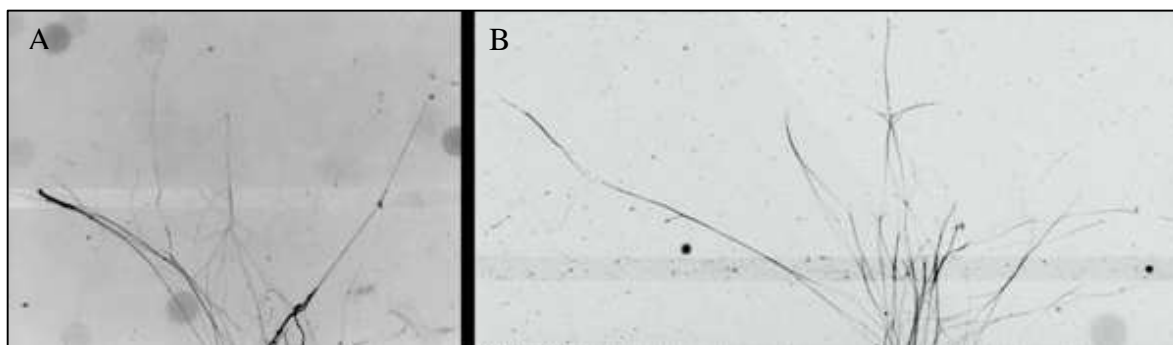
Figure 4.16 a further two experiments showing the effect of a modulated electrical stimulation waveform on regenerating sensory neurons. The neurons are confined near the electric field region, followed by a period of spreading and turning. This contrasts with the control outcome, in that they do not turn right. Colour inversion has been applied.

Figure 4.16 shows two further independent results using the modulated stimulation waveform, following on from the results shown in figure 4.15. These results were analysed using ImageJ image processing software, with the results of that analysis depicted in figure 4.17.
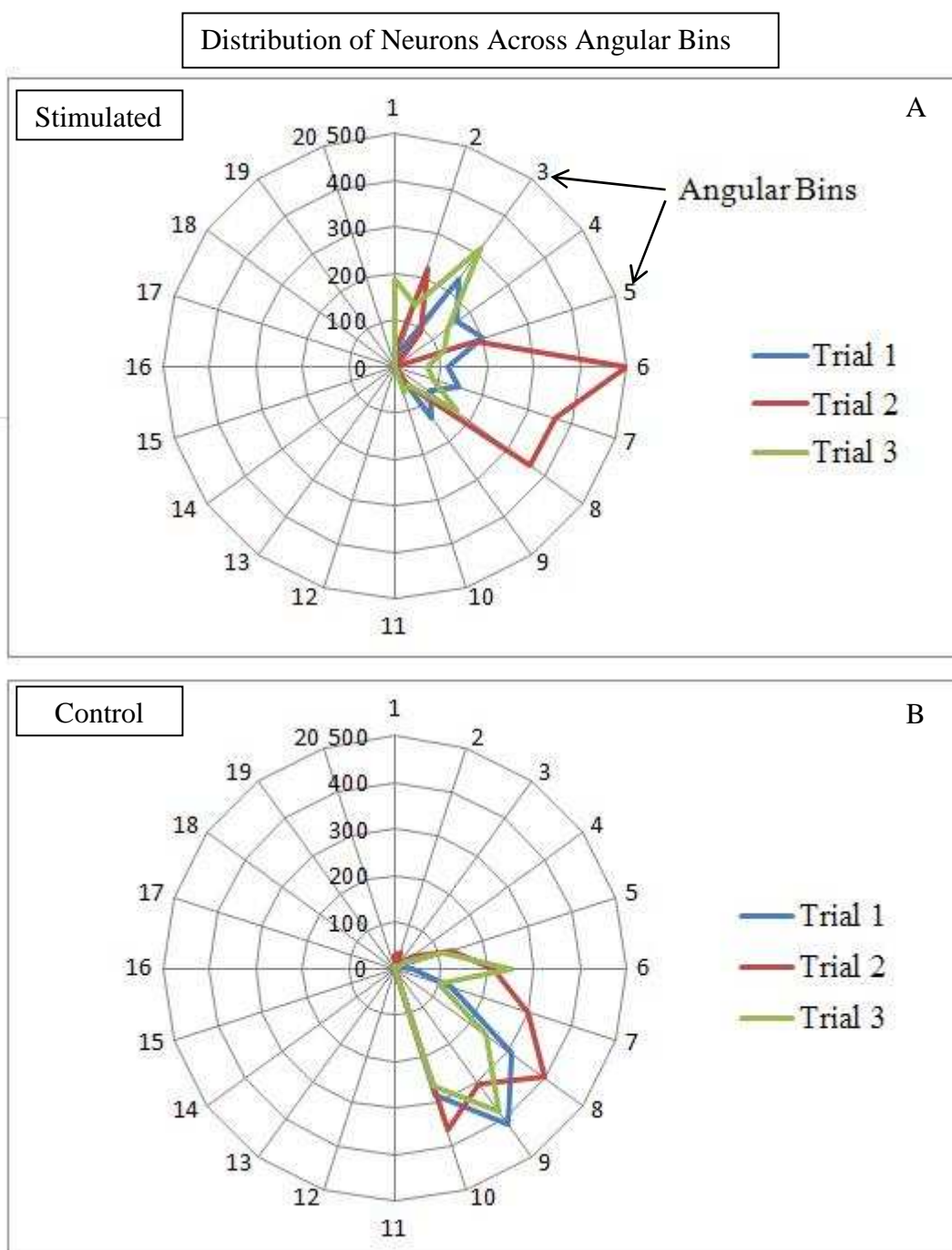
Figure 4.17 numerical analysis of perpendicular electrode experiments, quantifying the distribution of regenerating neurons after exiting the microgrooves. Three independent experiments for applied electrical stimulation are shown using three different colours (A). Similarly in (B) the three independent control experiments are represented with three different colours. The electric field, normal to the grooves, created a relatively even spread of neurons (A) versus the right-turning behaviour common to controls (B).

A circular selection was used to measure the light intensity distribution for each angle. Measurements were taken between 0 and 180 ° (a semi-circle), with 10,000 data points. These distributions were grouped into angular bins, in 20 degree intervals, shown in figure 4.16. A dark-threshold was defined for each image to quantify at what point at least one neuron crosses an angle. The number of crossings per angular bin was calculated and collated. The analysis has been performed in this manner to give an indication of the angular distribution assuming at least one neuronal crossing, thus removing ambiguity between light intensity and number of neurons. Graph A shows the stimulated cultures, with each independent trial represented by a different colour. Graph B shows three independent control experiments, again using three different colours to differentiate the independent experiments. The effect of the stimulation is two-fold. Initially, the applied alternating electric field attracts the neurons to the alternating electrode. Here they are held at this electrode before spreading left and right, as they seek space to grow into. The electrode is acting as a barrier to growth. Since a peculiar control growth profile is present, the stimulation appears to prevent the typical pattern of neurons turning right. It would be interesting to monitor this attraction, followed by a barrier effect and spreading, in comparison to a random control distribution. This barrier formation could have great utitily in neuronal confinement and control. Indeed this barrier effect was integral to the results reported in chapter 5, where two electrical barriers confined regenerating neurons, creating an alignment effect.

4.3.6 Square Electrode Results

The perpendicular electrode devices showed how a pair of electrodes generating an alternating electric field could influence neuronal growth. Whilst this is a good consistent outcome, it does not provide the sort of effect that is of positive utility within a nerve repair conduit. What would be of greater utility is the case where the neurons, upon leaving the grooves, continue to be aligned in the same direction by some applied field. This alignment should be capable of being applied to 'free' neurons once pre-aligned tests have identified the correct electrical stimulation parameters. The next three electrode designs all aimed to accomplish this through the alignment of neurons through a channel between the electrodes.
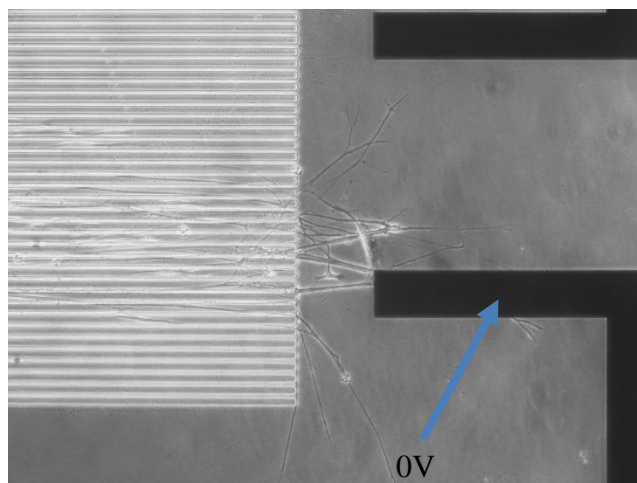
Figure 4.18 preferential growth on the 0V electrode (blue arrow) of regenerating neurons from a dorsal root ganglion on the square-wave electrode design. An alternating electric field was applied between the top electrode (stimulating) and the bottom electrode (0V).

The square-wave electrode designs feature two electrodes in a straight pattern, with regions of less electric field caused by a larger separation distance. It was expected that neurons could propagate through this channel, aligned to a certain degree; with less alignment observed in the wider sections. An interesting outcome was observed; the neurons preferred the 0V electrode, shown in figure 4.18. The neurons would emerge from the microgrooves, seek out the 0V electrode, and upon reaching it would retract back to the grooves. This 'memory' effect was observed on a number of samples and was completely unexpected. This observation led to the development of a symmetrical design, with four electrodes i.e. the straight electrode design.

Another interesting observation found using the square-wave electrode design was that the neurons were stretched, as illustrated in figure 4.19. This morphing of the network is an unexplained phenomenon. Note also that the neurons that have managed to enter the square wave electrodes seem to be truncated and almost aligned. This could be a promising effect, although it is one which has not been repeated.
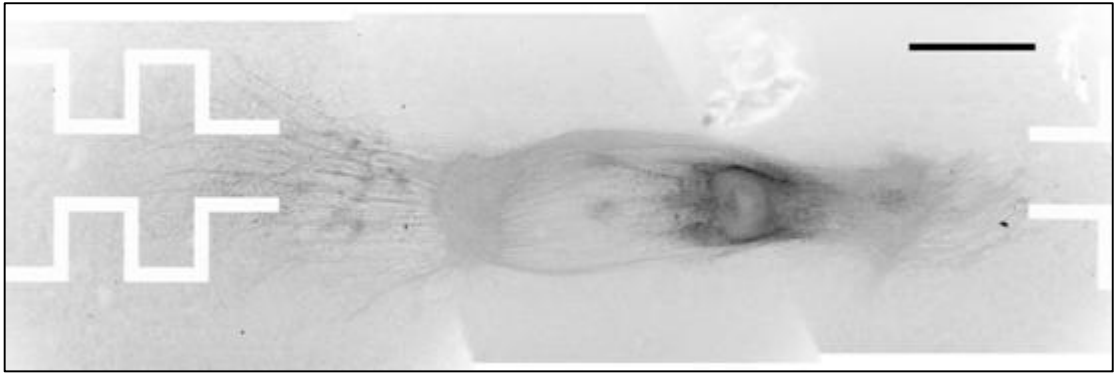
Figure 4.19 a regenerating dorsal root ganglion in the centre of the microgrooves, displaying some morphing of the regenerating neurons. Scale 1 mm.

4.3.7 Hairpin Electrode Results

The hairpin configuration was designed to guide the pre-aligned neurons through a channel, executing a series of turns as they propagated through. Results closely matched the square-wave designs for the same reasons: the neurons had difficulty entering the electrode channel; there was a preferential electrode effect, and there was in general a barrier effect which prevented the neurons from entering the channel. This design was in hindsight rather ambitious, but with optimisation of the electrical parameters perhaps such a design could demonstrate axonal turning and guidance in a controlled manner. Smaller fields and a wider spacing between the electrodes could also improve the results using the hairpin design. Figure 4.20 shows a stimulated result (left electrodes) versus a control (un-stimulated, right electrodes) using the same DRG. The difference in cell growth and orientation is clearly evident. Particularly, again, the right hand turn seen on control side, has been eliminated from the stimulated side through the application of the electric fields.
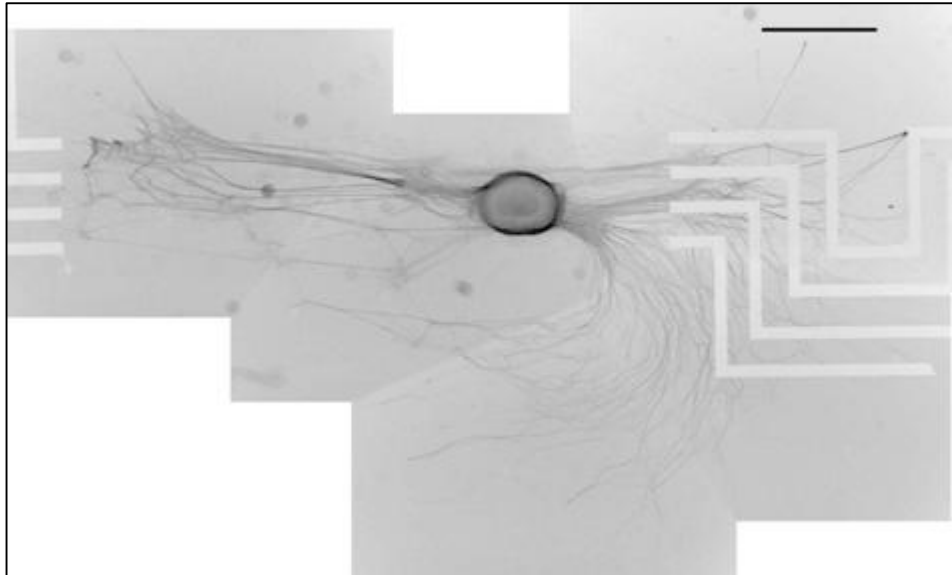
Figure 4.20 retraction of the neurons subjected to electrical stimulation (left side of the network))

versus the right-turning behaviour of the control side (right side of the network). Scale: 1 mm.

Stain: β3-tubulin.

4.3.8   Straight Electrode Results

In order to solve the issue of electrode preference, a symmetrical system was introduced. It was clear that using two electrodes, neurons were unable to move into the space between them. If four electrodes were used to create two electrical barriers, as in figure 4.21, perhaps some of the issues seen could be eradicated. These two barriers would enclose a region in the centre, having zero electric field. Regenerating neurons leaving the microgrooves should have no difficulty in propagating through this channel. Indeed they should be in fact *confined* to this channel by the surrounding electric field regions. If this hypothesis were proved to be true, this could illustrate progress towards the use of alternating electric fields as guidance tools *in vivo*.
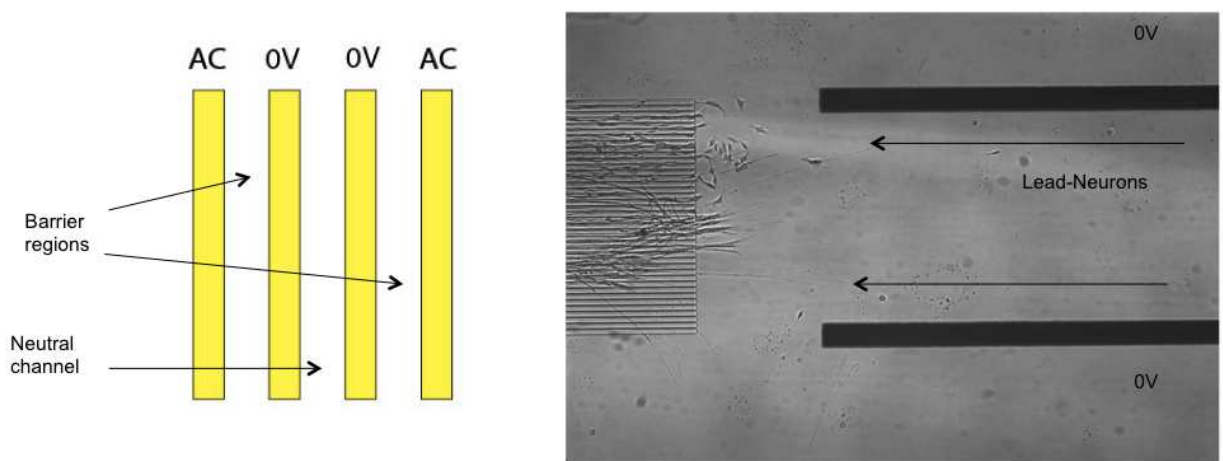
Figure 4.21 introduction of a neutral channel idea. Two barrier regions enclose a neutral zone, allowing neurons to align through the channel. This was designed based on observations from the perpendicular electrode devices.

Theoretically, using four electrodes configured to create a neutral channel enclosed by two barrier regions, the memory effect should be removed. The neurons when presented with a neutral 0V channel and being attracted to both electrodes should pass through the channel without bias. Results indicated that despite using a symmetrical approach, the neurons were in general unable to enter the neutral channel, shown in figure 4.21. It is perhaps the case that a series of ramp-tests as in the perpendicular experiments is required, in addition to tweaking of the modulation of the signal, would result in an increased flow of neurons into the channel. In addition, examining the effect of continuous stimulation versus 1 hour of stimulation could solve some of the issues observed to date.

4.4 Discussion

From sporadic alignment on electrode arrays, to consistent outcomes on hybrid devices, it is clear that alternating electric fields can have a variety of effects on the growth of sensory neurons. Using four different device designs, neurons were aligned with microgrooves as a first stage by topographical cues. Next, using different electrode patterns, and thus different electric field patterns, many electrical waveform parameters were explored. Perpendicular electrodes, orientated at 90 ° to the microgrooves, could enforce a barrier to neuronal growth. By introducing a modulated stimulation signal, unique to this work, retractions and tearing were replaced with safe confinement of neurons at the electrode site. Alternating fields have induced axonal turning at approximately 90 °; the first such display using charge-balanced waveforms. Efforts to use electrodes in a channel

configuration to continue the work of the topographical cues proved to be more difficult. Differences between stimulated and control cultures were observed, but results need further optimisation to prevent retractions and allow the neurons to enter these channels. An interesting observation on control cultures, whereby neurons persist in turning right upon exiting groove structures, remains a mysterious outcome.

4.5 Summary

The effects of alternating electric fields on sensory neurons *in vitro* have been analysed using a number of electrode configurations and both free neurons, and pre-aligned neurons. Pre-aligned neurons, obtained using SU-8 microtopography, show much promise due to their reduced experimental time and reliability in monitoring effects. The safe working electrical parameters to induce controlled effects on neurons have been identified; though have yet to be optimised further. A balance between obtaining a desired neuronal effect and achieving a sufficient level of cell proliferation remains the greatest challenge to using electric fields to significantly improve peripheral nerve repair outcomes for patients. It is hoped that the results documented here provide some insight as to how alternating fields should be applied and what fundamental waveform parameters should be applied. This method of fixing all parameters but one to examine the effect of electric fields on neurons has not been documented elsewhere. The results documented in this chapter form the foundation of progress towards an advanced, electro-activated conduit suitable for *in vivo* implantation. The following chapter describes the progress towards this and how the results in this chapter were used to gain a successful outcome from applied electrical stimulation on biodegradable substrates, powered inductively.

5 Alignment of Sensory Neurons Using Biodegradable Electronic Systems on Polycaprolactone

Injuries to the peripheral nervous system are extremely difficult to repair due to poor regeneration accuracy, scar formation, cell atrophy and axonal escape.[1, 2] Functionalised conduits are often used to improve repair outcomes using electrical, biological, chemical or mechanical cues. A novel inductively powered electrical stimulation circuit on sheets of a biodegradable polymer (polycaprolactone, PCL), has been used to apply alternating electric fields to sensory neurons *in vitro*. Gold microelectrodes and an inductor were fabricated on thin PCL sheets by contact printing and used to apply balanced sinusoidal electric potentials to organotypic cultures of regenerating sensory neurons, resulting in statistical improvements in the degree of longitudinal alignment versus control cultures. This work illustrates progress towards the use of alternating electric fields in an electro-active biodegradable device as an alignment tool with potential applications *in vivo* e.g. in nerve repair conduits. Functionalised biodegradable conduits using safe levels of balanced a.c. electric fields could improve the outcomes of peripheral nerve repair surgery, particularly if combined with other technologies, such as mechanical, chemical and biological growth cues.

5.1 Polycaprolactone

Polycaprolactone (often known as poly-ε-caprolactone) is a biodegradable polymer, found in a wide range of applications. It is characterised by a relatively long degradation time of approximately 2 years, depending on the formulation. It is biocompatible, with many examples of good cell growth when used as a tissue engineering substrate. It has a low melt temperature of approximately 60°C and is soluble in a number of solvents e.g. chloroform and toluene. In this work, polycaprolactone pellets (Sigma Aldrich, UK) with an average molecular weight of ~65,000, were dissolved in chloroform (75% chloroform, 25% PCL). The solution could then be spun onto a silicon or glass substrate. Once the chloroform has evaporated at room temperature, the PCL can be peeled from the substrate, or processed further. PCL has been selected for this project, primarily due to the biocompatibility, and its long degradation time, which is important considering the long period of time typically required for a successful nerve repair procedure. In addition to these properties, its flexibility (when in a thin-film) is an advantage, allowing the fabrication of tubular constructs designed to be wrapped circumferentially around a nerve bundle.

5.2   Design Procedure

The design procedure for a biodegradable receiver, and the inductive powering system, is provided below. The system shown in this chapter has been designed as a prototype to show efficacy in guiding regenerating neurons. Nevertheless, the requirements of an *in vivo* repair conduit have been at the forefront throughout. Whilst the substrate is degradable, those elements that are not degradable should be capable of remaining inside the patient indefinitely. These elements should be as small as possible and made from biocompatible materials. The metal and dielectric options that were considered for this project are:

- Gold
- Silver
- Platinum
- Palladium

- Titanium
- Silicon-Dioxide
- Silicon-Nitride
- Titanium-Dioxide

Materials such as these may be used with the biodegradable polymer PCL to produce electrically active conduits for peripheral nerve repair. PCL has been selected as a strong candidate for the substrate material due to its long degradation time and its compatibility with cell growth. Before describing the design flow in detail, it is useful to outline the target specifications of this system, which will play a key role in determining the requirements of the inductive powering system.

5.2.1   Inductive Link Design

The biodegradable receiver circuit is powered using an inductive link. The functional requirements of the design are shown below in figure 5.1. The transmitter must be capable of transmitting enough power to provide the electrical stimulation waveform to the numerous microelectrodes. Data must be sent over the link to provide the stimulation waveform. The receiver circuit must in turn be capable of retrieving this data and supplying the electrical stimulation waveform to the regenerating neurons. The link should have a certain degree of tolerance for lateral displacement and misalignment between the two inductors. The receiver should be capable of fulfilling these criteria at separation distances exceeding 5 mm. At present, the link is adjusted to give the required output voltage. Planned future developments include the requirement for an alignment technique, and the analysis of the effects of misalignment and their mitigation.
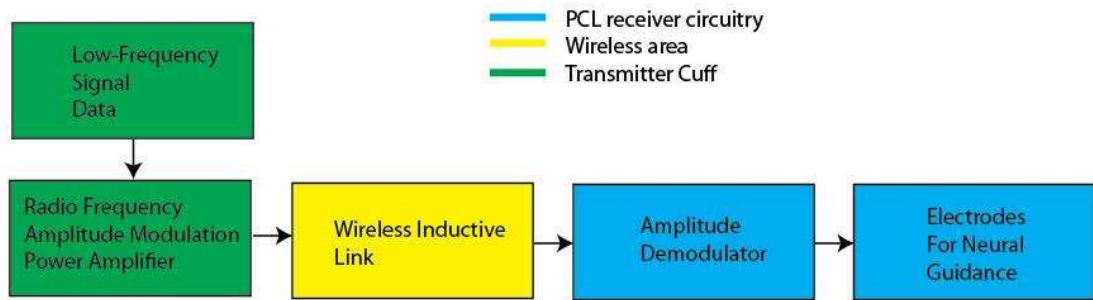
Figure 5.1 schematic outlining the functional requirements of the wirelessly powered, neural stimulator.

It is desirable to meet the following additional criteria. These have been set with a view to ensure the long-term goal of implantation *in vivo* is achievable:

- The quantity of receiver components should be minimised where possible.
- The size of the components should be on the order of 1 mm^2 or less.
- Components should be biocompatible and ideally biodegradable.

In this work, surface mount, off-the-shelf components were selected to develop the system with accurate values and tolerances. With an optimised circuit design and a successful array of biological results, work could turn towards the development and design of biocompatible components of known value and utility. When designing the receiver circuit, the dimensions of the components were at the forefront of considerations. For example, large capacitors, resistors and integrated circuits should be avoided. This led to practical compromises when designing the circuit. Organic thin-film transistors and diodes could be employed in a biodegradable system, increasing the functionality of the receiver. In the first design iteration, basic functionality was sought, with a view to optimisation over the long-term.

5.2.2   Receiver Inductor Design

The first design step centres on the receiver inductor. Often in bio-implantable devices the available space has been defined. In this case, a cylindrical nerve conduit on the order of tens of millimetres in length and approximately 5 millimetres in diameter defines the available substrate space. The receiver system should be produced in planar form, then wrapped around a nerve injury site by a surgeon. A choice of receiver inductor can be made based on these spatial and practical restrictions. A solenoid inductor could be wrapped around a nerve repair conduit, however some form of fastening would be required

to link each inductor turn together. This is impractical, and would have to be performed as part of the surgery. To avoid this complexity, a planar spiral inductor was selected as the most appropriate type to use. A planar spiral inductor can be produced with a single layer process. The only challenge is to wire-bond the central connection to the rest of the circuit. This is non-trivial on a thin-film polymer substrate with thin-film metal. The spiral inductor is superior to zig-zag and meander inductors due to its positive mutual inductance between turns; hence a larger voltage may be induced per unit area of the inductor.

Next, it is desirable to maximise the value of receiver inductance for the space available. However, with a view towards using a printing process for the fabrication, a trade-off must be made between inductance and printing yield. A 15 turn inductor measuring 6 mm x 6 mm has been selected to provide a sufficient value of inductance (1.2 μH), whilst being small enough to expect a reasonable level of printing success. The width of the inductor, when rolled around a nerve diameter of 5 mm, is chosen to ensure the inductor does not wrap underneath the conduit. The length, chosen to equal the width, could be increased to give a higher inductance value, but this again is a trade-off with printing yield. Efficiency and power transfer may be increased in the long-term with the use of a larger inductor.

The track width of 75 μm and spacing of 50 μm were selected to ensure sufficient conductivity and keep the self-resonant frequency of the inductor high. These values also ensured the inductor could have a relatively large number of turns (15). The inductor, as described in the fabrication section, is to be electroplated to increase its conductivity and therefore its quality factor. These values of geometry allow this process to produce the required thickness (30 μm) and prevent the tracks from touching (the track width will increase after electroplating). After electroplating, the inductor tracks are modified to 100 μm wide, with 25 μm spacing. These are approximate values and depend on the numerous electroplating factors.

5.2.3 Coupling Factor Simulations

Next, the transmitter inductor can be designed to match well with the receiver inductor. The transmitter dimensions should ensure a good value of coupling and a good tolerance for variations in lateral displacement. Finite element analysis software (Cobham Technical Services, Vector Fields Software, UK) has been used to observe the distribution of the magnetic flux density from a transmitter. A TOSCA magnetostatic simulation allows the calculation of the inductance and coupling factor for the receiver and transmitter. Straight bar ideal conductors model each inductor. A current of 1A has been chosen for the transmitter inductor to illustrate the distribution of the magnetic flux density across the

receiver location. The surrounding portions of the model have all been set to match that of air. This has been done to simplify the process of analysing many different coil geometries, assuming the magnetic permeability of human tissue is equal to that of air. The energy in the system was integrated to then calculate the inductance and mutual inductance as described in chapter 3.

The aim of this design exercise was to have a relatively constant level of magnetic flux density covering the location of the receiver inductor. This ensures that there is less variability in the coupling factor in response to lateral displacement. This is a trade-off with the value of coupling factor. This approach strikes an approximate balance between the value of coupling factor and the displacement tolerance.
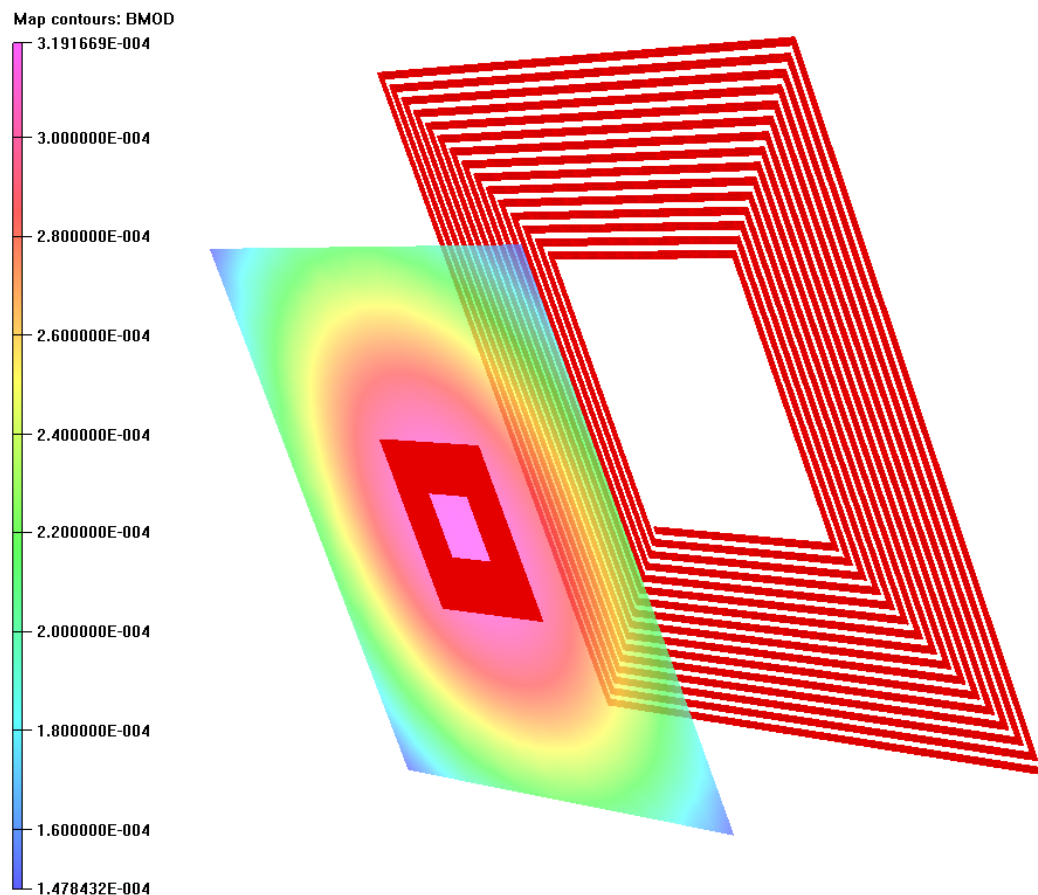
Figure 5.2 finite element analysis simulations assisted with the transmitter and receiver design. The transmitter was chosen to provide a region of constant magnetic flux density at the receiver. The magnetic flux density is expressed in Teslas; the transmitter current is 1 A. The separation distance is 10 mm.

Figure 5.2 shows the magnetic flux density resulting from current flowing in the transmitter inductor. Note the large area of near-uniform magnetic flux density enveloping the receiver. If improvements in efficiency take precedence, a smaller transmitter inductor

may be used at the expense of the displacement tolerance. The transmitter selected for this work is 25 mm x 25 mm, with a simulated inductance of 7 µH. The variation of coupling factor, and mutual inductance, as the separation distance is varied, is depicted in figure 5.3. It is envisaged that a graph such as this can be used as a reference for different injury types i.e. for the case of different distances to the injury site from the transmitter.
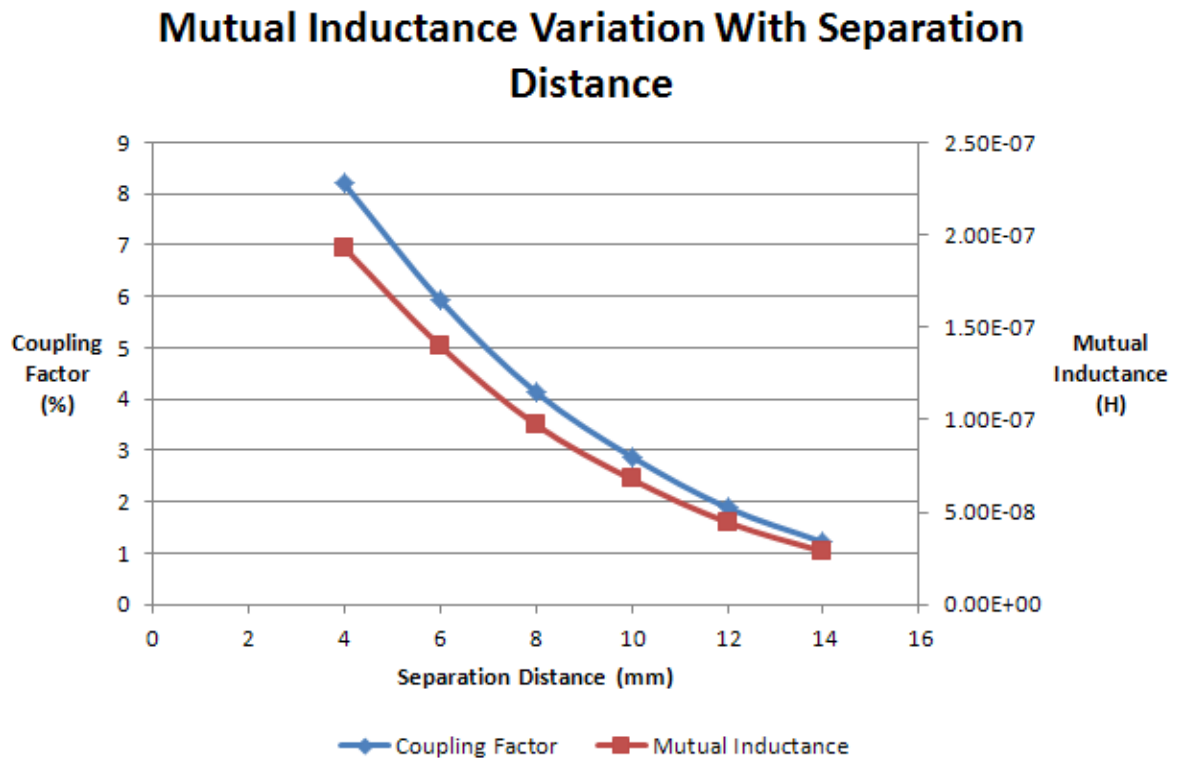
Figure 5.3 simulated coupling factor and mutual inductance variation with separation distance. Simulations were performed with Opera (Cobham Technical Services, UK) using magnetostatic analysis.

5.2.4 Transmitter Driver Design

The receiver and transmitter inductors have been defined; therefore the next step in the design flow is the selection of the driver circuit. The driver is required to provide the large alternating currents that must flow through the transmitter inductor. It also must provide some means of transmitting data to the receiver. This data is to be converted by the receiver to provide electrical stimulation waveforms to regenerating neurons. Contemporary inductive link transmitters often use a class E amplifier [58]. Whilst these amplifiers can reach efficiencies approaching 100%, their design is complex and must be revised for changes in transmission frequency and supply voltage. Design flexibility was a

key feature of this project, and for this reason, the class AB push-pull driver has been selected as the best candidate for the transmitter driver.

Bipolar darlington-pair devices were used in a push-pull configuration. Two PN junction diodes bias each darlington-pair device at two base-emitter voltage drops. This overcomes the distortion loss common to class B configurations, at the expense of some power loss when both transistors are briefly switched on (when the input voltage is zero). The output of the circuit is a parallel LC tank, tuned to the transmission frequency. This capacitor must be changed in order to retune the circuit. The output inductor is made from copper tracks on PCB, measuring 25 mm x 25 mm.

Amplitude modulation (AM) was selected as the best means of transmitting data to the receiver circuit. Demodulation at the receiver would involve a small number of components when compared with other data transmission schemes, and is therefore better suited for biodegradable applications. Base modulation was used here i.e. an amplitude modulated carrier signal was applied to the base of each transistor. The data signal was supplied from a signal generator (Tektronix, USA), typically with a modulation index of 50 %. Whilst this is a prototype, a battery powered transmitter cuff would contain a discrete signal source. The carrier frequency of 800 kHz was selected to balance efficient power transfer whilst being below the resonant frequency of the receiver inductor (13 MHz). The data signal was 100 Hz i.e. the desired electrical stimulation frequency, applied to the regenerating neurons.
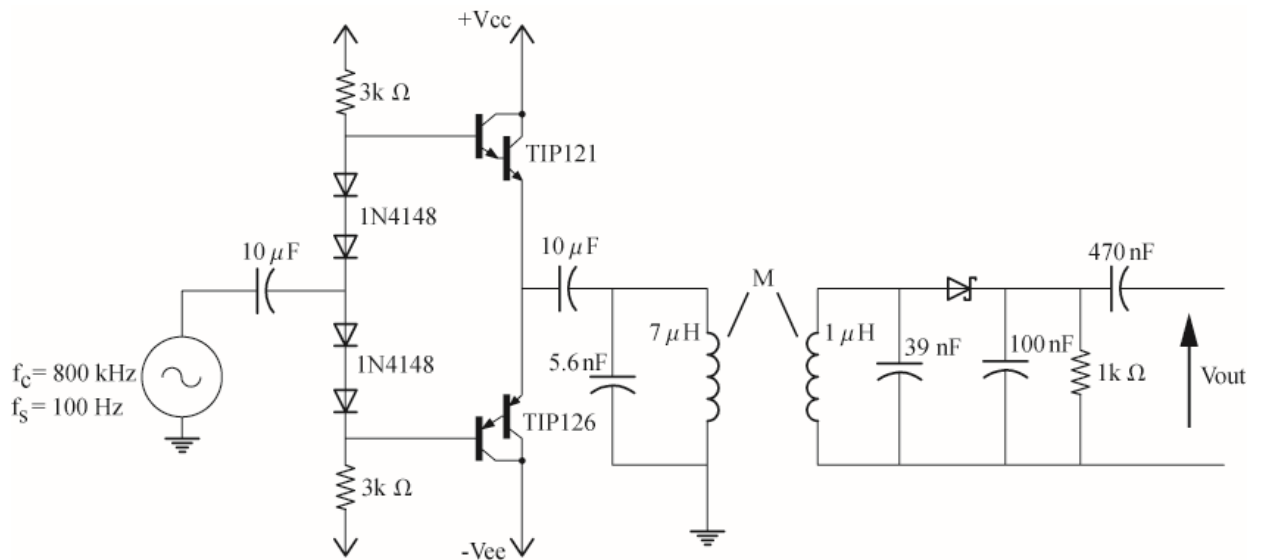
Figure 5.4 the inductive powering system schematic, with the transmitter on the left and the receiver on the right. The two transistors form a class AB push-pull driver capable of driving the large alternating current through the LC tank circuit. The transistors are biased with two PN diodes to minimise crossover distortion. The input signal is coupled in through a capacitor. This signal causes small changes in the base emitter voltage, causing large changes in the collector currents of the transitors. Each transistor conducts for one half-cycle. The resulting a.c. current through the inductor induces a voltage in the receiver inductor. This induced voltage is fed through an envelope detector and a d.c. blocking capacitor with the resultant output used as the electrical stimulation signal for the regenerating neurons. A schottky diode has been selected to lower the required induced voltage.

Simulated Receiver Voltages
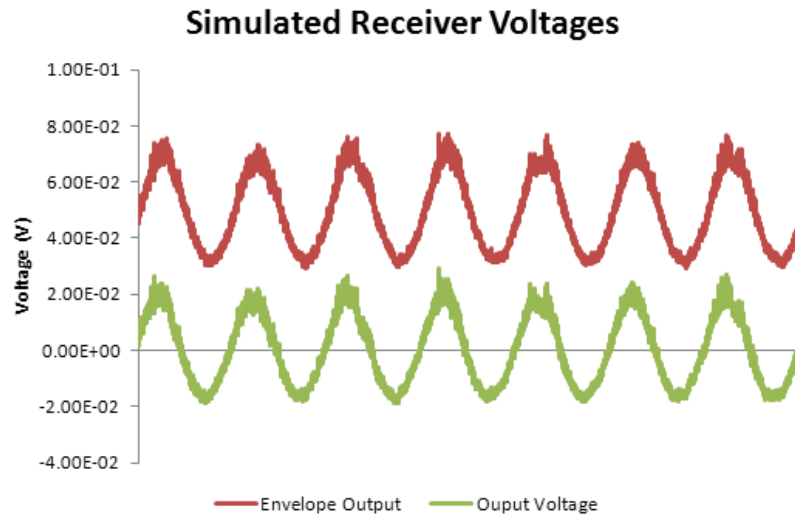
Figure 5.5 simulated receiver circuit voltages, showing the envelope detector output, and the

system output after the d.c. component has been removed. The simulations were performed with

pspice.

5.2.5 Receiver Circuit Design

With a suitable transmitter driver and data modulation scheme, the receiver circuit may be designed. The receiver must take the induced, modulated carrier signal at the receiver inductor, and extract the data signal. This signal can then be used to stimulate regenerating neurons. The receiver consists of an LC tank resonator, an envelope detector, and an output capacitor to remove the d.c. component from the envelope detector output. The LC tank, tuned to the carrier frequency, cancels the receiver leakage inductance. The impedance of this part of the circuit is therefore real and dominated by the parasitic resistance of the inductor. The induced voltage appears across this tank circuit. This induced voltage must be of sufficient amplitude to overcome the diode forward voltage. The power from the transmitter can be adjusted to ensure this is the case.

The schematic of the complete inductive powering system is shown in figure 5.4. The envelope detector consists of a Schottky diode, a bleed resistor and a smoothing capacitor. The envelope detector should track changes in the AM signal amplitude, filtering the carrier through the capacitor. The bleed resistor allows the capacitor to discharge during the negative half-cycle. These changes in amplitude centre around a d.c. voltage which must be removed before the signal can be applied to the regenerating neurons. This is done through a series output capacitor. The simulated receiver voltages are shown in figure 5.5. The values used for the output and filter capacitor have been selected with a view to

minimising their size. Larger capacitors would reduce the amount of carrier component present on the output signal. However, smaller components would have a greater impact on *in vivo* performance. Smaller component values are easier to design and build when producing biodegradable components, in addition to being of suitable size for implantation.

5.3 Fabrication Process Development

The conduit material (polycaprolactone, PCL), is a biodegradable polymer with a long degradation time and good cell growth properties. However there are a number of significant challenges to be overcome before producing an electrical stimulation system on PCL:

1. The polymer melts at approximately 55 °C. A photolithography process is therefore unsuitable.
2. The polymer is ideally thin and flexible when used as a nerve repair conduit, making it difficult to process using conventional techniques.
3. The polymer is mechanically weak, preventing the use of many polymer printing techniques, which often require a high imprint pressure.
4. The polymer is incompatible with most solvents used in wet-etching and lift-off, preventing their use for patterning metal films. In particular the inability to use acetone, methanol and isopropanol poses a significant challenge.

Despite the challenges in working with PCL, there are some advantages that have been exploited in this work. Some chemicals are known to be compatible with PCL; in particular the use of AZ400k photoresist developer allows the use of AZ series photoresist [113]. The low melt-temperature of the polymer is of great assistance during transfer printing, preventing features on the stamp from deforming due to excessive temperature or pressure. The steps below outline how patterned thin-films of Au can be transferred to the thin-film polymer , used in this work to create a 15.turn planar spiral inductor (6 mm x 6 mm area, 75 μm track width, 50 μm track spacing) as well as the electrical interconnect and component footprints, shown in figure 5.6.
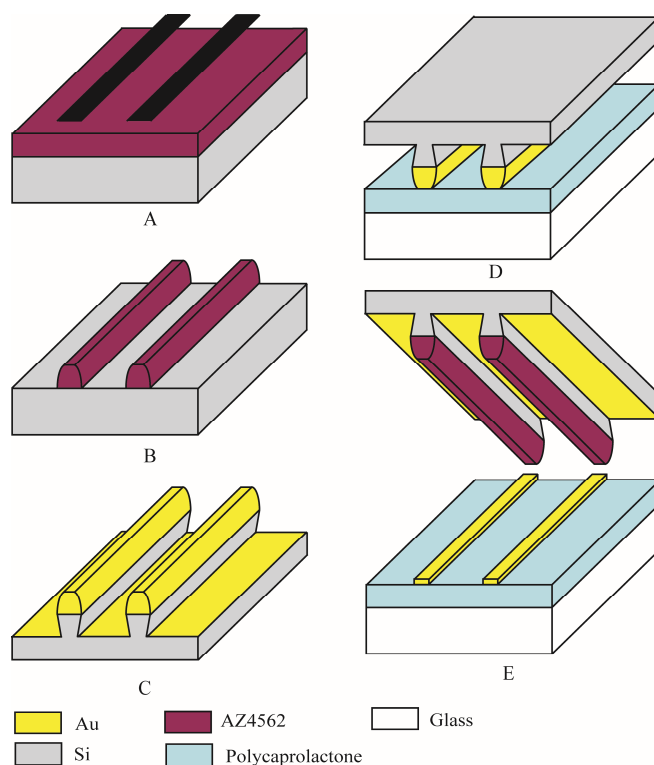
Figure 5.6 schematic of the transfer printing process to transfer patterned au films. AZ4562 photoresist, spun in two steps to a thickness of 30 μm, exposed through a photomask (A). Development of the photoresist (B). Dry-etching of the silicon substrate, followed by evaporation of 400 nm Au (C). The stamp is pressed into polycaprolactone on glass (D) at 65 °C. Removal of the stamp (E) completes the transfer printing process.

5.3.1 Stamp Production

The printing procedure is divided into two sections: stamp production and target substrate preparation. The stamp is produced using photolithography and dry etch techniques, described in a concise manner below. A detailed description can be found in Appendix B.

1. Two layers of AZ4562 photoresist are spun onto a silicon substrate to a thickness of 30 μm. The photoresist film is exposed to UV light through a photomask.

2. The exposed areas of photoresist are removed in AZ400k developer, leaving a patterned film on the substrate.

3. The substrate is dry-etched selectively, to a depth of 15 μm with an undercut profile.

4. The target substrate is prepared by spinning a layer of polycaprolactone (25 % in chloroform) onto a glass or silicon substrate.

5. The stamp is printed into the target substrate at 65 °C with minimal pressure. The stack is cooled to room temperature, followed by removal of the stamp. This yields selective pattern transfer to the target substrate.
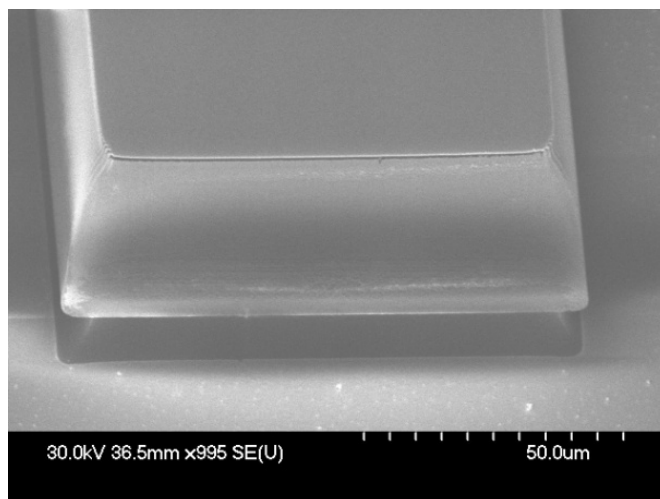
Figure 5.7 scanning electron micrograph showing a dry-etched silicon pillar with a sloping

sidewall profile. The AZ4562 photoresist column is on top. This profile isolates the metal on the

substrate from the metal on the photoresist film.

Figure 5.7 shows the printing stamp after step C. The photoresist film sits on top of a silicon column. The column has a sloped sidewall profile designed to induce a discontinuity in the gold metal film. This prevents the transfer of unwanted sections of metal and greatly improves the printing yield. This profile was achieved by using the Bosch process for deep dry-etching of silicon with an increased etch cycle, as described in appendix B.
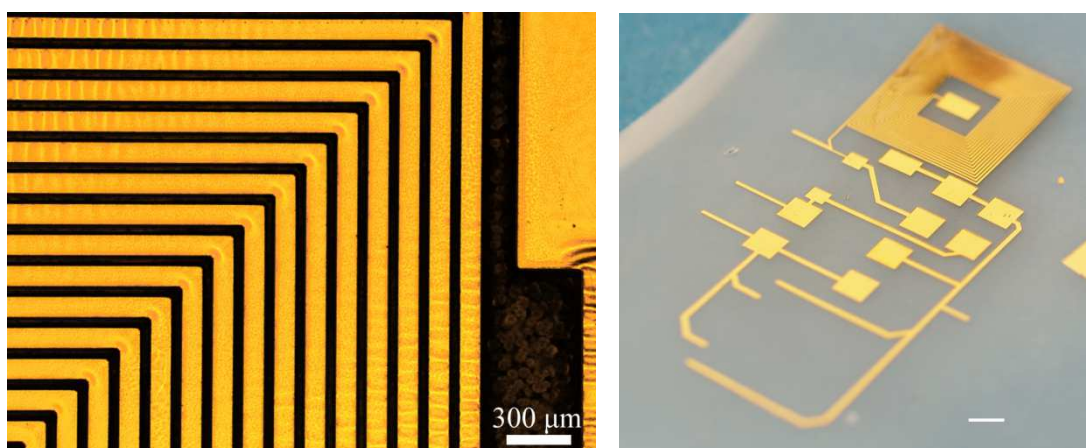
Figure 5.8 a micrograph showing a section of the 15 turn spiral inductor (left) and an image

showing the printed inductor and component footprints on polycaprolactone (right).

The fidelity of printed features is shown in figure 5.8. The 15 turn inductor segment depicts the accuracy of the printing process. The printed gold circuit (right) shows that the process is capable of printing accurate features across a large area (the inductor is 6 mm

square). Figure 5.9 shows a printed schematic after electroplating to 30 um thickness and the addition of gold wire bonds to connect the inner spiral inductor connection to the remainder of the receiver circuit. The debris seen either side of the circuit is a result of the silver conductive paint, required to connect every metal node to the electroplating substrate. This conductive paint is then removed prior to wire-bonding and the component attachment phase.
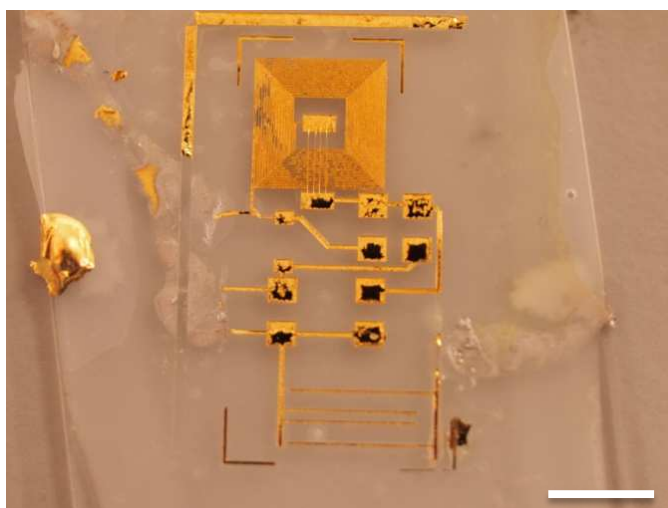
Figure 5.9 a printed receiver layout, featuring a 6 mm x 6 mm spiral inductor and component footprints. Gold wire bonds link the central pad to the outer circuit, completing the circuit. The printed gold is electroplated to a thickness of ~30 μm. Contacts have been made to the 'tabs' to allow electroplating. Scale: 5 mm.

5.3.2   Receiver Component Assembly

Components were attached to their respective footprints using silver conducting paint, as shown in figure 5.10. Surface mount components were selected, in 0805 packages, with a view to replacing these with biodegradable alternatives. These components offered accurate values and predictable tolerances, which would not have been the case with biodegradable components. This property allowed good replication of performance between experiments. It was undesirable at this stage to introduce another variable, when so many parameters remained as estimates. It is hoped that by publishing this work and highlighting the results obtained using this biodegradable approach, components may be sourced from interested authors in parallel to the development of these components as part of the future work and developments.
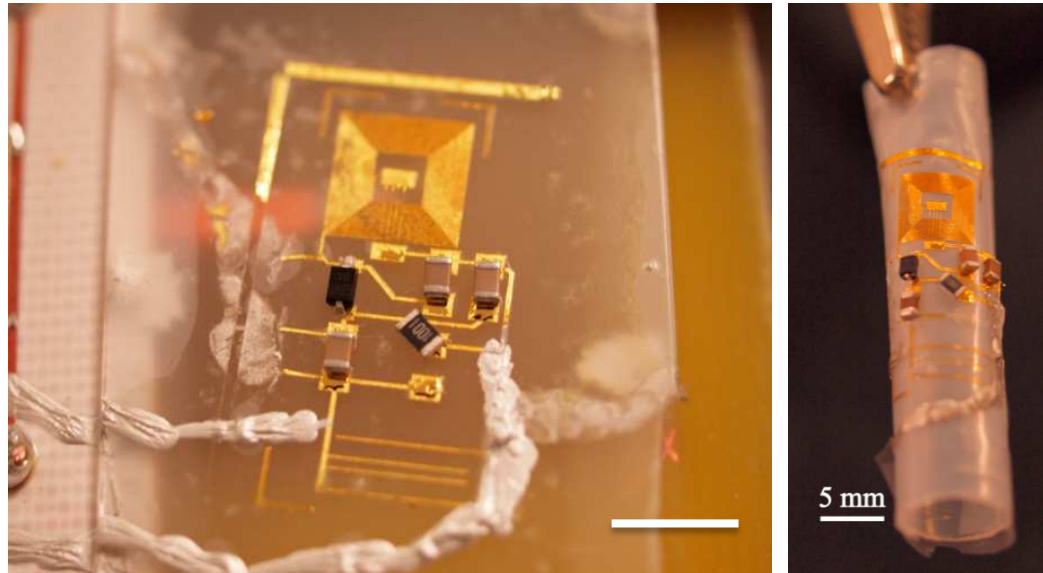
Figure 5.10 an assembled PCL receiver with surface mount components attached using silver conducting paint (left). The same receiver rolled around a plastic conduit. Components and wired bonds are orientated longitudinally to avoid detachment. Scale: 5 mm.

5.3.3 Quality Factor of Printed Inductors

A reasonable value of inductor quality factor is required for efficient power transfer. A value in the range 1 – 10 was selected. This ensures that the parallel receiver capacitor can adequately tune the receiver inductor to the transmission frequency, and reduces the energy lost per cycle. Figure 5.11 illustrates this effect. The input voltage can be thought of as the induced voltage in the receiver inductor. It can be seen that at reasonable quality factor values, the output voltage of the LC tank circuit is higher than the induced voltage. At quality factors lower than 1, the output voltage decreases as energy is lost in the parasitic resistance of the inductor. The skin and proximity effects have been assumed to be negligible at these frequencies. Simulations were performed using pspice. The parasitic capacitance has been included in the parallel capacitor (39 nF). The parasitic components of the parallel capacitor have been neglected, as the parasitic resistance of the inductor dominates in this case.
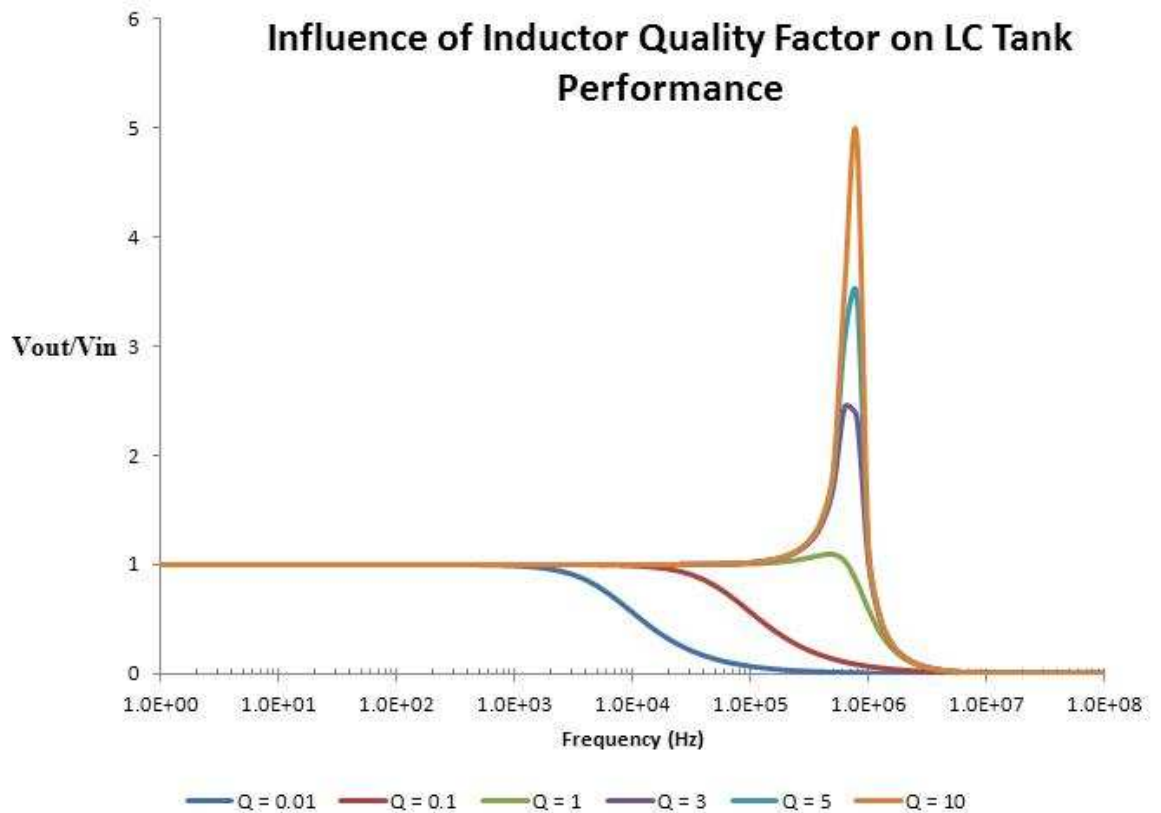
Figure 5.11 simulation values of the output voltage of a parallel LC tank circuit relative to the input voltage. Simulations were performed using pspice. The inductor value is 1.2 μH and the capacitor is 39 nF. The resistance of the inductor is calculated to give the quality factors shown, at a frequency of 800 kHz. It can be seen that below a unity quality factor the output voltage of the circuit falls below the input voltage. In a receiver circuit, this would put great pressure on the transmitter driver.

Prior to electroplating, the quality factor is on the order of 0.01, making it impossible to induce enough voltage in the receiver at practical transmitter power levels. The quality factor of the printed inductor was measured after the electroplating and wire-bonding steps. Printed inductors had a parasitic resistance in the range 3-17 Ω, which varied with the electroplating process. The thickness of the electroplated gold tracks is dependent on a number of factors, e.g. temperature, current density, seed-layer quality and surface roughness. It is this variability which impacts upon the range of resistances achieved. Also, any significant printing defects can result in higher resistances, which when accumulated along the full length of the inductor could have a significant impact. The measured quality factor shown in figure 5.12 is compared with a 1.2 μH inductor, with a parasitic resistance of 10 Ω. The measured quality factor allowed these printed inductors to be used practically

in the selected frequency band. Further improvements to the quality factor could be made by increased control of the electroplating, perhaps through the use of a commercial company. A larger inductor would also cause an increase in the quality factor; however the value here proved to be sufficient for the requirements of the project.
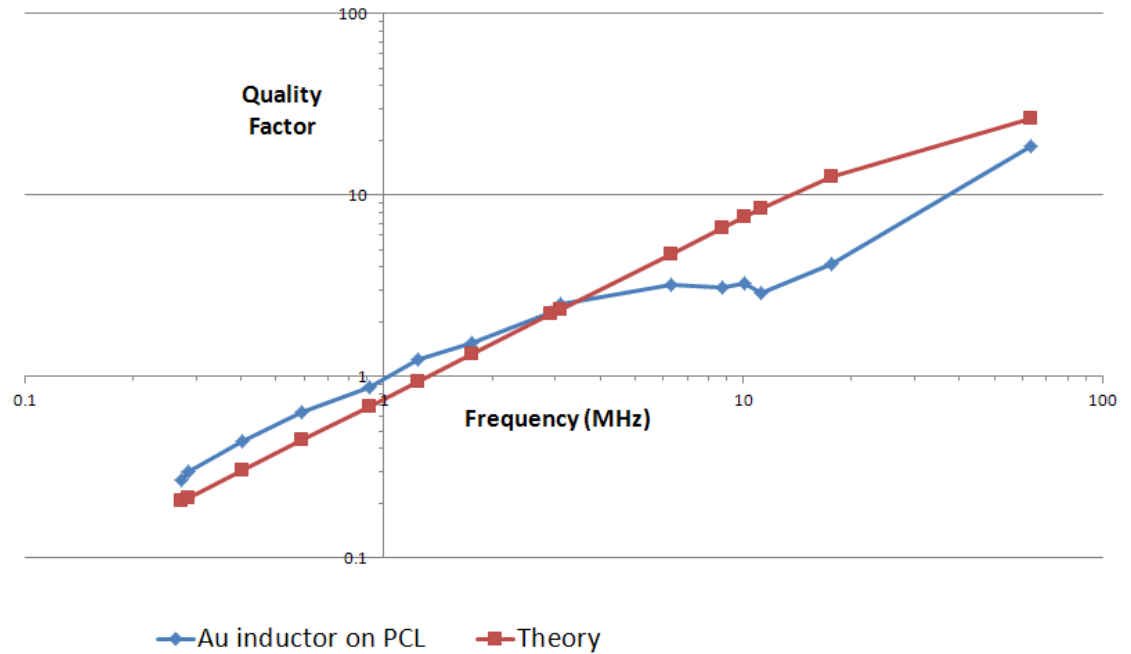
Figure 5.12 quality factor measurements of the printed inductor on the biodegradable polymer,

polycaprolactone. The theoretical value of quality factor for a 1.2 μH inductor with a parasitic

resistance of 10 Ω has been shown to provide a comparison. The self-resonant frequency of the

inductor is 13 MHz.

5.3.4 PCL Electrode Module Production

The same printing process was used to fabricate electrodes on PCL, used for cell culture and applying electrical stimulation to the neurons. The electrodes were made with 400 nm of Au. The planar PCL/electrode module, supported by a glass substrate, was then mounted on a PCB. The Au electrodes were connected to the PCB using silver conducting paint. Plastic tubes approximately 20 mm in diameter were attached using silicone sealant to the electrode modules to act as cell-culture wells.

5.3.5 Printing Reliability

One stimulation module was produced for *each* experiment, thus the reliability of the printing was critical to mass-producing these units. Approximately 100 stimulation test modules were produced for this project with a yield of around 85%. The fabrication yield was dictated in large part by the PCL substrate, which due to its high viscosity tended to

form numerous air bubbles or gaps when spun onto the substrate. Missing segments in the printed features would occur over the gaps. In order to achieve consistency between experiments, gaps in electrodes were not repaired using silver paint (or other method; only successfully printed electrodes were kept.

Printing success was approximately 40% for the printed receiver circuits, again due in part to the substrate and also due to the length of the inductor. Longer conductors have higher failure rates as any gap in the conductor is a failed print. The dimensions of the inductor, 6 mm x 6 mm, ensured a good balance between inductance (1.2 µH) and printing success. Larger inductors were printed but with a lower success rate. Larger inductors were held in reserve, should they be required. Printing success was dramatically improved by the addition of the dry-etch step. This step completely removed the possibility of undesired metal being printed, preventing the inductor tracks from being connected. With a dedicated machine or tool to apply the printing pressure, uniformity and yield would be sure to increase when compared with working by hand. In a commercial process, techniques like cold-welding or 3D stack printing could allow the repair of those printed samples that are almost complete. In this way, small sections of metal could be added, saving some devices which would be otherwise lost.

5.4   Experimental Set-up

5.4.1   Electrical Stimulation Protocol and Configuration –neutral channel
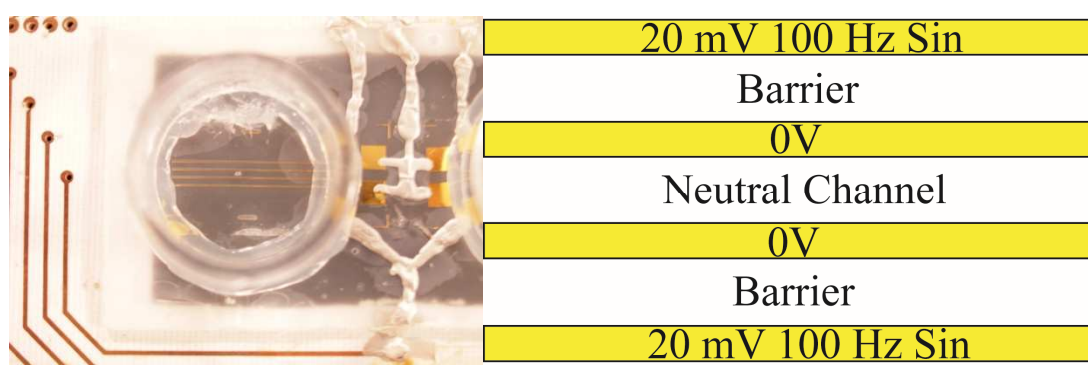
Figure 5.13 quad-electrode stimulation module (left) with DRG clearly visible in the centre. A cell-culture well was defined using a plastic ring, sealed with silicone sealant. Connections to a printed circuit board were made by silver conducting paint. The stimulus protocol and electrode configuration used to create a neutral channel is also shown (right).

Here, the problems described in the preceding chapter with neurons being unable to enter the straight electrode configuration were overcome. This was done by simply seeding the DRG in the centre of the electrode channel. The cell culture technique is outlined in

appendix C. The neurons were stimulated using a continuous stimulation protocol, using a 100 Hz sinusoidal signal of 20 mV amplitude (1 mm electrode spacing) depicted in figure 5.13. Four electrodes were used in a unique neutral channel configuration, designed to confine neuronal growth to this channel, creating a longitudinal alignment profile. Two inner electrodes, having a potential of 0 V, and two outer electrodes with the signal applied, created two a.c. barrier regions which the cells could not enter. The stimulation signal described here was applied over all independent experiments. The aim was to first document a change in the distribution of the neurons and to then repeat this observation over a large number of experiments. As this has proved successful, as will be shown in the results section, it is hoped that a series of experiments examining the effects of the electrical stimulation parameters may be employed. Linking the results achieved using wirelessly powered circuits, with those on pre-aligned neurons, could further reinforce the *in vitro* model described.

5.4.2 Hardware Set-up

Receiver circuits and stimulation modules were assembled on PCBs to keep them in place during testing, as shown in figure 5.14. The receiver was placed directly above the transmitter inductor, at a distance of 5 mm. This assembly was placed in a hot-room environment at 37 °C. Stimulation test modules were unplugged once per day to exchange the culture medium. Control cultures were placed in the same room, at 37 °C but were not connected. They were however, still connected to a PCB using silver conducting paint. Regenerating neurons from a DRG were stimulated for 7 days. This was an estimate based on the approximate number of days it would take to demonstrate an observable change on the growth of the network. It was paramount not to stimulate for too long, as the cells may retract or die. It is hoped that the duration of the experiment will be optimised and an effort will be made to make the PCL thin enough to facilitate time-lapse recording of the regenerating neurons.
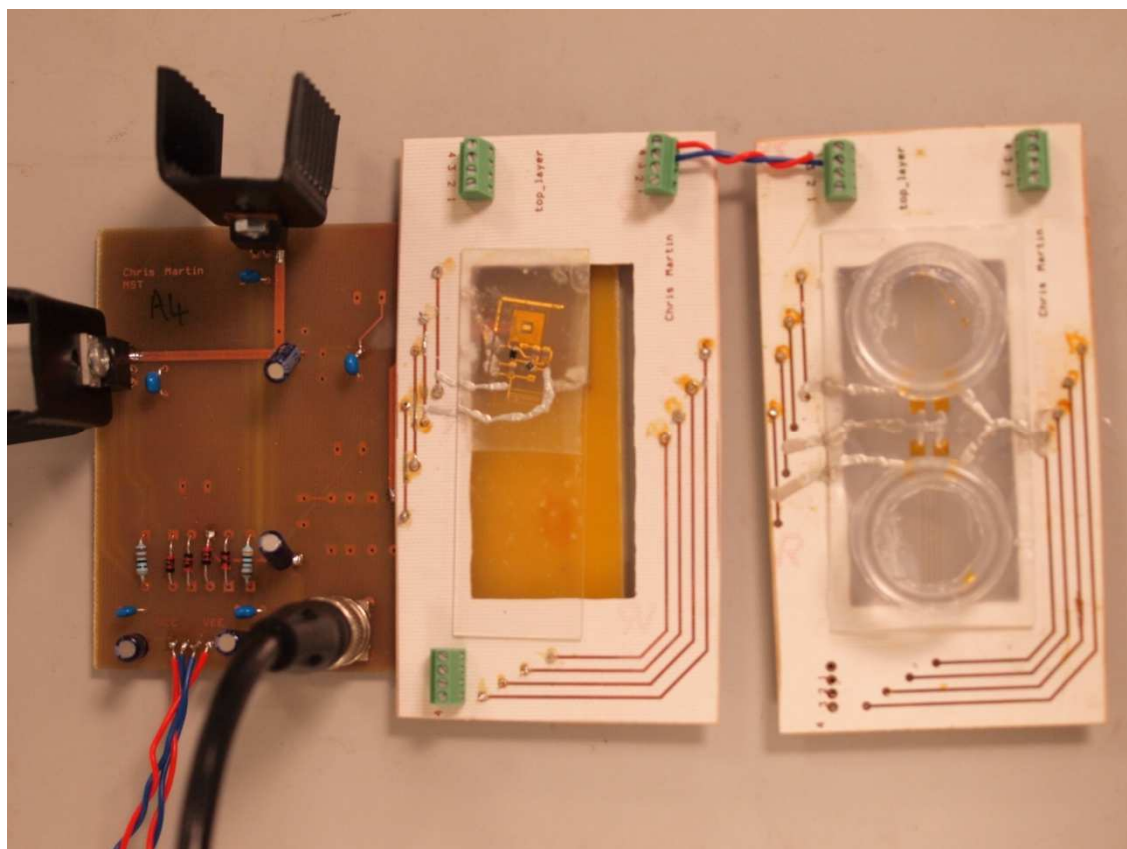
Figure 5.14 the class AB transmitter PCB, powering a receiver circuit on PCL. The receiver is then connected to a twin stimulation module. Silver conducting paint is used to connect PCB conductors to the gold electrodes on PCL.

5.5   Results

The results achieved using inductively powered receiver circuits on planar sheets of PCL are outlined below. Results are sub-divided into control and stimulated cultures. The aim, to confine neurons between electrodes, has been met here, demonstrating for the first time the action of alternating electric fields on regenerating neurons at the cellular level. Whilst planar devices have been used here, supported by glass substrates, progress is being made towards their implementation as *in vivo* nerve conduits.

5.5.1   Control Culture Results

Control cultures showed a random distribution and a preference for growing over the surface of the Au electrodes. It is hoped that with further experimentation using these devices, an explanation may be found identifying the cause of this behaviour. Despite this effect, the controls served as a good reference to compare any applied electrical stimulation growth profile. This was in contrast to the work on pre-aligned neurons, where unusual control results hampered the drawing of meaningful conclusions. With these control results, attention can now turn to analysing the stimulated results.
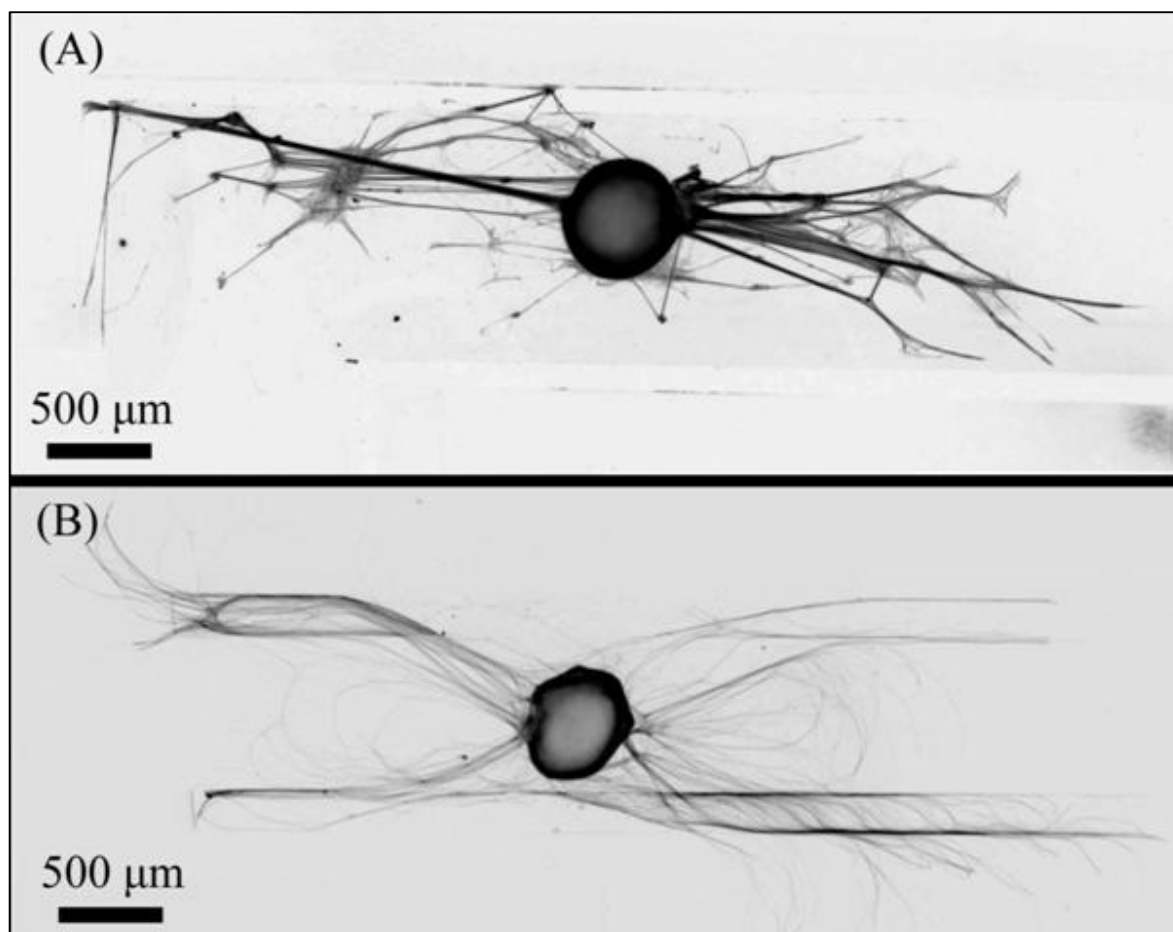
Figure 5.15 a comparison between the effects of electrical stimulation from a wireless receiver (A) and a control sample (B). The electrodes in the active sample are confining neurons to a channel.

5.5.2 Electrical Stimulation Results

Using the device described above, experiments and controls were conducted by applying a 20 mV, 100 Hz signal to the cells in culture. In the presence of the a.c. signal the induced potential barriers, with a maximum electric field of 0.2 Vcm^{-1}, confined the outgrowing support cells and the regenerating axons to the space between the electrodes. This phenomenon was not observed in the control cultures, where no a.c. stimulation was applied to the electrodes. Six stimulated and seven control results were used across three independent experimental trials. The micrographs in Figure 5.15(A and B) demonstrate this behaviour. Note that in the activated example (Figure 5.15(A)) there is no cell growth on the electrodes, whereas in the control (Figure 5.15(B)), growth is prolific over the electrodes. The behaviour is repeated across the three independent trials.
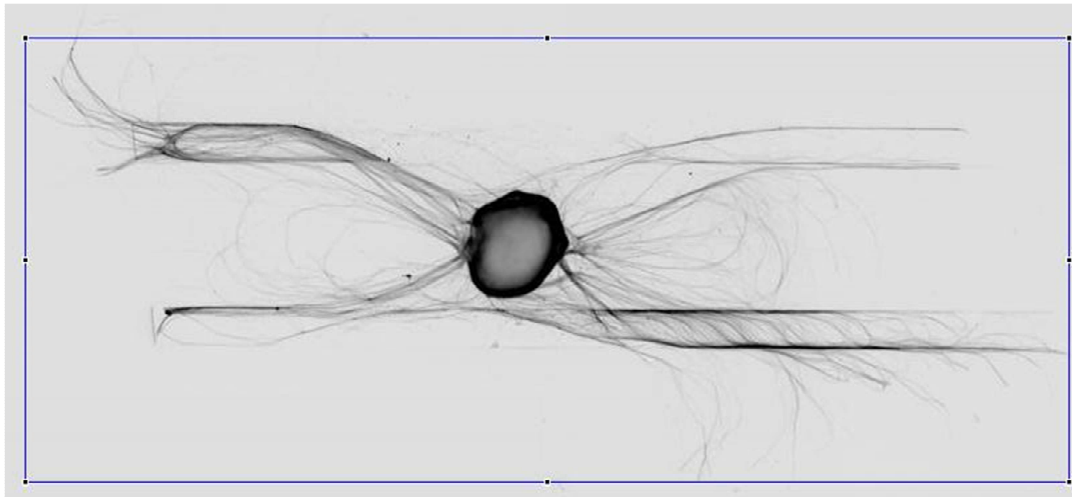
Figure 5.16 depiction of the aspect ratio measurement. the extent of the neuronal network in the x and y directions was measured three times for each experiment (shown with a blue rectangle). An average value was then taken and collated in terms of control and stimulation. This was performed using ImageJ. Colour inversion has been applied to the original image.

ImageJ software was used to measure the width and length of the axonal network for each sample, and its aspect ratio defined as the length of the network divided by the width, where the length was measured in the direction of the neutral channel, shown in figure 5.16. The standard error was used to quantify any uncertainty in the aspect ratio. Measured aspect ratios for stimulated cultures were significantly higher than for the control cultures, indicating a higher degree of longitudinal alignment as shown in figure 5.17.
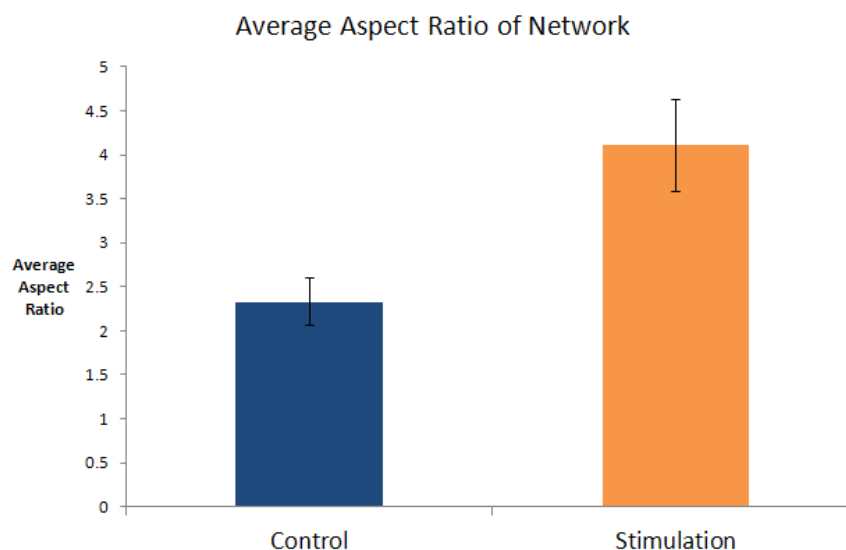
Figure 5.17 aspect ratio measurements from successful control and stimulation experiments, with the standard error included. Stimulated cultures had on average, higher aspect ratios, caused by the confinement from the electrical stimulation.

The angular distribution of axonal orientation also helped to quantify the effect of the electrical stimulation, with a distinct alignment profile for stimulated cultures. Polar angular measurements were obtained by setting a 'dark threshold' for each image, and plotting an oval profile of the number of crossings that exceed the threshold as shown in figure 5.18. Experiments were conducted in three batches, with each module stimulated for seven days at 37ºC.
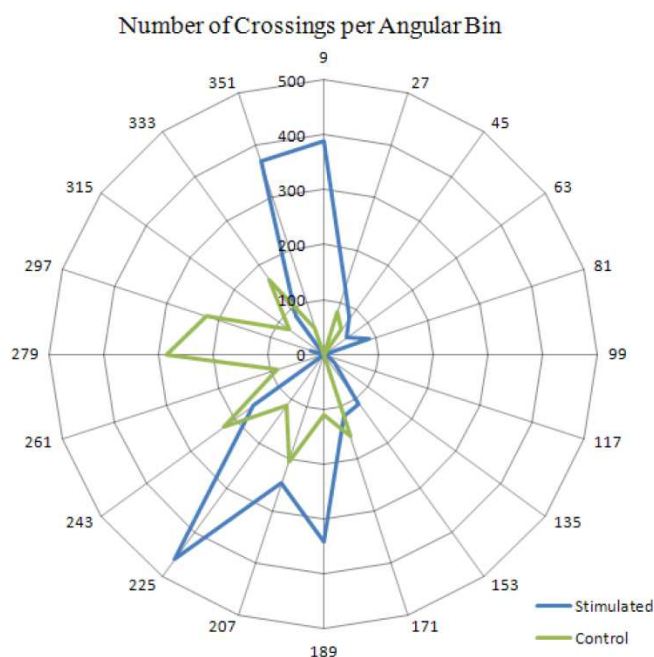
Figure 5.18 polar angular measurements depicting the distribution of the neuronal network. Stimulated cultures had an elongated profile when compared with control cultures.

5.6 Discussion

It has been shown here, for the first time, the use of alternating electric fields to influence neuronal growth at the cellular level by wireless stimulation of an electro-active device fabricated onto a biodegradable material. To do this a novel circuit on a biodegradable flexible membrane has been designed and implemented. Studies have shown the effectiveness of electrical stimulation applied during a PNS repair in a variety of ways. This study aims to provide the means to reliably fabricate a new type of device that will allow the use of electrical stimulation by applying sub-threshold inductively powered a.c. fields, and that is suitable for implantation. The findings reported here indicate that neurons can be confined near an electrode using a region of alternating electric field. By growing the neurons between two electrodes, the neurons are faced with a barrier on either side. It has been previously been established that neurons in culture will grow directionally in the presence of a d.c. voltage, with the growth cone being repelled by the anode and attracted to the cathode (cathode-preference) [13]. Because a wireless device was sought, the effect of applying a high frequency (> 1 kHz) a.c. stimulation was investigated, however there was no observable cellular response to the applied field. The majority of studies have shown the effects of electrical stimulation across the 1-200 Hz frequency band [31, 32, 114]. The detection of a change in the outgrowth from a regenerating dorsal root

ganglion (DRG) as a consequence of the application of a demodulated low frequency (100 Hz) signal has been described. This 100 Hz signal is slow enough to produce a barrier effect [112], whilst being of sufficient frequency to enable practical electronic implementation.

5.7 Conclusion

Electrodes printed by using a novel technique on PCL, a biodegradable polymer that has FDA approval, have been used to apply alternating electric fields to sensory neurons. The device is envisaged to be implantable, and delivers the electrical fields using inductively powered electrical stimulation from an external, wireless, source. The system has been used to demonstrate increased alignment of sensory neurons *in vitro* when compared with control cultures. This confinement has been shown to be possible using sub-threshold alternating electric fields by employing a novel four-electrode configuration, creating a channel with no electric field for neurons to propagate through. Further work is needed to study the rate of growth and percentage of aligned neurons by modifying the electrical parameters, and to show that an electro-activated neural conduit can be made.

Rogers et al have reported on the use of silk as a biodegradable substrate with biodegradable, wirelessly powered electronics [115]. They demonstrate complete degradation of their circuits in an effective manner. However, due to the thin-film nature of the receiver inductor, the transmission frequency is in the GHz range to overcome the large parasitic resistance. This contrasts with the lower transmission frequency reported here, aimed at allowing this device to be suitable for repairing injured nerve tissue deep within the body, on the order of a few centimetres or more. Using frequencies in the GHz range are also likely to induce large eddy currents in surrounding tissue and may not be capable of penetrating deep enough into the tissue for peripheral nerve repair applications, but are well suited to transdermal applications as demonstrated in the reported publication.

Other work, such as that reported by Vladu [116] place an emphasis on flexible electronic interconnect on a biodegradable substrate. These implants can generally withstand large deformations and are therefore highly applicable to wearing on the surface, or underneath, the skin. These circuits, made from predominately gold films, could be subjected to the electroplating process here to enable their use in peripheral nerve repair surgeries. These flexible interconnect devices offer much promise in including non-flexible items, such as CMOS chips and passive components, isolating them from mechanical damage.

The system reported in this chapter has the potential to be used *in vivo* to improve existing repair rates and functional outcomes. It is also comparable to contemporary wireless biodegradable electronics, in that further biodegradable component development is required here, but the practical peripheral nerve repair transmission frequency and stimulation frequency has already been shown. It is hoped that there is good scope for a valuable nerve repair system to be developed, perhaps with the inclusion of flexible interconnect and biodegradable refinements.

6 Wireless Electrical Cell Measurements

Electrical cell impedance sensing (ECIS) can represent cell-density and cell-death over time as changes in electrical impedance. A suitable method of measuring cell growth over time within an implant is sought here. A wireless interface, capable of detecting cell behaviour through measured data at the transmitter, was thought to be applicable for this task. Caco-2 cells were used for each experiment reported here. Caco-2 cells are a human epithelial cell line, which resemble the lining of the small intestine. They readily form a cell monolayer during tissue culture and are therefore ideal for measuring electrical impedance measurements as cells grow over the surface of electrodes. The cell culture and addition of the detachment agents was performed by Théo Dejardin in the Centre for Cell Engineering.

Impedance measurement differences between confluent caco-2 cells and cells removed using trypsin have been reported here. An inductive powering system allows these changes to be measured at the transmitter, with a view towards development of an implantable, biodegradable device. Wireless electrical measurements, using an inductive link powering a passive receiver circuit, illustrates how changes in the density of caco-2 cells can be detected by measuring the transmitter output voltage. Cell-death events were detected wirelessly in the same way. This *in vitro* wireless sensing technique could be enhanced and developed on biodegradable substrates, leading to systems suitable for implantation. There are many applications for this technique e.g. in wound repair, peripheral and central nervous system repair and in drug delivery, and integration with neural stimulation systems as a feedback mechanism.

6.1 Electrical Cell Impedance Sensing

As cells grow, changes in their size and density alter their contact area with the substrate. If these morphological changes occur over an electrode a change in electrical impedance can be detected. ECIS is implemented using dedicated instrumentation *in vitro* to measure changes in cell behaviour. In this way, measured changes in impedance over time can be used to indicate the level of cell density, the location of cells and the onset of mass cell atrophy (death). Electrode designs can be targeted to detect single, or multiple cell events. The interface between electrodes and solution is an important factor in cell-impedance measurement systems. When metal electrodes are immersed in an aqueous solution opposing charges accumulate on both sides of the metal/medium interface. The net charge on both sides of the interface is equal. This effect is termed the electrical double layer and an effective capacitance, the double layer capacitance, C_d, can model this effect.
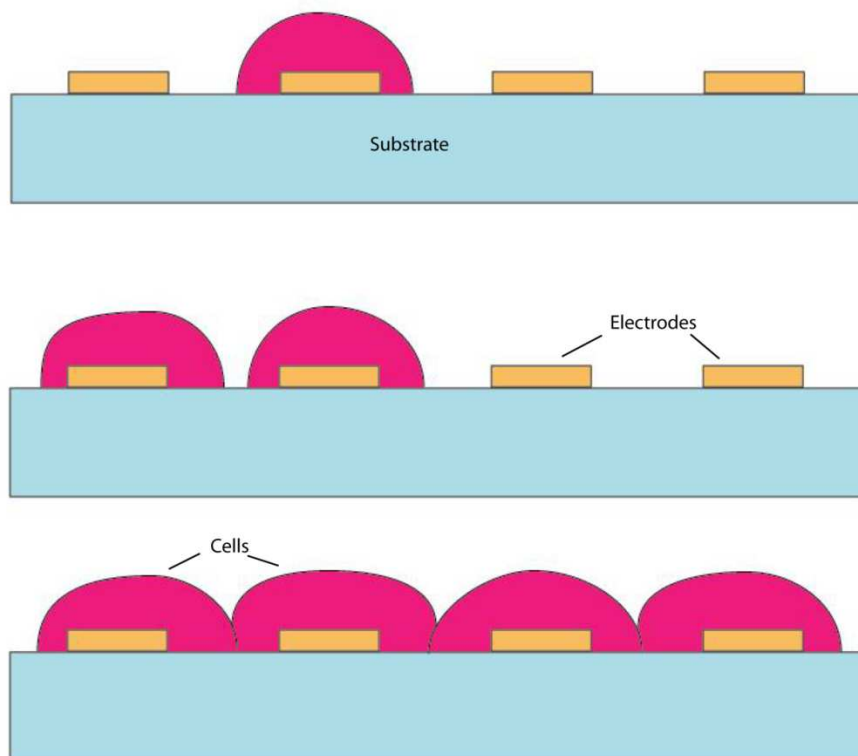
Figure 6.1 a schematic illustrating how, as cells grow and cover electrodes, the path between electrodes changes. This causes changes in the impedance between electrodes.

6.1.1 Electrical Model

The current flow in an electrode-solution system can be divided into two elements representing the faradaic and non-faradaic current flow. The faradaic element is modelled by the frequency dependant Warburg impedance and charge-transfer resistance in series. These elements model how the charge transfer current behaves. The non-faradaic process charges and discharges the electrical double layer, represented by the interface capacitance [117]. The faradaic and non-faradaic elements are in parallel, connected to the bulk resistance. The bulk resistance models the current flow through the solution. This must occur as the current flows through the bulk medium, to reach the return electrode. An equivalent circuit for one electrode-medium interface is shown in figure 6.2.
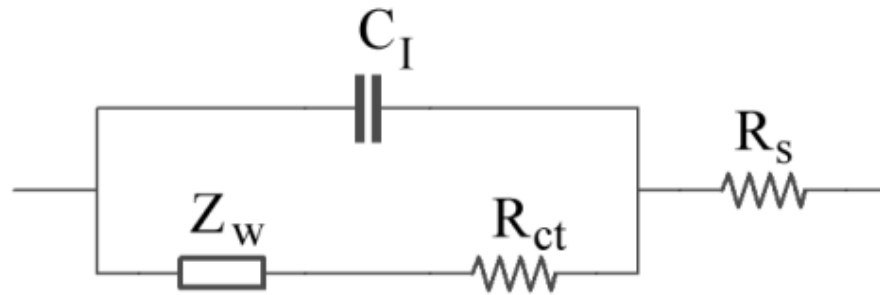
Figure 6.2 the schematic representation of an electrode/medium interface. Z_w is the Warburg impedance, C_I represents the interface capacitance. R_{ct} and R_s are the charge-transfer and spreading resistances [118].

When a cell or group of cells starts to cover an electrode, the cells block some of the current flow to the return electrode. At low frequencies, the current can flow laterally between the cell and substrate gap and hence the impedance should be the same with and without cells. However it has been reported in literature that the impedance, at low frequencies, is lower with cells present (this is unexplained). At higher frequencies, the cells block the current flow from the electrode, causing an increase in the impedance. This is the theoretical basis for changes in impedance caused by cells growing over electrodes [118].

6.2   Wireless Cell Impedance Measurements

The techniques described thus far, using instrumentation and dedicated software are *in vitro* systems. This section aims to introduce a method enabling wireless sensing of cell cell-growth powered from an inductive link. The development of these systems onto biodegradable substrates has been reflected in the choice of receiver circuit, and in other considerations.

6.2.1   Radio Frequency Identification

Radio frequency identification systems (RFID) is a technique for retrieving data from a passive receiver 'tag'. A transmitter inductor sends power to the receiver circuit when it is within range. Power is sent to the RFID tag and data is retrieved in the form of changes in transmitter voltage amplitude. This is caused by load modulation within the receiver. RFID technology is an example of changes in load impedance being detected at the transmitter inductor. If the changes in load impedance could be induced as a consequence of changes in cell-growth, this wireless scheme could provide the means for real-time feedback for the duration of many surgical procedures and wound patches. This passive approach to cell-sensing is ideally suited to a biodegradable implementation. Figure 6.3 illustrates how this

scheme may be developed on biodegradable substrates in conjunction with a neural stimulator.
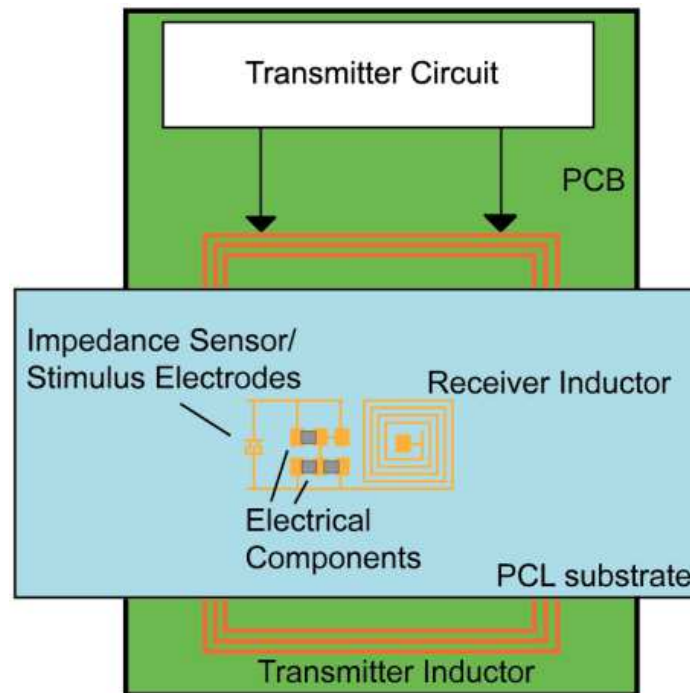
Figure 6.3 diagram showing the long-term goal of this topic, an integrated neural stimulator and sensor, within a biodegradable receiver circuit.

6.2.2   Reflected Impedance in an Inductive Link

It has been shown that impedance changes in a remote receiver, powered inductively, can be detected at the transmitter. Faraday's law of induction states that for two mutually coupled inductors, if the current in the receiver inductor changes, the current in the primary inductor must also change. Consider two mutually coupled inductors, with a coupling factor, k as in the schematic in figure 6.4(a). The equivalent load impedance, seen at the primary side is shown in figure 6.4(b) [109]. This reflected impedance will have a direct impact on the electrical performance of the primary circuit. Changes in the load impedance can be detected here due to the change in the reflected impedance. An equivalent circuit referenced to the primary side of the circuit can be created, assisting in the system design.
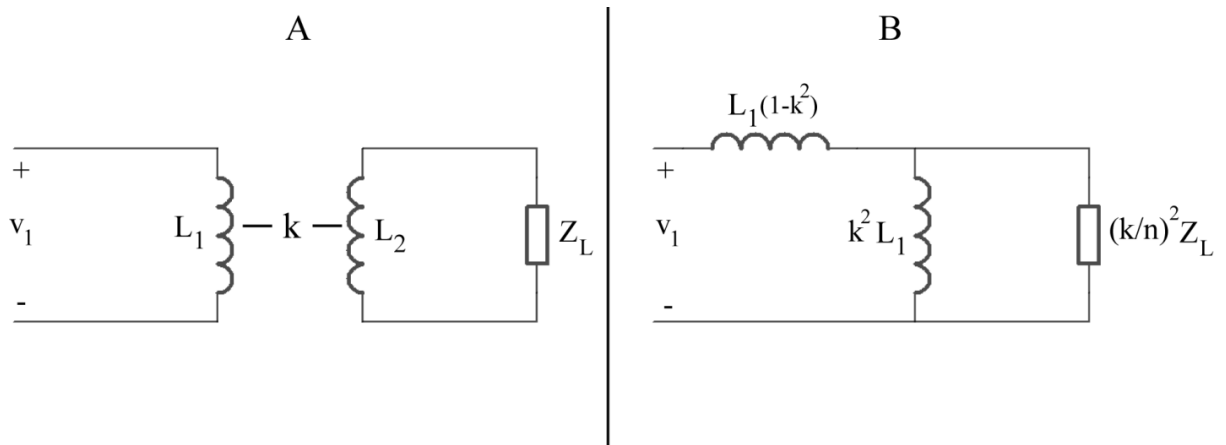
Figure 6.4 two mutually coupled inductors (a) acting as a non-ideal transformer. The load impedance can be expressed as a reflected impedance, reducing the circuit to the primary side (b).

6.3 Design

It is desirable to design a system capable of detecting changes in cell growth using a wireless, passive receiver circuit. The receiver should be designed with a view towards being implanted as part of a biodegradable sensor and stimulation system. The design centres on the detection of changes in impedance, caused by differences in cell coverage over microelectrodes. A suitable transmitter driver and receiver circuit must be defined to accomplish this. In addition, the coupling between the two inductors, which depends on a number of geometrical factors, must be sufficiently high for a given separation distance, in order to detect changes in impedance. The design sections below outline the steps taken to select the transmitter and receiver properties.

6.3.1 Transmitter Circuit Design

The choice of transmitter driver will have a significant impact on how changes in the load impedance of the receiver can be measured. The reflected impedance will appear in parallel with the output inductor. Hence the output circuit of the driver is an important factor in how changes in impedance will be measured. A class AB driver provides a good level of prototyping flexibility as it can drive a wide variety of load impedances. For example, this type of driver can operate with and without an output resonant capacitor, unlike many other topologies. This allows great flexibility in both the transmitter output circuit, and the receiver circuit. This allows ease of re-design as required, based on the level of impedance differences detected at the transmitter. A high-efficiency driver may be implemented beyond the prototype stage, to reduce the power consumption.

6.3.2 Receiver Circuit Design

With a suitable process to develop biodegradable components, for example diodes, transistors capacitors, inductors and resistors, further complexity can be included within the receiver. However, it was decided that the initial designs for a wireless impedance sensor should be as simple as possible to ensure a biodegradable implementation could be achieved. It was therefore desirable to minimise the number of components in the receiver. If a suitable degree of impedance change could be detected using this approach, a biodegradable system could be implemented. With this in mind, caco-2 cells cultured in MEAs were connected to a receiver inductor on PCB. The parallel combination of their impedance would be reflected across the inductive link to the output of the transmitter driver.

It was thought that this initial design would be sufficient to detect cell-impedance changes at the transmitter. Capacitors, or other components, could be added in series or parallel to change the response of the system. Components could be added at either the transmitter output, or receiver, or both as required. This could be of particular use when analysing the effect of resonance on the measured impedance changes. This approach could be developed on PCL with a printed inductor and cell-culture well. Complex receiver circuits, with active components, were not designed due to the early stages of the biodegradable circuit. It is hoped that in the future, the available components will allow for a more advanced design approach, if required. Receiver circuits on PCB proved to be effective in demonstrating the principle of operation. The electrical schematic is shown in figure 6.5.
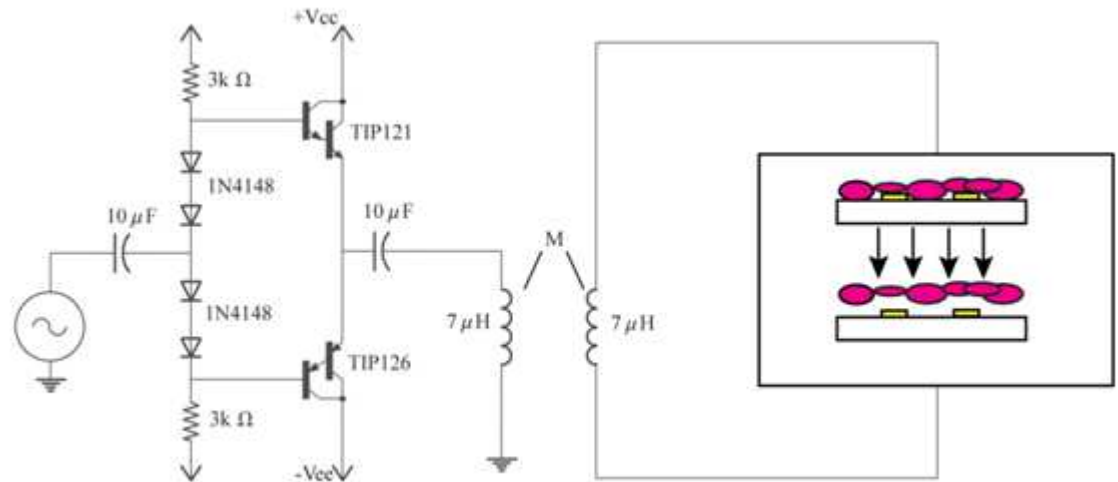
Figure 6.5 a schematic depicting the class AB driver and the receiver inductor, connected to confluent caco-2 cells. The cells were detached using trypsin or EDTA, causing a change in electrical impedance.

6.3.3   Low Coupling Reflections

Often, in bio-implantable applications the separation distance and tight space constraints lead to low coupling between the transmitter and receiver inductors. Since the reflected load impedance is proportional to the square of the coupling factor, low coil coupling makes it incredibly difficult to detect changes in load impedance when using a passive receiver. High transmitter power output is required to ensure that a significant amount of current flows to produce detectable changes in voltage. This case decreases the accuracy and increases the power required from the transmitter to retrieve data. Variations in coupling caused by movement of the inductors can be misinterpreted as meaningful data. This can be addressed in practice by designing the system to be relatively insensitive to coupling variations. In this section, the goal was to prove the concept, leading to design iterations aimed at improving coil displacement tolerance, signal noise and other performance indicators.

6.4   Experimental Procedure

A twisted pair of wires was used to connect the receiver inductor on PCB, to an MEA containing the cell culture. This enabled the use of time lapse recording. Confluent caco-2 cells were connected to the receiver of the inductive link for one hour prior to the application of trypsin or EDTA. These agents, upon breaking up the confluent cell mono-layer, should cause a detectable change in the load impedance. This change in impedance is measured as changes in the peak-to-peak transmitter output voltage. Cells were viewed

using time lapse recording, to verify that a change in the cell monolayer has caused a change in the measured transmitter voltage.

6.4.1 Labview Programming

Circuit voltages were acquired through a PXI data acquisition system (National Instruments). Acquisition was achieved using the NI-6259 analog input card housed within an NI-PXI-1033 chassis as shown in figure 6.6. Labview software (National Instruments, USA) was used to control PXI data acquisition hardware. Measurements were performed using a differential configuration, measuring the voltage difference across each inductor using sense-lines on the PCB. Data was sampled at twice the transmission frequency in accordance with the Nyquist sampling criteria. Data was acquired every minute for the majority of experiments. This was reduced to 10 seconds in subsequent experiments to reduce uncertainty in the measurement. Firewire cameras controlled using the IMAQ Labview platform facilitated the time-lapse recording of caco-2 cells, matching voltage changes with cell-density changes.
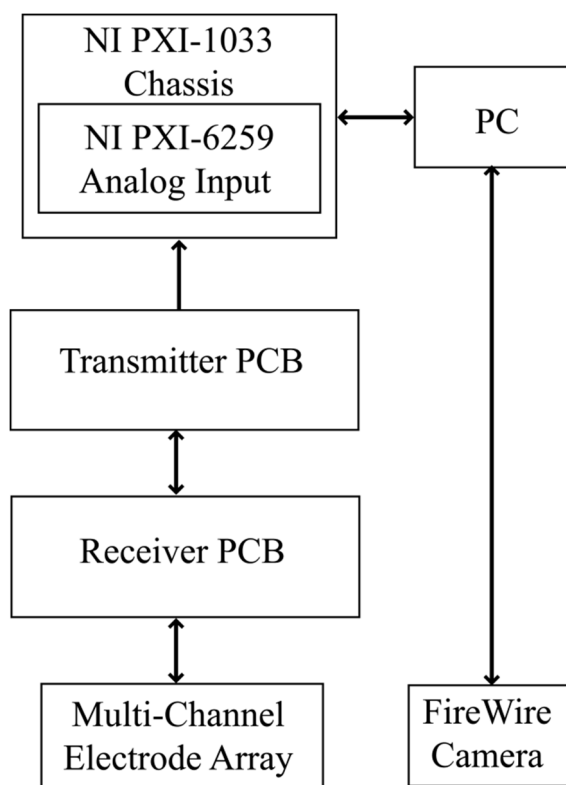
Figure 6.6 the hardware block diagram depicting the experimental set-up used for the impedance measurements.

6.4.2 Cell Culture

Caco-2 cells readily from a confluent monolayer *in vitro.* Their spreading across electrodes as they reach confluence provides the perfect conditions to measure changes in impedance caused by cell-growth. This behaviour provides a good representation of the general case of a wound or injury during the healing process. A detailed description of the cell culture procedure is provided in appendix C.

6.5 Results

The results can be divided into two sections: impedance measurements with a precision LCR meter; followed by measurements with a wireless inductive link. First, a precision LCR meter quantified the electrical impedance of a confluent layer of caco-2 cells. The same measurement was performed after the cells had been detached through the application of trypsin. Trypsin is an enzyme that breaks down proteins by damaging the peptide chains. This process has been used here to transform a homogeneous monolayer of caco-2 cells into separated, detached proteins, known as trypsinisation. Trypsinisation of the cell monolayer has been chosen as a method of measuring the change in electrical impedance from cell coverage, to cell detachment, as a means of modelling the initial and final conditions of cell-growth. These measurements were performed across a range of frequencies in order to asses which operating point provided the biggest difference in impedance. This experiment would prove pivotal in determining the optimum transmission frequency.

6.5.1 Impedance Measurements
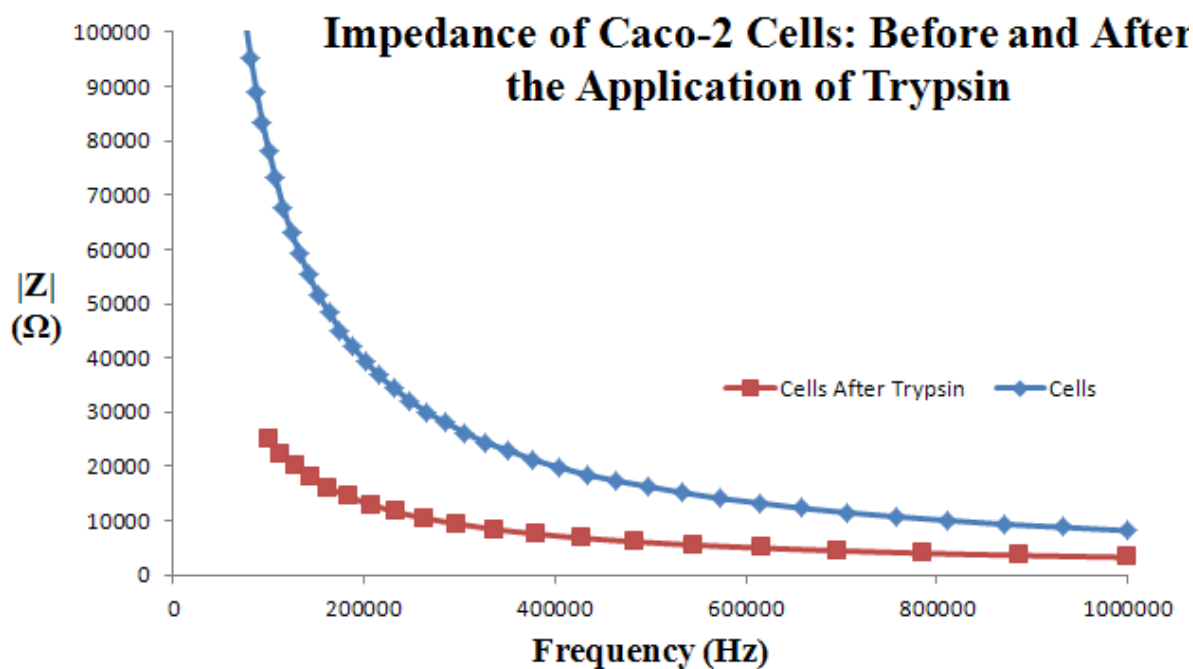
Figure 6.7 impedance magnitude values across frequency. Measurements were performed on confluent caco-2 cells and on the same cells after the application of trypsin, causing their detachment from the electrodes.

The impedance of a confluent monolayer of caco-2 cells was measured with a precision LCR meter, across the 100 kHz to 1 MHz frequency range. Measurements were repeated on the same sample after the application of trypsin. A clear difference in both the impedance magnitude (figure 6.7) and phase angle (figure 6.8) was evident from the measurements. The measured data showed good correlation with expected results and agreed with published literature showing the difference in impedance for cells versus no cells [118]. The larger impedance for the cell-monolayer case agrees with the theory set out at the beginning of this chapter. It was clear that lower transmission frequencies would yield larger differences in the measured change in impedance caused by cell-growth changes.

It was evident that working at a frequency of 100 kHz would allow for measurable changes in impedance, whilst achieving practical power transfer. Operating an inductive link below 100 kHz is impractical because of the high power consumption.

Figure 6.8 phase angle measurements of confluent caco-2 cells and detached caco-2 cells across frequency.

6.5.2 Wireless Measurement Results

Trypsin is quite an aggressive method of breaking up the confluent layer, and this is reflected in the measured transmitter voltage changes, depicted in figure 6.9. The peak-to-peak transmitter output voltage showed a large change after the application of trypsin, before settling to a steady state value. It was noted that the steady state value was different across experiments after the application of trypsin. Further work is required to quantify what the change in steady steady-state value signifies. Experiments with trypsin illustrated with clarity how detachment of cells from the electrodes had a dramatic effect on the load impedance and how these changes could be detected at the transmitter output circuit.
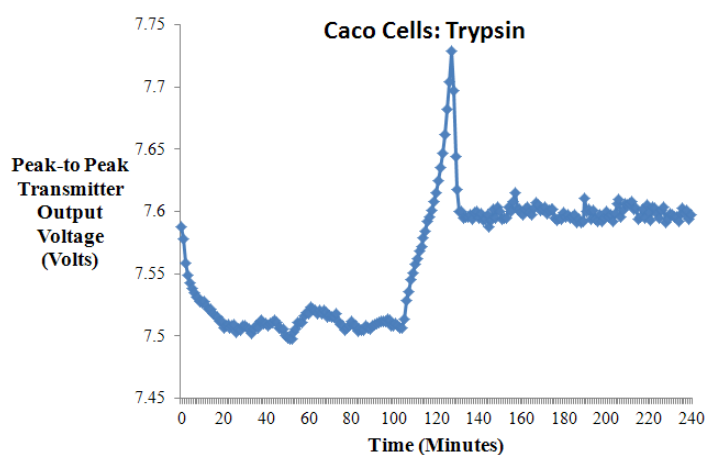
Figure 6.9 the peak-to-peak transmitter output voltage, showing how the application of trypsin after 100 minutes led to a large transition spike, followed by a different value of steady-state voltage. The output voltage reached steady-state after approximately 20 minutes.

Figure 6.10 shows another result obtained using trypsin, with the time-lapse images shown in Figure 6.11. The image on the left shows the confluent layer of cells on the electrode array. On the right, the layer has detached from the surface, and a tear in the monolayer is clearly visible. This shows how aggressive the addition of trypsin can be. Some variability in the results may be caused by the location of the holes in the monolayer. This may also serve to explain why the steady state-values can often differ between experiments. Further work is required to validate this experimentally and to explain why the transient behaviour is different for each experiment.
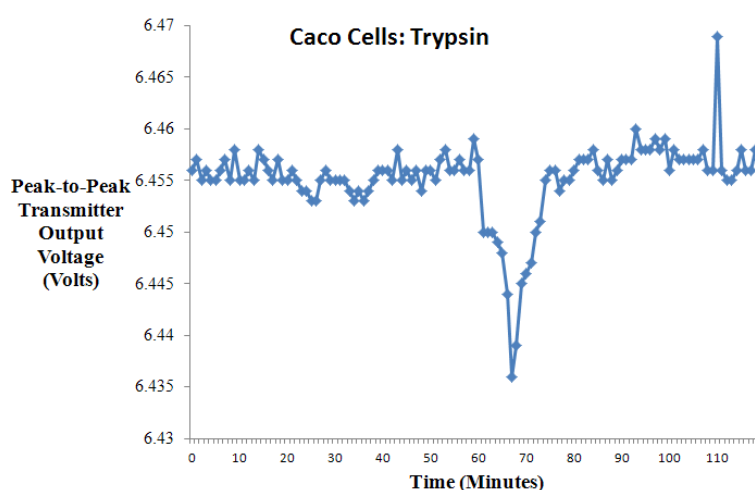
Figure 6.10 a second trypsin experiment, showing that the steady state value can return to the same level. The voltage change for this experiment was less than the previous experiment. Trypsin was added after 60 minutes.
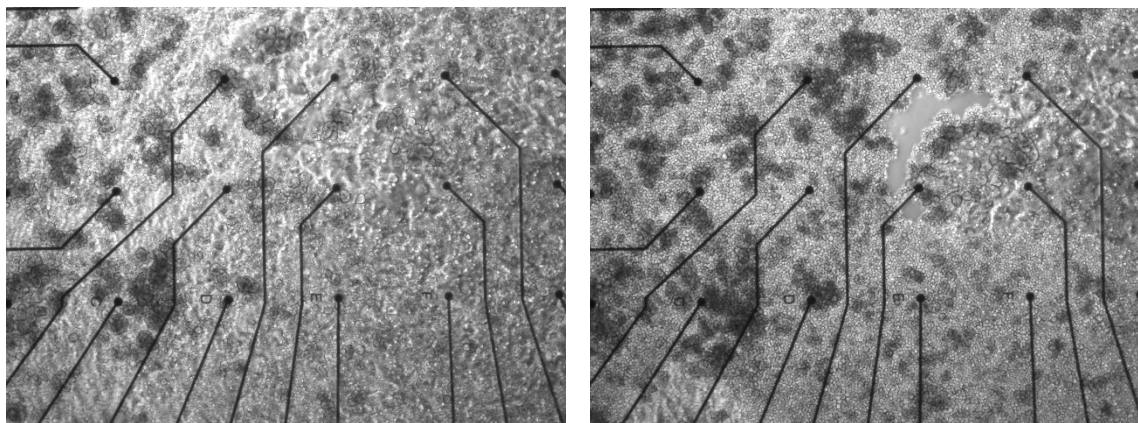
Figure 6.11 a confluent monolayer of caco-2 cells (left) and the layer after detachment of the monolayer by application of trypsin (right).

6.5.3 EDTA

EDTA has many applications, but is often used to detach cells for passaging (subculture). The cells remain functional and this is the primary difference between EDTA and trypsin. Hence EDTA is not as aggressive as with trypsin, and this is reflected in the electrical data because the cell monolayer is detached slower. Results were less distinct when applying EDTA, though some individual experiments, such as that depicted by figure 6.12, showed good levels of voltage change at the transmitter side. Differences between EDTA and trypsin were matched in subtle differences in the transmitter output voltage. This shows that this wireless cell impedance measurement technique is capable of differentiating between trypsin and EDTA as additive agents. However further work is needed at higher power output to obtain clear distinctions between a confluent layer and the application of EDTA and trypsin.
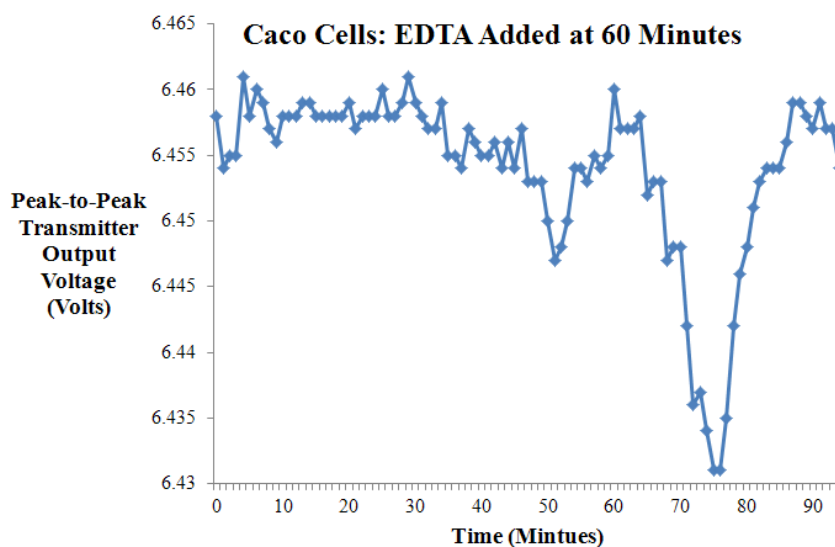
*Figure 6.12 transmitter output voltage showing how the application of EDTA induced a change.
EDTA was added after 60 minutes.*

6.5.4 Cell-Death
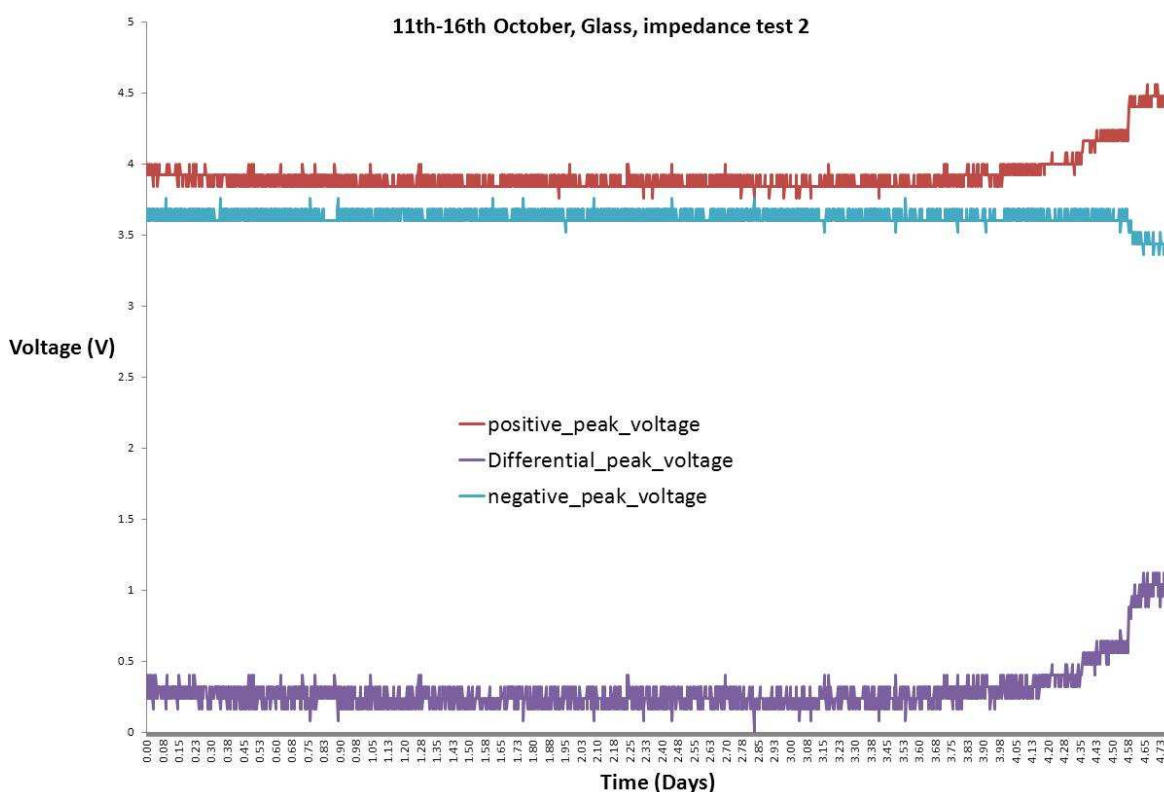
*Figure 6.13 the long-term transmitter output voltage showing the onset of cell-death. As the cells
die, a steady ramp is seen.*

Wireless electrical cell measurements performed on a confluent layer, and a layer that had
been detached, showed a steady state response, followed by a transient behaviour during
the detachment of the monolayer. These experiments provided a change in output

transmitter voltage caused by the switch from confluent cells to no-cells at the receiver circuit. This proved that reflected impedance was sufficient to detect changes in cell density. The degradation of the cell monolayer was also measured wirelessly over time, leading to a steady ramp caused by cell-death, shown in figure 6.13. Cell-death was observed and inferred through changes in the colour of the medium, and in viewing the cells through a microscope. A single experiment has been performed in this way. Further experiments could reinforce this behaviour.

6.5.5 Steady-Culture Impedance

The same wireless measurement technique was employed on a caco-2 culture as they reached confluence over a number of days. The experiment, like those described above, was conducted in a hot-room to allow space for the electrical systems, had to run completely without disconnecting the cells. Disconnecting the cells to feed and change the media would have made it unlikely that the electrical condition would be exactly the same. It was expected that as the cells grow, the output transmitter voltage would change gradually as the electrodes become covered. This experiment has yet to yield such a result, it is felt by further electrical and cell parameters optimisation, discrete changes may be observed. Experimenting with the number and size of electrodes used could also assist in this pursuit. Finally, executing the experiment within an incubator could drastically reduce the electrical noise.

This experiment was designed to show the true application of this wireless sensing technique. Trypsin experiments showed good results, but represented cell-growth in reverse. During an injury or wound healing procedure, cells would spread to confluence and it is this behaviour that is most desirable to document. The change in density would be slower, especially when compared with the rapid detachment of a monolayer as is the case during the application of trypsin.

6.6 Discussion

Some promising data has been obtained, particularly with the application of trypsin to remove the caco-2 cells from the electrodes. However, repeating the results on a consistent basis has proved troublesome due to a number of factors. The electrical variability is on the order of 5-10 mV over the course of the experiment, caused by the difficult experimental set-up. Within this margin there can be no certainty on any changes. Progressing towards a compact system, operating in an incubator will alleviate this characteristic. Some experiments, when progressing from a cell-monolayer, to a detached monolayer, could be

experiencing changes on this level of magnitude. It has been shown using the time-lapse recordings that as the cells detach, corresponding changes in transmitter voltage are observed. Using a compact system in an incubator i.e. with no time-lapse recording, could yield the expected variations in impedance on a more consistent basis. The incubator, acting as a Faraday cage, would reduce the electrical noise. An increase in transmitter output power could also be employed to make the system more sensitive to changes in cell behaviour or growth.

In terms of the steady growth experiments, a method of achieving good culture whilst maintaining the integrity of the electrical data is sought. With this improvement, culture will be reliable and data can be gathered that would more closely resemble the expected data *in vivo*. The number of electrodes used, and their size, could be altered. A large number of electrodes should yield step-changes in the impedance. This type of measurement would be useful in a nerve conduit, charting the cell proliferation through the conduit over time, indicating the success or failure of the procedure. Indeed using this, subsequent experiments could be enhanced based on the measured wireless impedance changes over time. Further enhancements to the receiver circuit could be made to include a higher degree of functionality. Encoding the data in a modulation scheme could be used to boost the signal at the transmitter. For example, by measuring changes in impedance, and encoding this as changes in the amplitude modulation as in RFID systems could greatly improve the accuracy and the amount of data that can be collected from within the receiver.

6.7 Summary

A series of impedance measurements, both wired and wireless, have been used to chart some cell outcomes, such as detachment, death and growth. Wireless electrical cell measurements *in vitro* can provide a good model for changes in cell behaviour and morphology. This model could be used as a template for an *in vivo* measurement system. It is hoped that such a system could be integrated with a nerve regeneration stimulator to design a bi-directional system capable of providing real-time cell growth information during the repair procedure. Addressing some of the issues reported here, such as noise and set-up difficulty could push this technique forward.

7 Conclusion and Future Work

7.1 Summary

Innovative approaches to improving peripheral nerve repair outcomes have been developed throughout this project. The effect of electrical stimulation on regenerating neurons was documented using a novel experimental set-up. This led to the demonstration of electrical stimulation in a wirelessly powered stimulation module on the biodegradable polymer, polycaprolactone (PCL). Finally, an effort was made to demonstrate the efficacy of reflected impedance changes caused by changes in cell growth as a passive sensing mechanism. The conclusions from these three topics are described in detail below.

7.1.1 Effects of electrical stimulation on regenerating neurons *in vitro*

The effects of alternating electric fields on regenerating sensory neurons were thoroughly investigated at the cellular level. Initial results on MEAs showed sporadic alignment on an inconsistent basis. Efforts were made to tune the electrical stimulation waveform to improve the results, but to no avail. In contrast, the design and fabrication of novel hybrid devices improved results dramatically. Hybrid devices, consisting of microtopography to first align the regenerating neurons, followed by a region of electrodes, allowed consistent experimentation on the effect of the stimulation. Electrical parameters, in particular the shape, frequency, amplitude and relaxation time were varied in a series of experiments designed to optimise the stimulation signal. From this, a number of effects were documented. An electrical barrier, neuronal turning, electrode preference and network-tearing were all observed using alternating fields on a number of electric field patterns. This represents the first such study of cellular effects on regenerating neurons *in vitro*. Furthermore, the use of mechanical cues to guide neurons to an electrical cue region is new, and could be used for other types of investigation e.g. different combinations of guidance cues. These mechanical cues were vital in increasing the rate of experimental data, when compared with results on MEAs, where the neurons were afforded a much higher rate of freedom.

7.1.2 Electrical Stimulation on Wirelessly Powered Biodegradable Polymers

A novel fabrication process was developed to produce a receiver inductor and inter-connect on the biodegradable polymer, PCL. In planar form, the PCL receiver circuit, powered wirelessly, was used to provide electrical stimulation signals to regenerating neurons, also on planar PCL. This was done with a view to developing these systems for *in*

vivo, advanced conduit repair. These circuits demonstrated neuronal confinement between two pairs of electrodes. This offers much promise in developing conduits with an array of electrodes, leading to improved guidance of regenerating neurons to their targets. This system documents the first such use of alternating electric fields, powered wirelessly, on a biodegradable polymer.

7.1.3 Wireless Cell Impedance Sensing

With much inspiration from the multitude of applications of electrical cell impedance sensing (ECIS), progress has been made here in developing a wireless alternative. This wireless, passive approach to cell impedance sensing has been used here to demonstrate how changes in cell-growth over electrodes can be detected at the transmitter side of an inductive powering system. Using the caco-2 cell line to form a monolayer, additives designed to strip the monolayer resulted in two states of impedance. These changes, caused by the disruption of the monolayer, were detected at the transmitter side. This type of system could be included within an advanced, biodegradable conduit as a sensor, indicating how a repair is progressing. The system has been designed to be capable of integration with any biodegradable stimulation system.

7.2 Conclusion

To conclude this thesis, the five elements of this feasibility study will be described in terms of what has been learned and observed in reference to the original hypothesis listed in chapter 1.

7.2.1 Electrical Stimulation Parameter Space

At the beginning of this study it was unknown what effect each electrical stimulation parameter has on regenerating neurons. This study aimed to identify, through a series of *in vitro* experiments, an approximate working value for each parameter. The work in chapter 4 was effective in achieving this aim. A stimulation signal of amplitude 20 mV, sinusoidal shape, 100 Hz frequency and occurring 20 times per second throughout the experiment proved to be a good working point for the different trials. It is recognised that this does not represent the *optimum* stimulation signal. It does however allow the reliable execution of a multitude of experiments, with the knowledge that growth of cells will occur and that a discernible outcome may be observed. It is hoped that this information, particularly in the accurate control of electric fields at the cellular level, may allow other researchers to further explore electrical stimulation of neurons and to optimise the electrical waveform.

7.2.2 Manipulation and Control of Neurons through Electrical Stimulation

The identification of a 'working electrical stimulation protocol' allowed a large amount of experiments to be conducted, each displaying effects on the outgrowth of regenerating neurons. Through the use of 4 different electrode layouts, and mechanical guidance cues to provide alignment, a number of effects were observed. Neurons, when faced with an alternating electric field that is normal to their outgrowth, are repelled by this field. This gives rise to a barrier effect. With careful consideration of the electrical stimulation protocol, neurons were able to be held at this barrier prior to their decision to turn at right-angles to it. This turning effect is thought to be the first demonstration using alternating electric fields.

A number of interesting effects, though not of use, were observed. A memory effect was prevalent in unbalanced electrode configurations, leading to the preferential growth of neurons towards one electrode. Upon reaching this electrode, the neurons are repelled, never to return to the contact-site. This effect was overcome in the work in chapter 5 by employing a balanced set of barrier effects, presenting the neurons with two 0V electrodes. This memory effect thus directly contributed to the understanding and successful outcomes obtained on wirelessly powered substrates.

An interesting control outcome, that of neurons always turning to the right, remains unsolved in its origin. Further work should seek to identify this as it may indeed be a unique guidance mechanism in its own right.

7.2.3 Enabling Technologies for Electronics on Polycaprolactone

A novel printing technique capable of producing patterned thin-film gold on polycaprolactone has been developed. It has been used to produce over 200 viable devices. Wire-bonding and electroplating were also possible through empirical process design and have proved invaluable, particularly in reaching a practical working transmission frequency of 800 kHz.

7.2.4 Design and Set-up of a Wireless Link and Biodegradable Stimulator

The development of a reliable printing process for PCL has resulted in the demonstration of the effectiveness of alternating electrical stimulation in aligning neurons from a wirelessly powered device. These devices, on biodegradable substrates, show that alternating electric fields can confine neurons to a neutral channel. This confinement, were the device to be implanted, could result in increased numbers of neurons reaching their targets and thus improving functional outcomes for patients.

7.2.5 Passive Wireless Impedance Sensing

It was the aim of this work to develop a passive wireless cell impedance sensor, ultimately capable of inclusion with a biodegradable conduit design. Initial results reported here show its ability to detect detachment of cell-monolayers from the substrate. It is therefore feasible, but as can be seen from the results in chapter 6, further designs and experiments are required to improve the repeatability. Efforts to detect subtle changes in growth over time have proved difficult, but it is hoped that future experiments will overcome this challenge. Another interesting outcome from this section has been in the detection of cell-death events. This could provide a means to chart life/death over time within a conduit, leading to design iterations aimed at improving nutrient flow and cell proliferation within an implant.

7.3 Future Work

Some of the key developments aimed at making progress towards the development of a system capable of *in vivo* implantation are described in this section.

7.3.1 Electrical Stimulation Parameter Optimisation

The investigation of applied electrical stimulation parameters to regenerating sensory neurons has opened up a number of possible avenues to explore. The interesting results for control cultures on hybrid devices warrants further experimentation. It is desirable to achieve a random control distribution, which has as yet not been achieved on these devices. Perhaps a re-design of the electrode layout with added passivation would remove the tendency to turn right. Next, a multitude of experiments, in the same vain as documented here, could be carried out to further optimise the stimulation waveform. In particular, being able to allow the regenerating neurons to enter the straight, hairpin and other configurations is a primary goal. With a re-design of the system to allow for smaller electric field values, this may be achieved.

Taking data and observations from the hybrid devices, it would be interesting to see how these results could be introduced back to 'free' neurons. Using an MEA or custom electrode module *without* any mechanical guidance cues, this study would aim to show some of the effects and outcomes without their assistance. This is important in progressing towards an *in vivo* implementation. Other electrode designs could also be developed, perhaps with different materials.

7.3.2 Biodegradable Conduit Developments

Work here has shown how wirelessly powered circuits on planar PCL can confine neurons between electrodes. There are a number of experiments that can be carried out to lead to a conduit design, capable of implantation. Further optimisation of the electrical stimulation waveform in conjunction with the work on hybrid devices could yield improvements in the level of cell growth, and in the observed effect. The development of biodegradable components has been discussed and metal-insulator-metal (MIM) capacitors could be suitable for this task. Work has begun on investigating the use of TiO_x films between two metal layers as a high dielectric material, providing a large capacitance per unit area. Conventional MIM components using silicon dioxide or nitride are well documented and could also be implemented. Diodes, also made from TiO_x could take the place of the Schottky diode. A Pt-TiO_x-Ti structure has been investigated but further work is needed to produce a practical diode. ZnO is another possible material, commonly used in organic diodes. Many research groups have documented a plethora of organic thin-film transistors. These could lead to enhanced functionality within the receiver circuit, and in particular could greatly enhance the capability of any wireless impedance sensor. It is hoped in future work to develop these components, or to seek collaboration with research groups that produce them.

The wireless sensing results reported here are in their infancy. Further work is needed to demonstrate the use of the circuits on PCL. Achieving a level of consistency is also required, to ensure changes observed in transmitter voltages are representative of cell behaviour. Interesting work could centre around the use of neurons, charting their growth through a conduit. Alternatively, their action potentials could be recorded and transmitted over the wireless link. This would require a more advanced level of circuitry, but is not entirely impossible. This would require the use of transistors leading to a more active receiver circuit. Work on steady growth of cells and charting that as changes in reflected impedance is on-going. To date this has proved difficult to implement due to challenges associated with the experimental set-up and the exchange of the culture medium (which changes the level of impedance as the cells are removed and plugged back in). Continuous experimentation led to failed cell-culture, and it is hoped that in future this can be addressed. Biodegradable transistors would improve the level of voltage change seen at the primary, by increasing the changes in receiver load current. This load-modulation scheme is at the heart of radio frequency identification (RFID) technology.

Implementing a wireless impedance sensor, based on reflected impedances, on the same circuit as the electrical stimulator offers many challenges. However both systems have been designed with a view to achieving this aim. Both use the same transmitter and data modulation scheme. Using different transmission frequencies, separate branches of the transmitter could be employed to separate the transmitted data from the received data. Again, this would be much easier should the receiver contain biodegradable transistors.

Reference List

[1] J. IJkema-Paassen, K. Jansen, A. Gramsbergen, M. F. Meek, *Biomaterials* **2004**, *25*, 1583.

[2] A. Hart, G. Terenghi, M. Wiberg, *Tissue Engineering for Peripheral Nerve Regeneration* **2010**.

[3] L. Dvali, S. Mackinnon, *Clin Plast Surg* **2003**, *30*, 203.

[4] G. Lundborg, L. B. Dahlin, N. Danielsen, R. H. Gelberman, F. M. Longo, H. C. Powell, S. Varon, *Experimental Neurology* **1982**, *76*, 361.

[5] G. Lundborg, B. Rosén, L. Dahlin, J. Holmberg, I. Rosén, *The Journal of Hand Surgery: British & European Volume* **2004**, *29*, 100.

[6] S. P. Lacour, R. Atta, J. J. FitzGerald, M. Blamire, E. Tarte, J. Fawcett, *Sensors and Actuators A-Physical* **2008**, *147*, 456.

[7] T. Gordon, T. M. Brushart, K. M. Chan, *Neurological Research* **2008**, *30*, 1012.

[8] H. Millesi, in *How to Improve the Results of Peripheral Nerve Surgery* (Eds: H. Millesi, R. Schmidhammer), Springer Vienna **2007**, 37.

[9] S. P. Lacour, J. J. FitzGerald, N. Lago, E. Tarte, S. McMahon, J. Fawcett, *Ieee Transactions on Neural Systems and Rehabilitation Engineering* **2009**, *17*, 454.

[10] S. M. Kim, S. K. Lee, J. H. Lee, *Journal of Craniofacial Surgery* **2007**, *18*, 475.

[11] S. Madduri, K. Feldman, T. Tervoort, M. Papaloizos, B. Gander, *Journal of Controlled Release* **2010**, *143*, 168.

[12] A. A. Al-Majed, C. M. Neumann, T. M. Brushart, T. Gordon, *Journal of Neuroscience* **2000**, *20*, 2602.

[13] T. Gordon, O. A. R. Sulaiman, A. Ladak, in *International Review of Neurobiology* (Eds: Stefano Geuna, Pierluigi Tos and Bruno Battiston), Academic Press **2009**, 433.

[14] C. E. Schmidt, J. B. Leach, *Annual Review of Biomedical Engineering* **2003**, *5*, 293.

[15] M. Merle, A. L. Dellon, J. N. Campbell, P. S. Chang, *Microsurgery* **1989**, *10*, 130.

[16] K. Seunarine, D. O. Meredith, M. O. Riehle, C. D. W. Wilkinson, N. Gadegaard, *Microelectronic Engineering* **2008**, *85*, 1350.

[17] J. M. Corey, D. Y. Lin, K. B. Mycek, Q. Chen, S. Samuel, E. L. Feldman, D. C. Martin, *Journal of Biomedical Materials Research Part A* **2007**, *83A*, 636.

[18] J. W. Xie, M. R. MacEwan, A. G. Schwartz, Y. N. Xia, *Nanoscale* **2010**, *2*, 35.

[19] T. B. Bini, S. J. Gao, S. Wang, S. Ramakrishna, *Journal of Materials Science-Materials in Medicine* **2005**, *16*, 367.

[20] J. J. FitzGerald, S. P. Lacour, J. W. Fawcett, *Recording with microchannel electrodes in a noisy environment*, IEEE, NEW YORK **2008**.

[21] J. H. Huang, L. Lu, J. B. Zhang, X. Y. Hu, Y. G. Zhang, W. Liang, S. Y. Wu, Z. J. Luo, *Plos One* **2012**, *7*.

[22] J. J. FitzGerald, S. P. Lacour, S. B. McMahon, J. W. Fawcett, *Ieee Transactions on Biomedical Engineering* **2009**, *56*, 1524.

[23] N. Lago, D. Ceballos, F. J. Rodriguez, T. Stieglitz, X. Navarro, *Biomaterials* **2005**, *26*, 2021.

[24] G. C. W. Ruiter, M. J. A. Malessy, M. J. Yaszemski, A. J. Windebank, R. J. Spinner, *Neurosurgical Focus* **2009**, *26*.

[25] B. Pomeranz, J. J. Campbell, *Brain Research* **1993**, *603*, 271.

[26] C. D. McCaig, A. M. Rajnicek, *Exp Physiol* **1991**, *76*, 473.

[27] R. K. Aaron, D. M. Ciombor, *Journal of Cellular Biochemistry* **1993**, *52*, 42.

[28] E. W. Kellogg, M. G. Yost, E. J. Reed, A. P. Krueger, *International Journal of Biometeorology* **1985**, *29*, 253.

[29] J. M. Kerns, I. M. Pavkovic, A. J. Fakhouri, K. L. Wickersham, J. A. Freeman, *Journal of Neuroscience Methods* **1987**, *19*, 217.

[30] D. L. Zealear, R. J. Rodriguez, T. Kenny, M. J. Billante, Y. Cho, C. R. Billante, K. C. Garren, *Journal of Neurophysiology* **2002**, *87*, 2195.

[31] M. C. Lu, C. Y. Ho, S. F. Hsu, H. C. Lee, J. H. Lin, C. H. Yao, Y. S. Chen, *Neurorehabilitation and Neural Repair* **2008**, *22*, 367.

[32] W. L. Cheng, C. C. K. Lin, *Journal of Trauma-Injury Infection and Critical Care* **2004**, *56*, 1241.

[33] G. E. Loeb, W. B. Marks, J. A. Hoffer, *Journal of Neurophysiology* **1987**, *57*, 563.

[34] M. O. Kelleher, R. K. Al-Abri, D. V. Lenihan, M. A. Glasby, *Journal of Neurosurgery* **2006**, *105*, 610.

[35] B. F. Sisken, M. Kanje, G. Lundborg, E. Herbst, W. Kurtz, *Brain Research* **1989**, *485*, 309.

[36] L. Hinkle, C. D. McCaig, K. R. Robinson, *Journal of Physiology-London* **1981**, *314*, 121-&.

[37] V. R. Gaddam, J. Yernagula, R. R. Anantha, S. Kona, S. Kopparthi, A. Chamakura, P. K. Ajmera, A. Srivastava, *Smart Structures and Materials 2005: Smart Electronics, Mems, BioMems, and Nanotechnology* **2005**, *5763*, 20.

[38] V. R. Gaddam, Remote power delivery for hybrid integrated bio-implantable electrical stimulation system, in , Louisiana State University **2005**.

[39] W. H. Ko, S. P. Liang, C. D. F. Fung, *Medical & Biological Engineering & Computing* **1977**, *15*, 634.

[40] C. M. Zierhofer, I. J. Hochmair-Desoyer, E. S. Hochmair, *Ieee Transactions on Rehabilitation Engineering* **1995**, *3*, 112.

[41] E. Margalit, M. Maia, J. D. Weiland, R. J. Greenberg, G. Y. Fujii, G. Torres, D. V. Piyathaisere, T. M. O'Hearn, W. Liu, G. Lazzi, G. Dagnelie, D. A. Scribner, E. de Juan Jr, M. S. Humayun, *Survey of Ophthalmology* **2002**, *47*, 335.

[42] J. Wu, V. Quinn, G. H. Bernstein, *Mems Components and Applications for Industry, Automobiles, Aerospace, and Communication* **2001**, *4559*, 43.

[43] H. M. Lu, C. Goldsmith, L. Cauller, J. B. Lee, *Ieee Transactions on Magnetics* **2007**, *43*, 2412.

[44] G. Vandevoorde, R. Puers, *Sensors and Actuators A-Physical* **2001**, *92*, 305.

[45] M. Ghovanloo, K. Najafi, *Ieee Transactions on Circuits and Systems I-Regular Papers* **2004**, *51*, 2374.

[46] P. E. K. Donaldson, *Journal of Medical Engineering & Technology* **1987**, *11*, 23.

[47] D. C. Galbraith, M. Soma, R. L. White, *Ieee Transactions on Biomedical Engineering* **1987**, *34*, 265.

[48] C. M. Zierhofer, E. S. Hochmair, *Ieee Transactions on Biomedical Engineering* **1990**, *37*, 716.

[49] K. Fotopoulou, B. W. Flynn, *Ieee Transactions on Magnetics* **2011**, *47*, 416.

[50] N. Futai, N. Futai, K. Matsumoto, I. Shimoyama, *Sensors and Actuators A-Physical* **2004**, *111*, 293.

[51] J. T. Kuo, K. Y. Su, T. Y. Liu, H. H. Chen, S. J. Chung, *Ieee Microwave and Wireless Components Letters* **2006**, *16*, 69.

[52] H. M. Greenhouse, *Ieee Transactions on Parts, Hybrids, and Packaging* **1974**, *PHP-10*, 101.

[53] S. S. Mohan, M. D. Hershenson, S. P. Boyd, T. H. Lee, *Ieee Journal of Solid-State Circuits* **1999**, *34*, 1419.

[54] X. L. Tang, H. W. Zhang, H. Su, Y. Shi, X. D. Jiang, *Microelectronic Engineering* **2005**, *81*, 212.

[55]   J. G. Hubert, R. J. Kakalec, *Proceedings: Electrical Electronics Insulation Conference and Electrical Manufacturing & Coil Winding Conference* **1993**, 707.

[56]   H. A. Wheeler, *Proceedings of the Institute of Radio Engineers* **1928**, *16*, 1398.

[57]   W. J. Heetderks, *Ieee Transactions on Biomedical Engineering* **1988**, *35*, 323.

[58]   P. Troyk, Z. Hu, *Ieee Transactions on Biomedical Engineering* **2013**, *60*, 1414.

[59]   M. Nardin, K. Najafi, "A multichannel neuromuscular microstimulator with bi-directional telemetry", presented at *The 8th International Conference on Solid State Actuators, and Eurosensors IX.*, Stockholm, Sweden, **1995**.

[60]   J. A. Vonarx, K. Najafi, *Transducers 97 - 1997 International Conference on Solid-State Sensors and Actuators, Digest of Technical Papers, Vols 1 and 2* **1997**, 999.

[61]   J. Perelaer, C. E. Hendriks, A. W. M. de Laat, U. S. Schubert, *Nanotechnology* **2009**, *20*.

[62]   S. Magdassi, M. Grouchko, O. Berezin, A. Kamyshny, *Acs Nano* **2010**, *4*, 1943.

[63]   M. Hummelgard, R. Y. Zhang, H. E. Nilsson, H. Olin, *Plos One* **2011**, *6*.

[64]   H. J. H. Chen, L. C. Chen, C. H. Lien, S. R. Chen, Y. L. Ho, *Microelectronic Engineering* **2008**, *85*, 1561.

[65]   L. Y. Jiao, H. J. Gao, G. M. Zhang, G. Y. Xie, X. Zhou, Y. Y. Zhang, Y. Y. Zhang, B. Gao, G. Luo, Z. Y. Wu, T. Zhu, J. Zhang, Z. F. Liu, S. C. Mu, H. F. Yang, C. Z. Gu, *Nanotechnology* **2005**, *16*, 2779.

[66]   G. S. Ferguson, M. K. Chaudhury, G. B. Sigal, G. M. Whitesides, *Science* **1991**, *253*, 776.

[67]   C. Kim, M. Shtein, S. R. Forrest, *Applied Physics Letters* **2002**, *80*, 4051.

[68]   C. Kim, P. E. Burrows, S. R. Forrest, *Science* **2000**, *288*, 831.

[69]   N. Lee, Y. Kim, S. Kang, J. Hong, *Nanotechnology* **2004**, *15*, 901.

[70]   G. Kumar, H. X. Tang, J. Schroers, *Nature* **2009**, *457*, 868.

[71]   L. R. Bao, L. Tan, X. D. Huang, Y. P. Kong, L. J. Guo, S. W. Pang, A. F. Yee, *Journal of Vacuum Science & Technology B* **2003**, *21*, 2749.

[72]   X. D. Huang, L. R. Bao, X. Cheng, L. J. Guo, S. W. Pang, A. F. Yee, *Journal of Vacuum Science & Technology B* **2002**, *20*, 2872.

[73]   J. H. Choi, D. Kim, P. J. Yoo, H. H. Lee, *Advanced Materials* **2005**, *17*, 166-+.

[74]   C. Chung, M. Allen, *Journal of Micromechanics and Microengineering* **2005**, *15*, N1-N5.

[75] W. Dai, K. Lian, W. J. Wang, *Microsystem Technologies-Micro-and Nanosystems-Information Storage and Processing Systems* **2005**, *11*, 526.

[76] F. Axisa, D. Brosteaux, E. De Leersnyder, F. Bossuyt, M. Gonzalez, M. V. Bulcke, J. Vanfleteren, *6th International IEEE Conference on Polymers and Adhesives in Microelectronics and Photonics, Proceedings 2007* **2007**, 280.

[77] W. Zhao, H. Y. Low, *Journal of Vacuum Science & Technology B* **2006**, *24*, 255.

[78] L. R. Bao, X. Cheng, X. D. Huang, L. J. Guo, S. W. Pang, A. F. Yee, *Journal of Vacuum Science & Technology B* **2002**, *20*, 2881.

[79] K. Ojima, Y. Otsuka, T. Matsumoto, T. Kawai, K. Nakamatsu, S. Matsui, *Applied Physics Letters* **2005**, *87*.

[80] Y. C. Lee, C. Y. Chiu, *Journal of Micromechanics and Microengineering* **2008**, *18*.

[81] Q. Chen, C. Martin, D. Cumming, *Plasmonics* **2012**, *7*, 755.

[82] J. M. Helt, C. M. Drain, G. Bazzan, *Journal of the American Chemical Society* **2006**, *128*, 9371.

[83] A. J. Tunnell, V. W. Ballarotto, D. R. Hines, E. D. Williams, *Applied Physics Letters* **2008**, *93*.

[84] A. F. Kaplan, T. Xu, Y. K. Wu, L. J. Guo, *Journal of Vacuum Science & Technology B* **2010**, *28*, C6O60-C6O63.

[85] D. R. Hines, A. Southard, M. S. Fuhrer, *Journal of Applied Physics* **2008**, *104*.

[86] H. Schmid, H. Wolf, R. Allenspach, H. Riel, S. Karg, B. Michel, E. Delamarche, *Advanced Functional Materials* **2003**, *13*, 145.

[87] Y. L. Loo, R. L. Willett, K. W. Baldwin, J. A. Rogers, *Applied Physics Letters* **2002**, *81*, 562.

[88] J. W. Kim, K. Y. Yang, S. H. Hong, H. Lee, *Applied Surface Science* **2008**, *254*, 5607.

[89] D. Y. Lee, D. R. Hines, C. M. Stafford, C. L. Soles, E. K. Lin, G. S. Oehrlein, *Advanced Materials* **2009**, *21*, 2524-+.

[90] J. Y. Chen, P. Mela, M. Moller, M. C. Lensen, *Acs Nano* **2009**, *3*, 1451.

[91] D. M. Fang, X. N. Wang, Y. Zhou, X. L. Zhao, *Microelectronics Journal* **2006**, *37*, 948.

[92] S. S. Lee, T. Nishino, T. Yuasa, Y. Yoshida, M. Taguchi, *Journal of Micromechanics and Microengineering* **2006**, *16*, S96-S101.

[93] L. Gu, X. X. Li, *Microelectronic Engineering* **2008**, *85*, 697.

[94] J. B. Yoon, B. K. Kim, C. H. Han, E. S. Yoon, C. K. Kim, *Ieee Electron Device Letters* **1999**, *20*, 487.

[95] R. J. Rassel, C. F. Hiatt, J. DeCramer, S. A. Campbell, *Ieee Transactions on Magnetics* **2003**, *39*, 553.

[96] Z. Wu, X. Li, *Electronics Letters* **2009**, *45*, 409.

[97] T. M. Liakopoulos, C. H. Ahn, *Sensors and Actuators A-Physical* **1999**, *77*, 66.

[98] J. Wegener, C. R. Keese, I. Giaever, *Experimental Cell Research* **2000**, *259*, 158.

[99] T. Schwarzenberger, P. Wolf, M. Brischwein, R. Kleinhans, F. Demmel, A. Lechner, B. Becker, B. Wolf, *Physiological Measurement* **2011**, *32*.

[100] J. H. Yeon, J. K. Park, *Analytical Biochemistry* **2005**, *341*, 308.

[101] C. Xiao, J. H. T. Luong, *Toxicology and Applied Pharmacology* **2005**, *206*, 102.

[102] M. L. Guo, J. H. Chen, X. B. Yun, K. Chen, L. H. Nie, S. Z. Yao, *Biochimica et Biophysica Acta-General Subjects* **2006**, *1760*, 432.

[103] H. Kalvoy, L. Frich, S. Grimnes, O. G. Martinsen, P. K. Hol, A. Stubhaug, *Physiological Measurement* **2009**, *30*, 129.

[104] S. J. Carter, C. J. Linker, T. Turklehuslig, L. L. Howard, *Ieee Transactions on Biomedical Engineering* **1992**, *39*, 1123.

[105] P. Mirtaheri, S. Grimnes, O. G. Martinsen, *Ieee Transactions on Biomedical Engineering* **2005**, *52*, 2093.

[106] G. A. Snook, A. J. Urban, M. R. Lanyon, K. McGregor, *Journal of Electroanalytical Chemistry* **2008**, *622*, 225.

[107] J. D. Kraus, *Electromagnetics*, McGraw-Hill, Singapore **1984**.

[108] A. Sanni, A. Vilches, C. Toumazou, *Ieee Transactions on Biomedical Circuits and Systems* **2012**, *6*, 297.

[109] K. VanSchuylenbergh, R. Puers, *Inductive Powering: Basic Theory and Application to Biomedical Systems*, SPRINGER, NEW YORK **2009**.

[110] K. Van Schuylenbergh, R. Puers, *Inductive Powering Basic Theory and Application to Biomedical Systems*, Springer **2009**.

[111] E. S. Hochmair, *Ieee Transactions on Biomedical Engineering* **1984**, *BME-31*, 177.

[112] C. R. Keese, J. Wegener, S. R. Walker, L. Giaever, *Proceedings of the National Academy of Sciences of the United States of America* **2004**, *101*, 1554.

[113] D. K. Armani, C. Liu, *Journal of Micromechanics and Microengineering* **2000**, *10*, 80.

[114] A. Eberstein, S. Eberstein, *Medicine and Science in Sports and Exercise* **1996**, *28*, 1463.

[115] S. W. Hwang, H. Tao, D. H. Kim, H. Cheng, J. K. Song, E. Rill, M. A. Brenckle, B. Panilaitis, S. M. Won, Y. S. Kim, Y. M. Song, K. J. Yu, A. Ameen, R.

Li, Y. Su, M. Yang, D. L. Kaplan, M. R. Zakin, M. J. Slepian, Y. Huang, F. G. Omenetto, J. A. Rogers, *Science* **2012**, *337*, 1640.

[116] M. Irimia-Vladu, E. G+éowacki, G. Voss, S. Bauer, N. S. Sariciftci, *Materials Today* **2012**, *15*, 340.

[117] A. J. Bard, L. R. Faulkner, *Electrochemical Methods Fundamentals and Applications* **1980**.

[118] X. Q. Huang, D. Nguyen, D. W. Greve, M. M. Domach, *Ieee Sensors Journal* **2004**, *4*, 576.

Appendix A: Hybrid Stimulation Device Fabrication

SU-8 microgrooves have been shown to be effective in aligning neurons, which when coupled with the fact that SU-8 is transparent, makes it a suitable choice as the material for the microgrooves. The fabrication process consists of two stages, the metal electrode patterning and the topographical groove section, depicted in figure A.1. The fabrication steps were carried out in the James Watt Nanofabrication Centre within the University of Glasgow. Quartz microscope slides (Newcastle Optical) were used as the substrate material because of their strong adhesion to SU-8. The substrate was cleaned in acetone, propan-2-ol and methanol for 5 minutes each, followed by a rinse in deionized (DI) water, again for 5 minutes. The substrate was then baked at 180 °C for 5 minutes to remove any moisture. S1818 photoresist (Shipley, USA) was spun onto the quartz substrate at 4000 rpm for 30 seconds. After a soft bake of 95°C for 2 minutes the resist was immersed in MF319 developer (Shipley, USA) for 1 minute to create a suitable sidewall profile for the lift-off technique. The resist was then exposed to UV light through a photo-mask using an MA6 mask aligner tool (SUSS MicroTec, Germany) for 8 seconds. The resist was developed using MF319 developer for 75 seconds. Using a Plassys metal deposition tool (Plassys Bestek, France), 20 nm of Ti followed by 200 nm of Au were evaporated onto the patterned resist film prior to immersion in acetone at 50 °C to perform lift-off, yielding patterned metal electrodes on the quartz substrate.
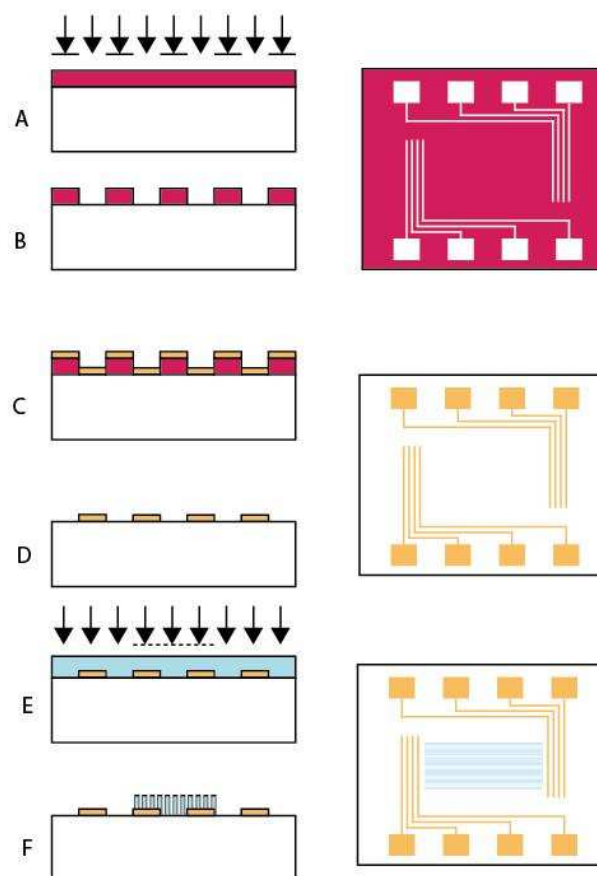
Figure A.1 exposure of S1818 photoresist (A) followed by pattern development (B). Evaporation of Au electrodes (C) and metal lift-off (D). SU-8 groove definition using UV exposure (E) followed by pattern development in EC solvent (F).

The next stage of fabrication is the patterning of SU-8 microgrooves. The quartz substrate, containing the newly added microelectrodes is cleaned for 5 minutes in acetone, propan-2-ol and methanol followed by a rinse in DI water. The substrate was then baked at 180 °C for 5 minutes to remove any moisture. SU-8 3005 photoresist (Micro Chem, USA) was spun at 4000 rpm for 30 seconds. Following a ramped soft-bake of 65°C (1 minute), 95°C (3 minutes) and 65°C (1 minute) the sample was exposed to UV light through a photomask for 25 seconds. The mask aligner was used to ensure the grooves were patterned in the correct location. After exposure, a post exposure bake is required to further cross-link the exposed regions of the resist. The post exposure bake uses the same baking cycle as the soft-bake with the exception that the 95°C step lasts for 2 minutes. The unexposed areas of SU-8 are then removed from the substrate by immersion in EC solvent (Shipley, USA). The sample is then cleaned using propan-2-ol. Patterned SU-8 microgrooves 12.5 μm wide, spaced 12.5 μm are left on the substrate. The final step, hard-curing of the SU-8

photoresist, is achieved at 180 °C for 20 minutes to harden the resist film. This final step prevents the microgrooves from delaminating during aqueous processing e.g. during cell-culture.

# Appendix B: Fabrication Process Development: Electronics on PCL
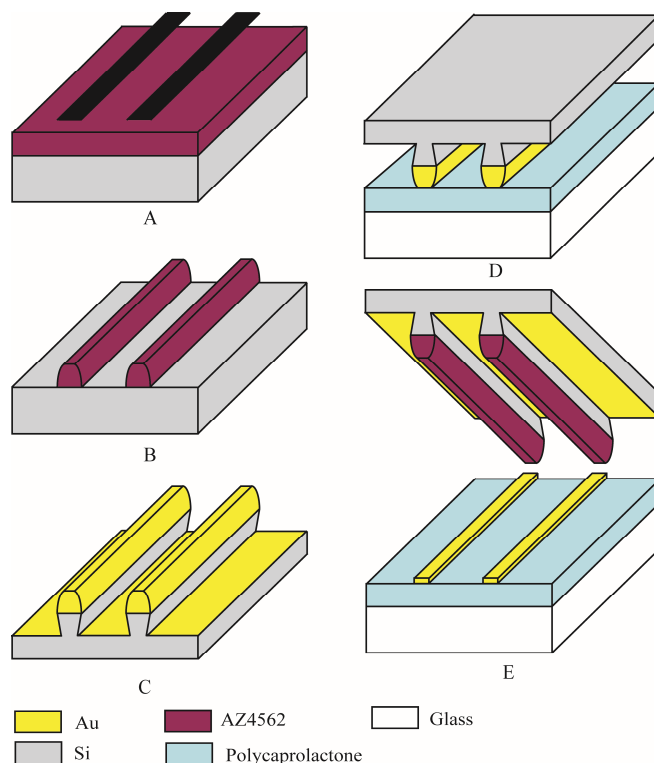
Figure B.1 schematic of the transfer printing process to transfer patterned au films. AZ4562 photoresist, spun in two steps to a thickness of 30 μm, exposed through a photomask (A). Development of the photoresist (B). Dry-etching of the silicon substrate, followed by evaporation of 400 nm Au (C). The stamp is pressed into polycaprolactone on glass (D) at 65 °C. Removal of the stamp (E), completing the transfer printing process.

Stamp Production

The printing procedure is divided into two sections: stamp production and target substrate preparation. The stamp is produced using photolithography and dry etch techniques in the following way. First, a Si substrate is cleaned in acetone, methanol, isopropyl alcohol (IPA) and deionized (DI) water, each for 5 minutes, followed by a blow dry in a pressurized stream of N_2. A dehydration bake in a 180°C oven for 5 minutes removes any residual moisture from the cleaning procedure. A layer of AZ4562 photoresist is spin-cast onto the Si substrate using a spin speed of 1000 rpm with an acceleration ramp of 250 rpms^{-1} for 30 seconds. A soft-bake on a hot-plate for 15 minutes at 90°C causes the solvent to evaporate from the photoresist. A second layer of AZ4562 is then applied in the same way; resulting in a 30 μm thick film of photoresist (2 x 15 μm) on the Si substrate. This resist height is sufficient to prevent the PCL substrate coming into contact with the silicon wafer during printing and was found experimentally. The resist film was left to rehydrate overnight prior to executing the exposure step. Exposure to UV light was

performed through a photo-mask for 110 seconds using 10 second bursts between 10 second relaxation periods to allow any N_2 to escape (preventing the accumulation of N_2 bubbles in the resist film). The exposed regions of AZ4562 were removed using AZ400k developer in DI water (1:3) for 5 minutes. Any residual photoresist layer was removed using an O_2 plasma ash at 80 W for 2 minutes. The residual layer must be removed before dry-etching to ensure the correct profile is achieved.
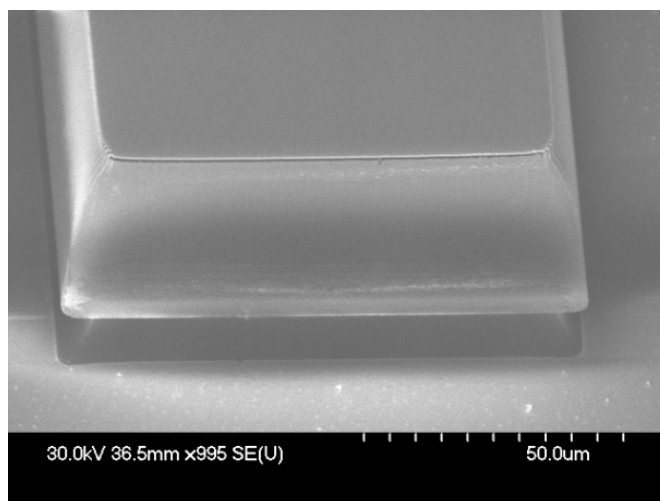

Figure B.2 scanning electron micrograph showing a dry-etched silicon pillar with a sloping sidewall profile. The AZ4562 photoresist column is on top. This profile isolates the metal on the substrate from the metal on the photoresist film.

Next the stamp is dry etched using the Bosch process for deep dry-etching of silicon in an STS-ICP machine. A modified Bosch process is used here to create an undercut sidewall profile by increasing the flow rate of SF_6. An increased rate of SF_6 etches the protective polymer coating the sidewalls, resulting in the etching of the sidewalls. This causes a sloping undercut rather than a vertical profile as shown in figure B.2. The modified process uses an SF_6 flow rate of 40 sccm, platen power of 10 W, ICP power of 600 W, and a pressure of 10 mT for 5 minutes. This procedure leaves any undesired regions of metal deep within a silicon trench, with no connection to the metal on the resist sidewall, preventing the transfer of undesired metal to the PCL substrate. Prior to metal evaporation the photoresist film is subjected to a flood-exposure of 120 seconds, allowing the subsequent use of AZ 400k for resist stripping. Evaporation of 400 nm of Au in a Plassys metal deposition machine is the final step in the stamp fabrication process. The target substrate must now be prepared before the printing step can begin.

Target Substrate Preparation

A SiO$_2$ substrate is cleaned in acetone, methanol, IPA and DI water, each for 5 minutes, followed by a blow dry in a pressurized stream of N$_2$. PCL in chloroform (1:3) is spin-cast at 400 rpm with an acceleration ramp of 100 rpms^{-1} for 60 s. The chloroform is evaporated at room temperature until a 50 μm thick layer of PCL remains on the SiO$_2$ substrate. Both the target substrate and printing stamp are now complete and ready to use in the printing step.
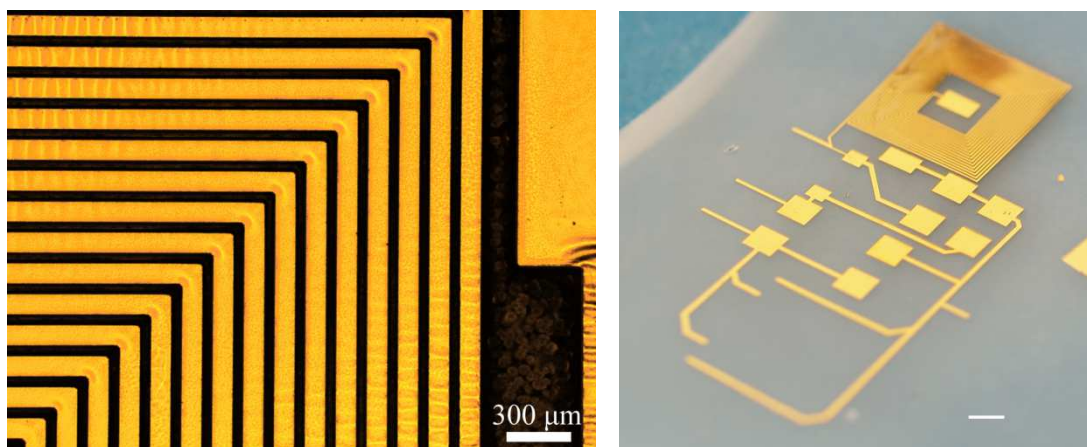

Figure B.3 a micrograph showing a section of the 15 turn spiral inductor (left) and an image showing the printed inductor and component footprints on polycaprolactone (right).

Transfer Printing

To begin the transfer printing, both the stamp and the substrate are placed on a 65°C hot-plate. This temperature is chosen to be above the melt-temperature of PCL. Upon reaching a temperature of 65°C, the stamp is placed onto the PCL sample with enough pressure to push the stamp into the polymer and left for 5 minutes. After this time the stamp-substrate stack is removed from the hot-plate and allowed to cool to room temperature. The stamp is then peeled from the substrate using tweezers. Removal of the stamp causes selective pattern transfer to the substrate due to the poor adhesion of the resist film to the Si substrate. If the height of the photoresist is insufficient, the PCL will come into contact with the sidewalls of the silicon substrate, adhering strongly to them, causing a failure of the printing step because the stamp cannot be removed save for excessive force being applied (pattern deformation is certain). At this stage, metal has been transferred to the PCL substrate in a pattern defined by the photomask used, as shown in figure B.3. The device is almost ready to be used but for two final steps: electroplating and wire-bonding.
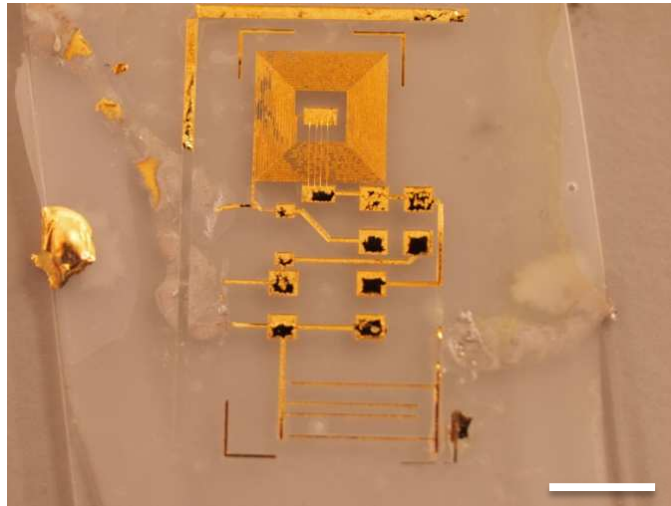
Figure B.4 a printed receiver layout, featuring a 6 mm x 6 mm spiral inductor and component footprints. Gold wire bonds link the central pad to the outer circuit, completing the circuit. The printed gold is electroplated to a thickness of ~30 μm. Contacts have been made to the 'tabs' to allow electroplating. Scale: 5 mm.

Electroplating and Wire Bonding

Printed samples were then electroplated in gold plating solution at room temperature for 5 to a thickness of 30 μm. This plating step reduces the resistance of the inductor from several hundred Ohms down to a few Ohms, increasing the quality factor and thus improving the performance of the inductive link. The electroplating step also facilitates the use of wire bonding to connect the central inductor connection to the rest of the circuit. In CMOS technology, planar spiral inductors are connected to the rest of the circuit using a via on a separate metal layer. Several wire bonds were added to connect the inner contact of the spiral inductor to the rest of the circuit, shown in figure B.4. By wire bonding in this way, only one printing step is required, with the wire bonds used as the second layer.

Appendix C: Cell Culture Technique

Electrical Stimulation Modules on Polycaprolactone

Dorsal root ganglia (DRG) were isolated from 2-day old neonate Sprague-Dawley rats and placed between the electrodes on the PCL/electrode modules. The DRGs were then grown for 15 days at 37 °C, 5% CO_2 with L15 media (Sigma) supplemented with 10% FBS, NGF 2.5S (10ng/ml) (Invitrogen), n-acetyl-cystein (50μg/ml) and 1% antibiotics antimycotic (PAA p11-002). Half of the media (150 μl) was exchanged every day. Cells were fixed and immunostained for β-tubulin (mouse anti-TU-20 Santa Cruz). After the experiment was complete, DRG were fixed in 4% formaldehyde/PBS solution for 15 minutes at 37°C. They were then permeabilized in perm buffer (10.3g sucrose, 0.292g NaCl, 0.06 g MgCl2, 0.476 g HEPES 0.5ml Triton X-100 per 100ml PBS Sigma, UK) at 4 °C for 15 minutes. A blocking solution of 1% BSA/PBS was added at 37°C for 5 minutes. The blocking solution was replaced by 1% BSA/PBS solution containing anti-b3-tubulin antibodies (1:100; mouse anti-TU-20 Santa Cruz, California) and anti-S100 antibodies (1:100; rabbit Ab868 S100 Abcam, UK). The samples were incubated at 37 °C for two hours then washed three times with a PBS/Tween20 (Sigma, UK) 0.5% solution. They were then incubated for 1 hour at 37 °C in 1% BSA/PBS solution containing 1:100 secondary Texas-red anti-rabbit antibodies (Vector Laboratories, UK) and 1:100 biotinylated anti-mouse antibodies (Vector Laboratories) and washed three times with Tween 20 0.5%/PBS. Fluorescein Streptavidin 1:100 (Vector Laboratories) in 1% BSA/PBS was then added to the sample for 30 minutes at 4 °C, before washing them again. The samples were viewed by fluorescence microscopy, and imaged using a Zeiss Axiovert 200m, with a QImaging camera, running on ImagePro+ (Media Cybernetics, UK). A total of 13 successful cultures were used for the experiments.

Multichannel Electrode Array Experiments and Hybrid Device Experiments

DRGs were isolated from 2 day old neonate Sprague-Dawley rats and were seeded in the electrode construct. DRGs were then grown for 15 days at 37°C, 5% CO2 in well L15 media (Sigma) supplemented by 10% FBS, 10 ng/ml NGF 2.5S (Invitrogen), 50 μg/ml n-acetyl-cystein and 1% antibiotics antimycotic (PAA p11-002). Half of the media (150 μl) was changed every day. Cells were fixed and immunostained for β-tubulin (mouse anti-TU-20 Santa Cruz). Samples were recorded by time lapse light microscopy one frame every two minutes. At the end of an experiment, samples were viewed by fluorescence microscopy.

Caco-2 Cell Culture Technique for Impedance Experiments

Caco-2 cells readily from a confluent monolayer *in vitro.* Their spreading across electrodes as they reach confluence provides the perfect conditions to measure changes in impedance caused by cell-growth. This behaviour provides a good representation of the general case of a wound or injury during the healing process. Caco-2 cells were seeded on the MEA at a density of 10^6 cell/mL in 600μL of DMEM (Invitrogen, Scotland) supplemented with 10% fetal bovine serum (FBS, Invitrogen, Scotland) and L-glutamine (2mM, Sigma) and grown until confluence for 10 days at 37°C and 5% CO_2. For those experiments that rely on a detachment of the cell-monolayer, either trypsin or EDTA were used to detach the cell monolayer, in order to induce a sharp change in impedance. Confluent Caco-2 cells were rinsed in 2.38g/L Hepes solution (Sigma, UK) and detached from the MEA aggressively by a 0.25% Trypsin (Sigma, UK) in Versene/EDTA (0.2 g/L) solution, or slowly by the Versene/EDTA solution only.